APPLICATION OF THE FINITE ELEMENT METHOD

TO

LAMINATED FIBER COMPOSITES

by

SOHAIL A UMAR-KHITAB, B.A.Sc., M.A.Sc.

A Thesis

Submitted to the School of Graduate Studies

in Partial Fulfillment of the Requirements

for the Degree

Doctor of Philosophy

McMaster University

Copy 7

LAMINATED FIBER COMPOSITES

DOCTOR OF PHILOSOPHY (1991)
(Mechanical Engineering)

McMASTER UNIVERSITY
Hamilton, Ontario

TITLE : Application of the Finite Element Method to Laminated Fiber Composites.

AUTHOR : S.A. Umar-Khitab, B.A.Sc. (University of Toronto)
M.A.Sc. (University of Toronto)

SUPERVISOR : Professor M.A. Dokainish

NUMBER OF PAGES : xvii, 208

Abstract

This thesis deals with the application of the Finite Element Method to the analysis of laminated fiber composites. Specifically, it addresses the problem of representing the variation of material properties through the element volume in order to reduce the number of degrees of freedom required to represent a laminated composite. This is accomplished by a modification in the evaluation of the element stiffness matrix, whereby the through thickness integration is evaluated separately for each ply of the laminate. This modification results in a significant reduction in the core memory requirements.

The modification is implemented in a finite element code and used to investigate various aspects of laminate behaviour using a design philosophy based upon the laminae constituents rather than the more usual laminate properties. Problems involving lamina coupling, edge and surface deformations are solved for symmetric and unsymmetric laminates. The tensile behaviour of a particular laminate is predicted, and the ability to back calculate the specimen composition parameters is demonstrated. An explanation of the specimen size limitation for tensile tests is verified.

Views of plate edge deformations are obtained that are not predicted by classical laminated plate theory, and that are currently unavailable in the literature.

The modified element formulation is also used to implement a method whereby laminates of various lamination sequences may be ranked in terms of their energy absorption potential when subjected to quasistatic loading conditions by comparing the total energy absorbed before catastrophic failure. This is accomplished by the used of a damage analysis method that is based upon element integration point failure rather than the usual first ply failure criterion.

Acknowledgements

The author wishes to thank Professor Dokainish, his research supervisor, and the members of the supervisory committee for their support and guidance through the period of this research. Thanks are due to Professor Sivakumaran for his input on plate theory, Professor Sowerby on his suggestions with regards to damage analysis, and Professor Weaver for his suggestions with regards to experimental confirmations using simulated tension tests.

Thanks are also due to Mr. B.Tole and Mr. R.Underhill for the many useful suggestions made during the course of our discussions. It was a pleasure working with such talent. Likewise, the author wishes to acknowledge the contributions of his fellow graduate students, too numerous to mention, whose assistance and feedback were an important factor in the completion of this thesis.

Finally, the author wishes to express his sincere thanks to his family for their continuous support; especially to his mother and wife for their encouragement during the final phase of the research.

Table Of Contents

List Of Tables

List of Figures

Nomenclature

σ = Applied normal stress

τ = Applied shear stress

Γ = Surface energy

θ = Counter clockwise inplane rotation angle from the global reference axis to the material reference axis.

c = Diameter of void

q = Non-dimensional material constant

W = Elastic strain energy

$^{o}\phi$ = Value of representative quantity for virgin material

$^{n}\phi$ = Value of representative quantity for failed material

μ_b = Poisson's ratio of the binder

σ_f = Failure strength of fiber

r_f = Radius of fiber

r_m = Radius of matrix tunnel

u^o = Midplane displacement in x-direction

u_i = Element displacements at node points

v^o = Midplane displacement in y-direction

w^o = Midplane displacement in z-direction

Γ_f = Surface energy of fiber

Γ_m = Surface energy of matrix

D_m = Damage parameter

E_b = Elastic modulus for binder

F_i = Strength tensor of rank two

G_b = Shear modulus for binder

L_l = Lower limit of integration

L_u = Upper limit of integration

M_i = Initial slope

N_i = Shape function associated with node i

R_e = External reactions

R_i = Internal reactions

S_p = Sampling point for Gauss Integration

S_w = Sampling weight for Gauss Integration

U_e = Elastic strain energy
or
External displacements

U_i = Internal displacements

V_b = Volume fraction of binder

V_v = Volume fraction of voids

W_b = Weight fraction of binder

W_c = Weight fraction of composite

W_f = Weight fraction of fiber

W^* = Complementary strain energy

V_f = Volume fraction of fiber

$0j_\epsilon$ = Intercept strains for the j'th load step.

ϵ_{xx} = Normal strain in x-direction

ϵ_{yy} = Normal strain in y-direction

ϵ_{xy} = Shear strain in xy-plane

τ_{xy} = Shear stress in xy-plane

μ_{ij} = Poisson's ratio for strain in the j-direction when stressed in the i-direction.

σ_{xx} = Normal stress in x-direction

σ_{yy} = Normal stress in y-direction

gpr = Number of integration points in r-direction

gps = Number of integration points in s-direction

gpt = Number of integration points in t-direction

n_{00} = Number of 0 degree plies

n_{90} = Number of 90 degree plies

D_{ch} = Material creep constant

E_{ii} = Elastic modulus in the i-direction.

E_{00} = Elastic modulus of 0 degree plies

E_{90} = Elastic modulus of 90 degree plies

F_{ij} = Strength tensor of rank four

G_{ij} = Shear modulus in the ij-plane.

K_{ch} = Material creep constant

L_{db} = Critical debonded length of fiber

N_{ij} = Force per unit crossection

M_{ij} = Moment per unit crossection

Q_{ij} = Component of transformed reduced plate stiffness matrix

S_{iC} = Compressive failure strength in the i-direction

S_{iT} = Tensile failure strength in the i-direction

S_{ij} = Shear failure strength in the i-j plane

U_{db} = Energy for fiber debond formation

U_{po} = Pullout energy

W_{dg} = Energy expended during damage growth

[A] = Plate extensional stiffness matrix

[B] = Plate coupling stiffness matrix
or
Element strain-displacement matrix

[D] = Plate bending stiffness matrix
or
Element stress-strain matrix

[J] = Jacobian transformation matrix.

[K] = Element stiffness matrix

[L] = Linear differential operator

[T] = Rotation matrix

ϵ_{xx° = Midplane normal strain in x-direction

ϵ_{yy° = Midplane normal strain in y-direction

ϵ_{xy° = Midplane shear strain in xy-plane

μ_{f12} = Poisson's ratio of the fiber for strain in the 2-direction due to a stress in the 1-direction

μ_{f23} = Poisson's ration of the fiber for strain in the 3-direction due to a stress in the 2-direction

μ_{f31} = Poisson's ration of the fiber for strain in the 1-direction due to a stress in the 3-direction

σ_{eff} = Effective stress

dVol = Differential volume element

k_{xx}° = Midplane curvature in x direction

k_{yy}° = Midplane curvature in y direction

k_{xy}° = Midplane twist curvature in xy plane

Den_b = Density of binder

Den_f = Density of fiber

D_{mji} = The j'th damage parameter for the i'th load step

$^{j}En_{\varepsilon}$ = Stored elastic strain energy for j'th load step

E°_{ii} = Undamaged elastic modulus in the i-direction

E_{f11} = Elastic modulus in 1-direction for fiber

E_{f22} = Elastic modulus in 2-direction for fiber

E_{f33} = Elastic modulus in 3-direction for fiber

F_{ijk} = Strength tensor of rank six

G°_{ij} = Undamaged shear modulus in the ij-direction

G_{f12} = Shear modulus of fiber in the 1-2 plane

G_{f23} = Shear modulus of fiber in the 2-3 plane

$^{ij}En_s$ = Elastic strain energy lost for the j'th step

$u^{\circ}(x,y)$ = General midplane displacement

$(\delta D_m/\delta t)$ = Time rate of change of damage growth

$(\delta D_m/\delta \epsilon)$ = Strain rate of change of damage growth

$(\delta D_m/\delta N)$ = Stress reversal rate of change of damage growth

$U_{(x,y,z)}$ = Overall plate displacement.

$\delta^n w^{\circ}(x,y)$ = N'th derivative of the thickness displacement.

1.0 Introduction

1.1 Fiber Composites

The traditional approach to the design of engineering structures has been to start with a given material and design stress level, and detail appropriate members to carry the specified loads without exceeding the material allowable strengths. These strengths are usually defined as a certain percentage of the material's tensile ultimate (F_{tu}) or yield strength (F_{ty}). The advent of advanced fiber composites has given the impetus for a major change in the normal design philosophy. Rather than being constrained to designing a structure with a given set of material properties, it is now possible to tailor the required properties into the material itself, thereby rendering the finished product much more efficient in the role for which it is required. This is what may generally be known as Zero-Based design.

The term composite refers to a mixture of two or more materials that are microscopically distinct but together form a single macroscopic entity. Such materials have a long history, and in the past two decades they have found widespread usage in the aerospace industry. In current engineering terms the word has come to refer to materials made of stacked layers of a fibrous reinforcement material

held in place by a rigid binder. Such materials have been extensively utilized in aerospace applications in the form of long fibers embedded in a carrier matrix to make thin plates or shells. Combinations of such materials have several advantages in that they tend to exhibit the best qualities of their constituents as well as other qualities that neither possess. This has resulted in a broad range of investigation of these materials using various techniques.

Long fibers of any given material are inherently much stiffer and stronger than the same material in bulk form. This is mainly due to the high alignment of the crystals in the fiber and the lower defect concentration. Geometrically the fibers are characterized by their high length to diameter ratio and their crystal-sized diameter. Their main disadvantage is the relative lack of compression strength, for which they require some sort of binder. Their main advantage is the ability to fabricate structures with preferential directional properties.

The usage of fiber composites has gone through several stages. The first of these was a demonstration phase during which confidence was built on the reliability and commercial viability of fiber composite parts. The second stage involved the direct replacement of existing non-critical secondary structure. Following this was a

production stage during which parts of a structure were designed using fiber composites from the outset for the purpose of weight savings. The past decade has seen an increased use of fiber composites in the energy absorption field. Kevlar laminates are being used in the energy absorption and protection role for ships as well as army field personnel. Closely related to this is the protection of spacecraft from micrometeorite impact, the integrity of fan blade containment rings for jet engines and the safety of nuclear reactor containment vessels from tornadobourne debris.

Currently the design of fiber composite structures employs some form of lamination theory to construct the material of the structural element required. Laminated fiber composites refer to materials built up of layers of a fiber reinforced matrix. While control of the individual constituents and their relative abundances in the lamina may be used to tailor the lamina orthotropic properties, control of the lamination sequence and fiber orientation may be used to tailor the finished material to the specific design requirements of the structural element being built.

Fiber composite laminates can be manufactured to perform a variety of functions that are not possible when using isotropic materials. The coupling between

extensional and bending deformations allows one to fabricate parts for a variety of applications such as tail rotor blades for helicopters, and forward swept wings for advanced jet aircraft. In the former the centrifugal loading from an increased rotational velocity can be used to apply a twisting moment to the tail rotors, generating a horizontal lifting component that would offset the rotational moment from the main rotor blades. In the latter the bending moment caused by an increase in lift can be used to twist the wing planform in a direction that would prevent catastrophic divergence.

1.2 Methods of Analysis

The usual elasticity approach to solving engineering problems is to assume an unknown stress function over the region of interest, and substitute this into the compatibility equations [1]. Application of the boundary conditions then determines the necessary constants for a correct representation of the solution. Unfortunately this procedure is cumbersome for all but the simplest of problems. It is practically impossible to apply this method to complex geometries.

The most common approach used in the structural analysis of laminated composites involves some variation of Classical Laminated Plate Theory (CLPA). In this case

the laminate displacements are represented through the thickness by a linear function in terms of the midplane displacements and curvatures [2]. Unfortunately this approach is limited to thin plates since the effects of shear deformations is not taken into account.

The utilization of laminated composites is not, however, limited to thin plates. Applications also exist for thick laminates, in which case the classical theory cannot be applied. Many higher order laminated plate theories have been proposed to overcome the difficulties encountered due to the thickness effects [3,4,5], however they are all variations on a given theme. These theories attempt to take care of the zero shear stress requirement at the top and bottom surfaces of the laminate with varying degrees of success. Unfortunately they do not take care of the free edge effects at the longitudinal and lateral extremes of the plates. These effects become of paramount importance in considerations of failure for plates loaded along their edges.

Current design procedures for laminated fiber composites involve a number of independent steps to arrive at a viable design. One must evaluate the lamina properties, perform a laminate analysis, test for failure and decide if any modifications are necessary. Often it is difficult to predict the deflection response from a

knowledge of the stresses within the laminate. It would be advantageous to be able to predict the deflection response of thick laminated fiber composites simply from a knowledge of the lamina orientations, the laminae constituents and the applied loading. The Finite Element Method allows one to integrate the above steps into one easily mastered process.

The underlying concept of the displacement based Finite Element Method is the division of a structure into a series of subregions or elements. The behaviour over each element is described by a set of assumed functions for the displacements. The form of these assumed functions is such that the displacement continuity is satisfied at the element boundaries. The local behaviour is described by the use of an appropriate function valid for the region of interest. The advantages of this method lie in its application to complex geometries. In addition, the method may be applied to 3D analysis with much greater ease than either of the previous two.

The Finite Element Method, is not without its limitations. The plate or shell elements currently available in commercial codes such as ASAS, ANSYS, MARC and the like cannot be used to predict the three dimensional stress fields encountered in problems related to thick plates. Formulations of thick plate and shell

elements found in the literature involve the use of an increased number of variables to overcome some of the limitations inherent in thin plate theory, however they still represent the entire laminate thickness by one element.

1.3 Objectives

To overcome the limitations imposed by the use of plate and shell elements, several solid elements may be used to represent the laminate thickness. The use of this element allows inclusion of all laminate stresses as well as end effects in the analysis of thick laminates. The properties of each ply would be assigned to one element, and a stack of these would represent the plate behaviour in the thickness direction. Unfortunately, this would lead to an excessive computational demand, and some method must be found whereby those degrees of freedom not germane to the problem are eliminated.

Current methods of solution for fiber composite problems require knowledge of the lamina orthotropic properties. These are usually evaluated experimentally using various test methods. Such tests are expensive to perform, and the results are valid only for the particular lamina being tested. However, it is also possible to compute the lamina properties from a knowledge of the

properties of the constituents and their relative abundances in the laminate.

The serviceability design for laminated fiber composites is usually based upon a first ply failure criteria. The laminate is considered to have passed its structural limit at the onset of failure in one of its lamina. This is a conservative approach, and does not take into account the significant residual strength of failed laminates. The problem is further complicated by unequal strengths in the tensile and compressive directions. Often failure of fiber composite laminates is based upon the deflection response rather than failure to carry a given load.

Laminates subjected to overloads exhibit a damaged behaviour that manifests itself in reduced material properties. The extent of this damage may be determined experimentally through ultrasonic C-Scan [6] methods or by measuring the response to a known load. Alternatively, if the vibration characteristics of the damaged laminate can be related to the extent of damage, a vibration test will suffice.

It was the purpose of this study to devise a method whereby the small deflection response of a laminated fiber composite may be computed based upon the known loading

conditions, the laminate constituents, the laminae orientations, their relative abundances and their respective material properties. The damage incurred due to overload was then used in an attempt to predict the energy absorption characteristics of particular laminates in a effort to rank them for an energy absorption role.

In order to accomplish the above, the following objectives had to be met:

1. The capability of representing several plies through the element thickness had to be provided.

2. A lamina analysis capability was found to be essential for the element stiffness routines in order that material properties for the elements could be generated from the basic lamina constituents.

3. Failure of the laminate required the incorporation of a damage progression model in order to realistically predict the response of the laminate to overloads.

4. Ranking of various laminates in terms of energy absorption required a method whereby the energy absorbed due to material failure could be tracked.

1.4 Scope

The scope of this thesis is limited to representation of the laminate deflections using small deflection theory. It does not deal with large strains and large deflections. In addition, dynamic effects such as those related to visco-elasticity and damping are not included in the analysis.

To this end a finite element code was developed that is capable of small deflection 3D analysis of laminated fiber composite structures. The code implements a 2D element for which the number of nodes can be varied from four to nine, and a 3D element for which the number of nodes can be varied from eight to twenty. The code can be easily expanded to handle large deflections and large strains by inclusion of the appropriate subroutines. The addition of an eigen analysis routine will allow vibration studies to be undertaken to determine the effect of material damage upon the vibration characteristics.

2.0 Literature Review

2.1 Laminate Analysis

The most common usage for fiber composites has been in the form of laminated plates. Individual layers of fibers are embedded in an epoxy or polyimide binder material and oriented in various directions to produce the desired anisotropy. The analysis of these kinds of structures has been done using what is known as Classical Laminated Plate Theory, which in turn is based on the Kirchhoff hypothesis for thin plates [7].

The theory embodies a reduction of the three dimensional elastic continuum to a two dimensional non-Euclidean continuum of the middle surface. The behavior of the plate is described by writing the overall plate displacements in terms of a power series expansion of the thickness coordinate. Due to the nature of the problem, a convective set of coordinates may be used which become curvilinear in the deformed state. Though reasonable, this approach leads to complications. Alternatively, a Lagrangian approach may be utilized in which the coordinates are embedded in the plate so that the middle surface is always at $z=0$ and the upper & lower surfaces are always at $z=+\frac{1}{2}h$ and $z=-\frac{1}{2}h$ respectively.

The general form of the displacement field is taken from Basset [8], where the displacement terms are directly specified in terms of the midplane displacements and their respective derivatives.

$$U_{(x,y,z)} = u^{\circ}(x,y) + z\,\delta w^{\circ}(x,y) + \ldots + z^{n}\,\delta^{n} w^{\circ}(x,y) \qquad (2.1.01)$$

where

$U_{(x,y,z)}$ is the overall plate displacement.

$u^{\circ}(x,y)$ is the midplane displacement.

$\delta^{n} w^{\circ}(x,y)$ is the n'th derivative of the thickness displacement.

z is the thickness coordinate.

Basset's paper can be considered to be a landmark in plate theory, since the displacement assumptions he put forward form the basis of nearly all plate theories used to model the behaviour of laminated fiber composites.

The Kirchhoff theory of plates utilizes a set of assumptions that can only be satisfied in the case of small deflections. The first of these assumptions is the Bernoulli hypothesis of a line originally straight and normal to the middle surface remaining so under deformation, implying zero transverse shearing strains. The second assumption requires that normals to the midplane have constant length, implying zero through thickness strain.

Under these assumptions the inplane plate displacements may be described by a truncation of the above series expansion to the first power in z. In the case of a flat plate the resulting inplane strains are then given by

$$\epsilon_{xx} = (\delta u^{\circ}/\delta x) - z\ (\delta^2 w^{\circ}/\delta x^2)$$
$$\epsilon_{yy} = (\delta v^{\circ}/\delta y) - z\ (\delta^2 w^{\circ}/\delta y^2) \qquad (2.1.02)$$
$$\epsilon_{xy} = (\delta u^{\circ}/\delta y) + (\delta v^{\circ}/\delta x) - 2\ z\ (\delta^2 w^{\circ}/\delta x \delta y)$$

which are usually written as

$$\epsilon_{xx} = \epsilon_{xx}^{\circ} + z\, k_{xx}^{\circ}$$
$$\epsilon_{yy} = \epsilon_{yy}^{\circ} + z\, k_{yy}^{\circ} \qquad (2.1.03)$$
$$\epsilon_{xy} = \epsilon_{xy}^{\circ} + z\, k_{xy}^{\circ}$$

The last term of the last equation represents the twist curvature of the midplane. It is evident that the variation of strain through the laminate thickness is linear. For the case of curved shells it is necessary to supplement the ϵ_{ii} terms with (w/r_{ii}) where r_{ii} is the radius of curvature.

Substitution of the strain variation into these equations allows one to express the stresses in the various plies in terms of the laminate midplane strains and curvatures.

The statically equivalent resultant forces and moments acting on a laminate may be obtained by integration of the stresses through the laminate thickness. These are given by

$$N_{ij} = \int_{-(t/2)}^{+(t/2)} \sigma_{ij}\, dz \qquad M_{ij} = \int_{-(t/2)}^{+(t/2)} \sigma_{ij}\, z\, dz \qquad (2.1.04)$$

where

N_{ij} = Force per unit crossection

M_{ij} = Moment per unit crossection

Due to the small thickness of the lamina, the stresses are assumed to be constant within each laminae. This allows the above integrals to be broken at the element boundaries and summed over the total laminate thickness. Substitution of the strain variation into these equations allows one to express the stresses in the various plies in terms of the laminate midplane strains and curvatures. For an orthotropic lamina the stress-strain relationship is given by

$$\begin{bmatrix} \sigma_{xx} \\ \sigma_{yy} \\ \tau_{xy} \end{bmatrix} = \begin{bmatrix} Q_{11} & Q_{12} & Q_{14} \\ Q_{21} & Q_{22} & Q_{24} \\ Q_{41} & Q_{42} & Q_{44} \end{bmatrix} \begin{bmatrix} \epsilon_{xx} \\ \epsilon_{yy} \\ \epsilon_{xy} \end{bmatrix} \qquad (2.1.05)$$

where [Q] is the transformed reduced stiffness matrix for the lamina [9]. Since [Q] may be different for each ply, the stress variation through the laminate thickness may not be continous.

Combining this with the power series representation of the displacements and realizing that the midplane values are not a function of the thickness coordinate then gives

$$N_{ij} = \sum_{n=1}^{m} [Q] \left[\epsilon_{ij}^{\circ} \int_{z(n)}^{z(n-1)} dz + k_{ij}^{\circ} \int_{z(n)}^{z(n-1)} z\, dz \right]$$

$$M_{ij} = \sum_{n=1}^{m} [Q] \left[\epsilon_{ij}^{\circ} \int_{z(n)}^{z(n-1)} z\, dz + k_{ij}^{\circ} \int_{z(n)}^{z(n-1)} z^2\, dz \right] \qquad (2.1.06)$$

which is usually written as

$$\begin{bmatrix} N_{ij} \\ M_{ij} \end{bmatrix} = \begin{bmatrix} A_{3x3} & B_{3x3} \\ C_{3x3} & D_{3x3} \end{bmatrix} \begin{bmatrix} \epsilon_{ij} \\ k_{ij} \end{bmatrix} \qquad (2.1.07)$$

where

[A] = Plate extensional stiffness matrix

[B] = Plate coupling stiffness matrix = [C]

[D] = Plate bending stiffness matrix

The presence of the B_{ij} terms in the stiffness matrix implies a coupling between the bending and extensional deformation. This means that an extensional force may result in bending and twisting of the laminate as well as an extension in the direction of the applied force. A similar statement may be made for the case of an applied moment. The coupling terms arise from geometric anisotropy due to the lamination sequence and lamina orientations, and have been investigated by Reissner & Stavsky [10].

The classical theory described above has been used extensively in the analysis of laminated fiber composite plates. However the theory considers only stresses in the plane of the laminate. Since the interlaminar stresses are not included in the analysis, the theory is incapable of providing any insight into some of the failure mechanisms associated with laminates. It is readily verified that the theory implies non-zero values of τ_{xy} at the free edges of the laminate. Though this is physically impossible, the Kirchhoff assumptions yield acceptable results from an engineering standpoint when the theory is applied to thin plates with small deflections.

Unfortunately the classical approach becomes invalid for applications involving stress distributions which are of a three dimensional nature. The mismatch of the

properties through the thickness leads to a violation of the Bernoulli hypothesis of plane sections remaining plane, and the theory becomes inadequate to describe the structural response. Also, the usual form of the theory uses statically equivalent stress and moment resultants which must be computed from the applied loads. These are generally valid only far from the point of load application.

The three dimensional equations of elasticity involve six components of stress which are related to six components of strain through Hooke's law. Furthermore the assumption of large deflections requires the use of Green's strain tensor to second order. An analytical solution using an asymptotic expansion in the powers of the plate thickness has been given by Fox [11]. The solution is obtained by considering the interior and boundary regions separately in terms of the full three-dimensional equations of elasticity. However the solution is valid only for small values of the plate thickness, and breaks down when applied to laminated fiber composites.

2.2 Higher Order Plate Theories

Higher order plate theories have been put forward by a number of investigators that overcome some of the above limitations. All involve displacement assumptions that

are truncated at increasingly higher powers of the thickness coordinate. Unfortunately these introduce other problems. For instance, in the case of a second order truncation of the displacements, transverse shearing stresses arise that do not satisfy the zero shear stress boundary conditions at the top and bottom surfaces of the plate.

The earliest consistent treatment of the effects of shear deformation on the bending of elastic plates is given by Reissner [12] using first order displacement approximations of the form

$$\begin{aligned} u &= u^\circ + z\,\delta w^\circ \\ v &= v^\circ + z\,\delta w^\circ \\ w &= w^\circ \end{aligned} \qquad (2.2.01)$$

where u°, v° and w° are functions of x & y, and the symbol δ stands for differentiation with respect to the appropriate coordinate.

The equations of equilibrium and the stress-strain relations were determined in the form of the stress resultants by use of Castigliano's theorem of least work. The solution is obtained in terms of two plane harmonic functions. The theory is applied to the problem of torsion of a rectangular plate and the plain bending and pure twisting of an infinite plate with a circular hole.

The results are reported to be accurate from a practical point of view.

Mindlin [13] later obtained the governing equations by a direct method using the same level of approximation but without using the corresponding stress distribution assumptions However the formulation requires a shear correction factor that must be determined by comparison to an exact elasticity solution, and so is not able to stand on its own.

Whitney & Leissa [14] have used the basic assumptions of thin plate theory, including inertia and thermal effects, to formulate the governing equations of a laminated anisotropic plate by integration of the nonlinear equations of elasticity. Closed form solutions to the linearized equations revealed that the coupling phenomenon increases transverse deflections and decreases buckling loads and fundamental vibration frequencies.

The inclusion of the effects of transverse shear deformation in a structural laminated orthotropic shell theory has been investigated by Dong & Tso [15]. Their derivation leads to Mindlin type correction factors in the transverse shear resultant-strain relation. As with the Mindlin plate theory, this formulation is also not able to stand on its own since the values of the correction

factors are based upon a match for the lowest cutoff frequency with that obtained by three-dimensional elasticity. Also although the theory reliably predicts displacements and stress & couple resultants, detailed stress and strain states cannot be described with the same degree of confidence.

Shear deformation theories based on the above set of assumptions are generally known as First Order Plate Theories (FOPT). In these kinds of theories the transverse normal component of the deformation is assumed to be independent of the thickness coordinate. This poses inherent limitations in problems of induced contact with a smooth surface. Essenberg [16] has investigated a theory based upon

$$\begin{aligned} u &= u^\circ + z\ \delta w^\circ \\ v &= v^\circ + z\ \delta w^\circ \\ w &= w^\circ + z\ \delta w^\circ + z\ \delta^2 w^\circ \end{aligned} \tag{2.2.02}$$

in an attempt to alleviate these limitations by deriving the corresponding one-dimensional plate theory.

Whitney & Sun [17] have also used these displacement assumptions to develop a refined theory for laminated anisotropic cylindrical shells. The effects of both shear deformation and transverse normal strain were shown to be significant factors in the accurate analysis of shells

with a small thickness-to-radius ratio. Reasonably good agreement was observed with exact elasticity solutions for static deformations.

Nelson & Lorch [18] have used full second order displacement approximations to model the highly dispersive character of axial waves in laminated orthotropic plates. This theory extends CLPT to include transverse normal, transverse shear and quadratic terms in the kinematic assumptions. The displacement assumptions are of the form

$$\begin{aligned} u &= u^\circ + z\,\delta w^\circ + z\,\delta^2 w^\circ \\ v &= v^\circ + z\,\delta w^\circ + z\,\delta^2 w^\circ \\ w &= w^\circ + z\,\delta w^\circ + z\,\delta^2 w^\circ \end{aligned} \qquad (2.2.03)$$

Composite correction factors are used to bring this theory into correspondence with exact elasticity solutions for the response of an infinite plate to plane harmonic waves. The theory accurately models the dynamic behavior of plates over the lower portion of the frequency spectrum for wavelengths greater than the plate thickness. Unfortunately there is an inconsistency in their use of the Mindlin shear correction factor since nonuniform shear stresses are implied by the assumed form of the displacements.

Hildebrand et al [19] have also examined a theory based upon a full second order expansion of the midplane

displacements, and have concluded that the inclusion of the quadratic terms in the inplane displacements does not provide a significant advantage over the lower order theories. Naghdi [20] has used these to derive a general theory of shells.

Reddy [21] has presented a nonlinear theory of plates with transverse shear deformation that accounts for the von Kàrmàn strains using

$$\begin{aligned} u &= u^\circ + z\,\delta w^\circ + z^2\,\delta^2 w^\circ + z^3\,\delta^3 w^\circ \\ v &= v^\circ + z\,\delta w^\circ + z^2\,\delta^2 w^\circ + z^3\,\delta^3 w^\circ \\ w &= w^\circ \end{aligned} \qquad (2.2.04)$$

Hamilton's principle is used to derive the equations of motion. This theory models the parabolic distributions of the transverse shear strains through the thickness of the plate and, in comparison with CLPT and FOPT, provides a better prediction of deflections, stresses and frequencies.

Riessner [22] has also presented a theory using higher order displacement approximations representing the lowest order correction to the classical theory for out-of-plane deformation effects. The inplane displacements are represented by incomplete cubics in z, and the out of plane displacement by an incomplete quadratic in z. Thus

$$u = z\ \delta w^{\circ} + z^3\ \delta^3 w^{\circ}$$
$$v = z\ \delta w^{\circ} + z^3\ \delta^3 w^{\circ} \qquad (2.2.05)$$
$$w = w^{\circ} \quad + z^2\ \delta^2 w^{\circ}$$

This theory gives accurate results when compared to the elasticity solution for the bending of a plate with a circular hole. Unfortunately all inplane deformation effects are not included due to the incomplete representation of the displacements.

These inplane deformation modes have been included by Lo et al [23] by virtue of a full cubic representation for the midplane displacements for u and v. The representation for w is truncated at the second power, which is consistent in that the transverse shear strains due to inplane displacements are of the same order in z as those determined by the transverse displacement. The displacement assumptions for this case are

$$u = u^{\circ} + z\ \delta w^{\circ} + z^2\ \delta^2 w^{\circ} + z^3\ \delta^3 w^{\circ}$$
$$v = v^{\circ} + z\ \delta w^{\circ} + z^2\ \delta^2 w^{\circ} + z^3\ \delta^3 w^{\circ} \qquad (2.2.06)$$
$$w = w^{\circ} + z\ \delta w^{\circ} + z^2\ \delta^2 w^{\circ}$$

The theory is applied to angle-ply and cross-ply laminates loaded by a sinusoidal pressure distribution on the top surface, for which displacements and flexural stresses are numerically computed. Exceptionally good agreement to elasticity solutions is obtained for the first case, and

close agreement for the second case. Unfortunately material discontinuities at the interfaces of the layers mitigate against good predictions of the flexural stresses at these locations.

It should be noted that the term "higher-order" as used in the above discussion refers not to the order of the differential equations representing the plate behavior, but to the level of truncation of the terms in the power series representation of the plate displacements. Although the use of these higher order theories has merits, their computational demands increase with each increasing power of the thickness coordinate. Also, although these higher order theories allow somewhat better predictions of thick plate stresses in comparison to CLPA, they are still valid only far from the plate edges. They are unsuitable for the prediction of the free edge effects responsible for delamination modes of failure.

2.3 Finite Elements

The above theories have usually been applied to analytical procedures for the purpose of solving specific problems involving homogeneous orthotropic plates. The technique of finite element analysis has been introduced by several investigators to solve problems involving

laminated fiber composites. Typically the higher-order theories mentioned above have been used to develop various forms of plate elements.

The method itself is based upon a representation of the overall behavior of a structure by it's discretization into a series of contiguous subregions, also known as elements. The behavior within each element is described in terms of a set of assumed displacement functions. The form of these assumed functions is such that displacement continuity is satisfied at the element boundaries.

The plate elements are formulated using the principle of virtual work. The kinematic relations are obtained from the general form of Green's strain tensor with the von Kàrmàn small deflection assumptions invoked [24]. These assumptions imply that the derivatives of the u and v displacements with respect to the x, y and z directions are very much smaller than the plate thickness. The plate stress distribution is then obtained from the strain energy expression using Castigilano's theorem.

Pica et al [25] have applied this technique using a Mindlin type of formulation to the investigation of geometrically nonlinear behavior of homogeneous isotropic plates. Numerical comparisons are given for square, skew,

circular and elliptic plates using Linear, Serendipity, Lagrange and Heterosis elements. Unfortunately, no discernable pattern of behavior emerged from this investigation.

Reddy [26] has used the assumptions of equation 2.2.01 and a combination of the Timoshenko and von Kàrmàn theories to formulate a geometrically nonlinear shear deformable laminated plate element. Transverse shear, rotary inertia and large deflections are accounted for in the development of the equations of motion. The theory is applied to study the dynamic response of simply supported and clamped plates with both isotropic and orthotropic material properties. Reference solutions are provided for layered composite plates, unfortunately the effects of material damping are not included in the analysis

Reddy and Chao [27] have used the assumptions of equation 2.2.01 and the thin plate Kirchhoff approach to study the small deflection elastic behavior of single layer and two-layer cross-ply plates loaded in the transverse direction. These materials are known to have a slightly different response in the tensile and compressive directions. This bimodular response of the materials was included in the analysis, which was found to significantly affect the results.

Unfortunately these elements suffer from a limitation in the description of the through thickness stress, in that plane stress assumptions are used in their derivation. Also the use of plate elements requires the use of a fully space averaged representation of the laminate properties through the thickness. It is not possible to represent the laminate by more than one element through the thickness. Consequently these elements cannot be used in the analysis of thick laminates.

As mentioned above, non-zero values of τ_{xy} are present at the laminate edges. These are usually neglected in engineering problems by appealing to Saint-Venant's principle. However in the case of fiber composites the characteristic decay length over which end effects are significant is several times longer than the corresponding length for isotropic materials [28,29]. Numerical results have shown that a complex three dimensional stress state is present in the region of the free edge [30]. Since delamination is an important failure mechanism for laminated fiber composites, accurate determination the state of stress at the free edges of the plate is essential.

The application of the Finite Element Method to the edge stress problem has been investigated by

Whitcomb et al [31]. They examined the normal stress distributions along the interface between the +45° and -45° plies of a $(\pm 45)_s$ graphite/epoxy composite using an 8-node plane isoparametric element. Layered fiber reinforced laminates have been examined by Lee [32] using an 8-node isoparametric solid element. A multilayer rectangular specimen subjected to a biaxial load was modelled with this element, and the damage progression monitored as a function of the applied load. Other investigators have also used various plane and solid elements in their investigations of laminated fiber composites [33,34]. However in all cases the through thickness modelling of the laminates has been done with constant properties throughout any given element volume.

2.4 Lamina Micromechanics

Since a fiber composite is made up of two distinct materials, the material behavior will be a function of the properties of the lamina constituents and their relative abundances. In the case of laminates, the behavior will also be affected by the lamination sequence. It is impractical to experimentally determine the elastic constants for all of the permutations and combinations that may be used in structural design.

The study of the detailed interaction of the lamina constituents for the purposes of investigating the behavior of a heterogeneous material is known as micromechanics. The prediction of lamina properties is an essential adjunct to the design process, and several authors [35,36,37] have obtained bounds on the elastic constants through the use of energy theorems from classical elasticity. The minimum potential energy theorem is used to yield the upper bound, whereas the lower bound is obtained from the minimum complementary energy theorem. However it is much more advantageous to mathematically derive the lamina properties on the basis of the constituent materials.

These methods utilize a basic set of simplifying assumptions consistent with the physical situation and based upon the principles of solid mechanics. The first of these assumptions is that the lamina can be considered to be macroscopically homogeneous, linearly elastic and generally orthotropic. Additionally, the fibers and binder are assumed to be homogeneous, linearly elastic and free of voids. The fibers are assumed to be regularly spaced and perfectly aligned, with complete bonding at the fiber matrix interface. Finally, the lamina is assumed to be in the stress free state.

The differences in the various methods arise from the degree to which each of these basic assumptions is relaxed. The theories range from a disjointed constituent response to sophisticated statistical methods. Unfortunately, not all of the assumptions are stated in the derivation of these theories. Further, many of the above assumptions tend to be unrealistic simplifications of the physical state of the materials being modelled.

Early investigators [38,39] made the assumption that the response in the fiber direction was governed solely by the reinforcement, with the binder governing the response in the transverse direction. This Netting analysis approach provides acceptable values for the longitudinal stiffness, but gives low values for the transverse stiffness and shear modulus. Its major use has been in the design and analysis of a large class of filament wound pressure vessels which, by their very nature, eliminate the major drawbacks of this method.

The basic mechanics of materials approach embodies all of the above assumptions. In addition, the fiber and matrix strains are taken to be equal in a direction parallel to the longitudinal fiber axis, and the fiber and matrix stresses are taken as equal in a direction perpendicular to the fiber axis. These assumptions have been used to evaluate preliminary estimates of various

elastic constants by Ekvall [40]. A square array with the ply subjected to a plane stress state provided good agreement with experimental data for E_1, but low values for E_3, G_{13} and μ_{13}. In a later work [41] the concept of a restrained matrix was introduced which gave better results for E_3.

Equations predicting the tensile moduli based upon a hexagonal array have been derived by Shaffer [42]. Two equations are developed for the transverse modulus, both of which predict low values when compared with experiment. Equations based upon a square array with transverse isotropy normal to the fibers have been derived by Abolin'sh [43]. In this case the Poisson effect normal to the fibers has been neglected. It was found that the value of E_3 fell close to the lower bound, whereas the value of μ_{23} fell between the upper and lower bounds.

The inclusion of voids in the binder was investigated by Greszczuk [44]. The equations derived in this case gave theoretical results that were in good agreement with experimental data. These were later extended [45] to predict values for the coefficients of thermal expansion in the longitudinal and transverse directions.

Equations predicting the thermal conductivities of composites with inclusions of various shapes have been

derived by Foster et al [46]. Good correlations were obtained between theory and experiment. Springer & Tsai [47] have provided similar equations based upon square and rectangular array models. Again, the values predicted were in reasonable agreement with experimental data.

Rigorous approaches to predicting the lamina elastic constants are generally referred to as self-consistent methods, of which there are two basic variations. The first variation involves an extension by Hill [48] of Hershey's [49] approach for aggregates of crystals. The model is that of a single fiber in an unbounded matrix. The assemblage is mathematically subjected to a uniform loading at infinity parallel to the fiber axis, and the strain field computed. This is then used to extract the elastic constants. The procedure has proved to be reliable for low fiber volume fractions, but unreliable for high values of this parameter.

The second variation of the self-consistent approach involves a modification of the procedure used to predict the viscosity of a Newtonian fluid containing a collection of equal elastic spheres [50]. The model is composed of three concentric cylinders, with the outer cylinder being unbounded. The inner cylinder is given the properties of the fiber, and the middle cylinder that of the binder.

The outer cylinder is given the properties of the composite. As before, a uniform loading is applied to the model, and the constants extracted using the resulting strain field. Whitney & Riley [51] approached the problem in a similar manner with a model consisting of a single filament surrounded by a cylinder of finite radius representing the binder. An energy balance was used to derive expressions for E_1, E_3 and μ_{13}. Whitney [52] later extended this to take into account the effect of filament twist on E_1.

The elasticity approach depends to a large extent upon the geometry of the laminae as well as the fiber and matrix characteristics. For instance, the fibers may be solid or hollow with a uniform or nonuniform elliptical or rectangular crossection. In addition the material comprising the fibers may not necessarily be isotropic. The entire laminate is assumed to be made up of a single repeating element upon which the analysis is based. The repeating element may be a single encased fiber or an array of fibers depending upon the regularity of construction. In general, the placement of the fibers in a lamina deviates from an orderly pattern to some extent. Their alignment is also not always perfect. The resulting elastic fields are averaged to obtain the expression for the desired elastic constants.

This approach has been used by Hermann & Pister [53] to obtain the elastic and thermoelastic constants for a square array of fibers by reducing the problem to that of a square boundary containing a circular inclusion. The solution of the reduced problem yielded values of the five elastic constants, two thermal expansion coefficients and two thermal heat conductivities. Unfortunately, no details of the solution were provided other than that the boundary conditions were satisfied exactly at the interface and by a point matching procedure [54] on the sides.

Adams & Dorner [55,56] utilized a finite difference scheme to solve this problem using a fundamental region that was rectangular in shape. A triangular repeating element representing a hexagonal array of fibers was used by Chen & Cheng [57] to obtain a series solution in polar coordinates. The boundary conditions were satisfied at the interface and at the sides by a least squares technique. Bloom & Wilson [58] solved the same problem using an infinite series selected such that the boundary conditions at the interface were satisfied identically.

The underlying assumptions behind the statistical approach is that the lamina thermoelastic properties can vary randomly with position, so the governing equations are partial differential equations with variable

coefficients. The variation is a combination of some mean value plus a fluctuating term determined by the field equations. The expressions for the desired constants are obtained by taking a statistical average, requiring the inclusion of all of the statistical moments. Unfortunately the sophisticated nature of the expressions obtained from this method, can lead to unmanageable computational difficulties [59]. The procedure can be simplified by neglecting moments of order higher than the second. However, unless care is taken in the application of these approximate expressions, they can deviate considerably from the true values.

In all but the mechanics of materials approach the solution of the laminae engineering constants are given by a fairly complicated set of relationships between the constituent properties. Furthermore, variations in manufacturing will always yield variations in the laminate geometry. This makes precise prediction of the required constants a difficult task. Even so, practically all theories predict some thermoelastic constants with reasonable accuracy when compared to experimental data.

Over the last 25 years the mechanics of materials approach has been used to derive equations for many different properties. Though of simple form, they are scattered throughout the literature. A unified set of

simple working equations has been provided by Chamis [60] with a view to providing experimental guidelines for maximum benefit and minimum testing. These equations provide a detailed quantitative insight into the strength and stiffness behavior, and are useful in parametric studies for the evaluation of various constituent parameters.

The ply properties defined by these equations are given with respect to the material axis orientation in terms of the properties of the constituents and their respective volume fractions. The mechanical properties are computed from

$$E_{11} = V_f E_{f11} + V_b E_b \qquad E_{22} = \frac{E_b}{[\ 1 - V_f^{\frac{1}{2}}\ (1-E_b/E_{f22})\ ]}$$

$$\mu_{12} = V_f \mu_{f12} + V_b \mu_b \qquad G_{12} = \frac{G_b}{[\ 1 - V_f^{\frac{1}{2}}\ (1-G_b/G_{f12})\ ]} \qquad (2.4.01)$$

$$\mu_{23} = \frac{E_{22}}{2\ G_{23}} - 1 \qquad G_{23} = \frac{G_b}{[\ 1 - V_f^{\frac{1}{2}}\ (1-G_b/G_{f23})\ ]}$$

where

V_b = Volume fraction of binder

V_f = Volume fraction of fiber

E_b = Elastic modulus of binder

E_{f11} = Elastic modulus of fiber in the 1-direction

E_{f22} = Elastic modulus of fiber in the 2-direction

G_b = Shear modulus of binder

G_{f12} = Shear modulus of fiber in the 1-2 plane

G_{f23} = Shear modulus of fiber in the 2-3 plane

μ_b = Poisson's ratio of the binder for strain in the 2-direction due to a stress in the 1-direction

μ_{f12} = Poisson's ratio of the fiber for strain in the 2-direction due to a stress in the 1-direction

The measurement of the constituent volume fractions is a time consuming task. It is usually quicker to measure the weight fraction of fiber by desolving the binder in a solvent according to method D3176 of the ASTM standards. The volume fractions can then be obtained from

$$W_b = W_c - W_f$$

$$V_b = \frac{[\ 1 - V_v\ ]}{[\ 1 + (Den_b/Den_f)((1/W_b)-1)\ ]}$$

$$V_f = \frac{[\ 1 - V_v\ ]}{[\ 1 + (Den_f/Den_b)((1/W_f)-1)\ ]} \qquad (2.4.02)$$

where

V_v = Volume fraction of voids

W_b = Weight fraction of binder

W_c = Weight fraction of composite

W_f = Weight fraction of fiber

Den_b = Density of binder

Den_f = Density of fiber

The volume fraction of voids depends to a large extent upon the temperature, the pressure and the cure cycle used in making the laminate. However for important applications these variables are tightly controlled. Typical values of this variable are in the range of 1-2%.

2.5 Lamina Failure Criteria

Structural analysis utilizes some form of failure criterion to determine the failure loads of a particular structure. These failure criteria are based upon maximum allowable strains or stresses for the material of which the structure is composed. The allowables represent the limit of elasticity under any possible combination of stress.

The determination of the onset of nonlinearity and degradation of material properties is much easier to determine for a unidirectional test specimen than it is for some general laminate. This is due to the nonlinear

behavior of general laminate configurations from the onset of loading. It would be uneconomical to experimentally establish strength allowables for all possible orientations of laminates that may be utilized. It is much simpler to establish strength allowables for each lamina at one orientation angle based upon its constituents, their respective weight fractions and the void volume fraction. The strains obtained from an analysis can then be transformed to the lamina axes and used to evaluate the resulting lamina stresses in the principal material directions.

The material properties for the laminae constituents are usually determined from tests in which the specimens are subjected to a uniaxial state of stress. This necessitates a logical method of approach to the application of uniaxial strengths to multiaxial loading conditions. There are a number of failure criteria available in the literature that may be used to predict ply failure in a fiber composite laminate. In the case of orthotropic materials subjected to a biaxial stress state three stress components will appear in the yield criterion and the resulting yield surface is a three dimensional figure. For the case of a triaxial stress state, up to six stress components will appear in the yield criterion.

The yield surface in this case is a surface in six dimensions.

In the Rankine theory the maximum stresses in the lamina principal directions are limited to values that are less than their respective failure strengths. Thus

$$\begin{aligned} S_{iC} < \sigma_{ii} < S_{iT} \qquad & \text{for } i \equiv \{1,2,3\} \\ |\sigma_{ij}| < S_{ij} \qquad & \text{for } ij \equiv \{12,23,31\} \end{aligned} \tag{2.5.01}$$

where

S_{iC} = Compressive failure strength in the i-direction

S_{iT} = Tensile failure strength in the i-direction

S_{ij} = Shear failure strength in the i-j plane

The assumption is made that if any one of the inequalities above is not satisfied the material has failed by the mechanism associated with that inequality. This is in effect a collection of six subcriteria since there is no interaction between the various modes of failure. The result is a set of cusps in the strength variation as a function of the orientation angle. These cusps are not borne out by experimental data.

The Tsai-Hill failure theory [61] is a modification of Hill's failure criterion [62] for anisotropic materials. The general form of Hill's criterion represents a hex-dimensional surface in stress space. This anisotropic yield criterion may be used as an

anisotropic strength criterion since both define limits on linear elastic behavior. Any point falling within the boundary of this surface represents an admissible state of stress.

For the case of fiber composites a state of simple anisotropy exists in which there are three mutually perpendicular planes of symmetry at every point. The principal axis of anisotropy lie on the intersections of these planes. In reference to these planes, Hill's criterion has the form

$$F\,(\sigma_{11}-\sigma_{22})^2 + G\,(\sigma_{22}-\sigma_{33})^2 + H\,(\sigma_{33}-\sigma_{11})^2 + 2\,(\,L\,\tau_{12}^2 + M\,\tau_{23}^2 + N\,\tau_{31}^2\,) = 1 \qquad (2.5.02)$$

where

$$F = (1/S_1)^2 + (1/S_2)^2 - (1/S_3)^2 \quad L = (1/2)\,(1/S_{12})^2$$
$$G = (1/S_2)^2 + (1/S_3)^2 - (1/S_1)^2 \quad M = (1/2)\,(1/S_{23})^2$$
$$H = (1/S_3)^2 + (1/S_1)^2 - (1/S_2)^2 \quad N = (1/2)\,(1/S_{31})^2$$

The constants F, G, H, L, M and N are parameters characterizing the anisotropy of the material.

This is very similar to the criterion first proposed by Huber in 1904 and later by von Mises & Hencky [63], of which Hill's theory is an extension. The former is obtained by equating the strain energy per unit volume due to dilatational stresses to the maximum distortion energy in simple tension. For orthotropic materials, the effects

of distortion and dilatation cannot be separated, therefore the above equation is not related to the energy of distortion. The theory has been used to analyze the strength characteristics of composite materials [64] with the assumptions that the yield strength and ultimate strength are identical. Primarily, the Tsai-Hill failure theory possesses several advantages over the Rankine theory. The variation of strength is a continuous function of the ply orientation angle. In particular, the theory models the interaction between the various principal failure strengths.

Unfortunately, as with the Rankine theory, the Tsai-Hill theory still suffers from inadequacies in the description of experimental data. In particular, the theory predicts the same failure stress for tension as for compression. This makes it necessary to use two separate yield conditions in order to realistically characterize the tensile and compressive strengths. Hoffman [65] has shown that if odd functions of σ_{11}, σ_{22} and σ_{33} are included, it is possible to use a single yield criterion. The resulting modification using linear terms gives

$$\begin{aligned} H_1 (\sigma_{22}-\sigma_{33})^2 + H_2 (\sigma_{33}-\sigma_{11})^2 + H_3 (\sigma_{11}-\sigma_{22})^2 \\ + H_4 \sigma_{11}^2 + H_5 \sigma_{22}^2 + H_6 \sigma_{22}^2 \\ + H_7 \tau_{12}^2 + H_8 \tau_{23}^2 + H_9 \tau_{31}^2 = 1 \end{aligned} \qquad (2.5.03)$$

where

$$H_1 = (1/S_{2C}\ S_{2T}) + (1/S_{3C}\ S_{3T}) - (1/S_{1C}\ S_{1T})$$

$$H_2 = (1/S_{3C}\ S_{3T}) + (1/S_{1C}\ S_{1T}) - (1/S_{2C}\ S_{2T})$$

$$H_3 = (1/S_{1C}\ S_{1T}) + (1/S_{2C}\ S_{2T}) - (1/S_{3C}\ S_{3T})$$

$$H_4 = (1/S_{1T}) - (1/S_{1C}) \qquad H_7 = (1/S_{12})^2$$

$$H_5 = (1/S_{2T}) - (1/S_{2C}) \qquad H_8 = (1/S_{23})^2$$

$$H_6 = (1/S_{3T}) - (1/S_{3C}) \qquad H_9 = (1/S_{31})^2$$

The predictions of this theory agree reasonably well with experimental results. Inspite of this, it must be pointed out that this is only a convenient empirical relation between experimental data. The physical significance of the modifications are not yet fully understood.

The correlation between theory and experiment can be improved by increasing the number of terms in the prediction equation. The use of strength tensors has been suggested by Gol'denblat & Kopnov [66]. They used

$$(F_i\ \sigma_i)^{\alpha} + (F_{ij}\ \sigma_i\sigma_j)^{\beta} + (F_{ijk}\ \sigma_i\sigma_j\sigma_k)^{\Gamma} = 1 \qquad (2.5.04)$$

where

F_i = Strength tensor of rank two

F_{ij} = Strength tensor of rank four

F_{ijk} = Strength tensor of rank six

and investigated the special case of $\alpha=1$, $\beta=\frac{1}{2}$ and $\Gamma=-\infty$. However the use of a sixth rank tensor results in the number of components in the criteria running into the

hundreds. Furthermore, the criteria is not practical since the failure surface is open ended. To overcome this difficulty, Tsai & Wu [67] have postulated a failure surface in stress space defined by 6 linear and 21 quadratic terms. The surface is given by

$$F_i \sigma_i + F_{ij} \sigma_i \sigma_j = 1 \qquad (2.5.05)$$

The linear terms represent the tensile and compressive failure strengths, and may be obtained through the use of a simple tension test. The quadratic terms represent the interaction between the normal stresses, and may be obtained from the use of a biaxial tension test.

The general character of a tensor failure theory lends itself to specific advantages when compared to the theories mentioned above. Tensor theories are invariant under rotation or redefinition of coordinates. The symmetry properties of these theories are similar to those of the laminate stiffness and compliance matrices, and they transform according to known tensor transformation laws. Thus employment of these theories is unambiguous.

The best failure criteria to use depends to a large extent upon the material it is applied to and the application. For instance, the Tsai-Hill failure criterion seems to be the most accurate for E-Glass/Epoxy composites. The biaxial interaction term has been

measured by Pipes & Cole [68] in various off-axis tests with a Boron/Epoxy composite. Although determination of this term was not precise, there was nevertheless excellent agreement between the Tsai-Wu tensor theory and experimental data. In addition, inelastic behavior of the lamina invalidates the prediction of the stress field used to evaluate the above failure criteria. In such cases criteria based upon strains rather than stresses may be utilized [69]. Also, design allowables may be expressed as limits on strains or stresses, so a single criteria is not always possible. However if the analysis is limited to elastic behavior at the lamina level, non-linear behavior at the laminate level is still a possibility. Therefore the systematic application of the criteria discussed above should suffice to describe the overall structural behavior.

2.6 Damage Mechanics

The general practice in laminate analysis is to use what is known as a first ply failure criterion [70]. The stresses in each ply of a laminate are computed from the strains, and a determination made as to whether or not the ply failure strengths have been exceeded. Lamina failure is categorized in terms of through thickness cracks that would cause failure if the material were not an integral

part of the laminate. If failure of the lamina has occurred, the material contribution of that ply to the remainder of the laminate is eliminated, and the strains recomputed from the modified laminate properties.

The problem with this approach from an engineering point of view is that it is overly conservative. Single laminae do not fail catastrophically after the onset of local damage since the load can be transferred over the fiber breaks through the binder material. Furthermore for a general structure in which the lamina stresses are a function of the position, the first ply failure criterion would lead to elimination of the contribution of areas of the laminate that are loaded to below the failure strength of the material. A more realistic approach is to model the damage caused by overloading, and to modify the material properties only in the region affected by the overload.

The methodology behind damage mechanics involves the introduction of new damage variables that take into account the degradation processes occurring in the material. These processes are generally related to some form of defect generation on a sufficiently small scale to be individually insignificant. These damage variables are then used at the macroscopic level in the prediction of material failure. This is not the same as the well known

study of fracture mechanics, whereby a single geometrically defined defect is used to gauge the structural integrity of a material. In contrast, damage mechanics starts with a virgin material free of defects and follows it through to the damaged state at which point fracture mechanics takes over.

The damage parameter D_m may be defined in relation to some measurable macroscopic quantity ϕ that is representative of the damage process by

$$D_m = ({}^{\circ}\phi - \phi) \; / \; ({}^{\circ}\phi - {}^{n}\phi) \qquad (2.6.01)$$

where

${}^{\circ}\phi$ = Value of representative quantity for virgin material

${}^{n}\phi$ = Value of representative quantity for failed material

The principles of damage mechanics were first applied to model high temperature tertiary creep in metals by Kachanov [71]. The nonlinear behavior just before failure was modelled by using an effective applied stress given by

$$\sigma_{eff} = [\sigma/(1-D_m)] \qquad (2.6.02)$$

where

σ = Applied stress

D_m = Damage parameter

which was then substituted into the usual creep law to give

$$\epsilon = K_{ch} \, [\sigma/(1-D_m)]^q \qquad (2.6.03)$$

where K_{ch} and q are material constants, q being non-dimensional.

The damage parameter represents a steadily increasing destroyed fraction of material, with catastrophic failure at the point where D_m is equal to unity. The change in D_m was represented by an evolution law of the form

$$(\delta D_m/\delta t) = D_{ch} \, [\sigma/(1-D_m)]^q \qquad (2.6.04)$$

where D_{ch} is a material constant. The material constants may be evaluated by a creep test to experimentally determine the time to failure as a function of the applied load. However, this has limited utility for most fiber composite materials.

Damage resulting from the creation and propagation of microcracks may be modelled by an increase in the surface energy of a material. This can be related to a reduction in the material stiffness by

$$\sigma = E^{\circ}(1-D_m)\epsilon \qquad (2.6.05)$$

The elastic strain (W) and complementary (W^*) energies are then given by

$$W = \int \tfrac{1}{2}\, \epsilon^2\, [E^\circ(1-D_m)]\, dVol$$

$$W^* = \int \tfrac{1}{2}\, \sigma^2/[E^\circ(1-D_m)]\, dVol \qquad (2.6.06)$$

The energy expended during damage growth is then given by

$$\begin{aligned} W_{dg} &= \sigma\ (\delta\epsilon/\delta t) - (\delta W/\delta t) \\ &= \tfrac{1}{2}\, E^\circ \epsilon^2 (\delta D_m/\delta t) \end{aligned} \qquad (2.6.07)$$

In order to follow the damage process and be able to predict the degradation of material behavior, a damage evolution law is required that will follow the damage process under a given load history. Both of the examples cited above involve a time dependent evolution law for the damage parameter. The time rate of change of damage growth may be modelled as a function of the applied stress and the current level of damage, giving

$$(\delta D_m/\delta t) = F_{D1}(\sigma, D_m) \qquad (2.6.08)$$

Sidoroff [72] has suggested two other types of evolution laws for the damage variable. In the case where the rate of damage growth is strain dependent, we may use

$$(\delta D_m/\delta \epsilon) = F_{D2}(\sigma, D_m) \qquad (2.6.09)$$

In the case of fatigue loading, it is more convenient to model the evolution of the damage parameter as a function of the number of stress reversals, thus

$$(\delta D_m/\delta N) = F_{D3}(\sigma_{max}, \sigma_{min}, D_m) \qquad (2.6.10)$$

Superposition of the above three equations then results in a general damage evolution law of the form

$$D_m = \int F_{D1}\, dt + \int F_{D2}\, d\epsilon + \int F_{D3}\, dN \qquad (2.6.11)$$

The discussion so far has been based upon the implied assumption that the damage, however caused, is isotropic in nature. Unfortunately defect patterns in fiber composites can be highly directional, so isotropic damage is not a reasonable assumption. Finally, there is more than one failure mechanism associated with fiber composites, and representation of these by a single damage variable is not realistic.

Due to these shortcomings, the application of damage mechanics to structural analysis requires an extension of the above approach to three dimensions. To this end the use of damage tensors has been suggested by a number of authors [73,74]. These tensors have been defined by statistical descriptions of the distribution and shape of

the defects, however they have not met with much success. Furthermore, they do not have any precise physical meaning.

Krajcinovic [75] has used a continuum damage approach to model the effect of matrix cracking using three independent damage parameters representing crack nucleation and growth due to longitudinal, transverse and shear loading. However the model is restricted to inplane behavior.

What is needed is a description of the damage parameter in terms of the failure modes of a fiber composite. The variables describing its evolution should include the effects of mircovoid coalescence, matrix cracking, fiber breakage, interfacial debonding and interlaminar delamination.

2.7 Energy Absorption

Studies of the energy absorption characteristics of materials is an important consideration in impact studies. Considerable effort has been expended in this area, and some data published in the literature is concerned with experimental investigations of various fiber/matrix combinations. Unfortunately the bulk of this data remains

classified since the investigations were performed under defence department contracts.

Most of the published data relates the energy absorption to some form of impact parameter such as the peak force or the maximum deflection. However, the calculation of the actual energy absorbed by the impact is a difficult task, due mainly to the various failure mechanisms encountered. These include, but are not limited to microvoid formation and coalescence, fiber/matrix debonding, fiber pullout and interlaminar delamination.

Microvoid formation and coalescence may be modelled by a modified Griffith [76] approach, whereby material failure is treated as resulting in the formation of a strain free sphere. The strain energy released is equated to the energy of the new surfaces created by the void.

$$\int_{Vol} \sigma \, \epsilon \, dVol = \pi c^2 \Gamma \qquad (2.7.01)$$

where

c = Diameter of void

Γ = Surface energy

Fiber/matrix debonding results from shear forces that are generated at the interface as a result of the

differential moduli between the two constituents of the lamina. Debonding occurs if this shear force exceeds the interfacial bond strength. The energy absorption depends upon the length of the debond, the fiber diameter and the interfacial bond strength. The critical debonded length of fiber can be defined as

$$L_{db} = [\sigma_f r_f / 2\tau] \qquad (2.7.02)$$

where

σ_f = Failure strength of fiber

r_f = Radius of fiber

τ = Applied shear stress at interface

Since the fiber failure strength can have a statistical distribution about some mean value [77], the critical pullout length will also have a similar distribution. The energy absorbed in the formation of the fiber debond is then given by

$$U_{db} = 2\pi L_{db} (r_m \Gamma_m + r_f \Gamma_f) \qquad (2.7.03)$$

where

r_m = Radius of matrix tunnel

r_f = Radius of fiber

Γ_m = Surface energy of matrix

Γ_f = Surface energy of fiber

Different expressions for the fiber debonding energy have been given by Beaumont [78], Phillips & Tetelman [79] and Wells [80] .

Once the fibers have broken, stress transfer is still possible due to friction between the fiber and matrix due to differential thermal expansion of the two materials. The differential compressive stresses are a direct result of the fabrication process. The phenomenon of crack bridging occurs if the matrix crack propagates past the unbroken fibers, resulting in the fibers being literally pulled out of the binder.

Energy is dissipated as heat as the fibers displace relative to the binder due to the work done against the interfacial shear stress. This pullout energy is given by

$$U_{po} = 2\tau\pi r_f L_{db}^2 \qquad (2.7.04)$$

The main drawback of the above expressions is that they involve knowledge of the material surface energy, which is generally not known. Though Griffith showed how to obtain this for glass fibers, the procedure is not simple for fibers of advanced composite materials.

There are two experimental methods whereby energy absorption is evaluated for laminated fiber composites. The method used by various military establishments is to

fire a projectile of a given mass at a flat target and measure what is known as the ballistic limit (V50) of the material. This is the velocity at which 50% of the projectiles penetrate the target. Commercial research establishments use a much cheaper ball drop or Charpy test in which the energy absorption is related to the impact load and the maximum plate deflection. These methods are not used so much to measure the absorbed energy as they are to rank the materials tested in terms of their energy absorption potential.

As mentioned above, little data is available on the energy absorption characteristics of laminated fiber composites. What data is available indicates that the results depend to a large extent upon the lab that performs the testing. Wardle [81] has indicated that plain weave fabrics absorb more energy than those with more complex weave styles, whereas Winkle & Adams [82] indicate that satin weave fabrics are better energy absorbers. Harding & Welsh [83] have indicated that fracture strengths and failure modes are unaffected by strain rates, and Hull [84] has indicated that the energy absorption characteristics are also not strain rate dependent. In contrast, Ohlson [85] has found that the peak load and flexural modulus increased with increasing loading rate up to a maximum, and decreased thereafter.

None of the methods mentioned above are able to provide any insight into the damage process or the failure progression. Furthermore, they are only useful as a method of ranking the various lamination sequences. Both tests require the use of a large sample size for a reliable result, the manufacturing costs of which contributes significantly to the overall cost of the test. For specimens involving thicknesses larger than about ¼ in (0.635 cm), complications arise in the cure cycle due to heat and mass transfer problems in the center of the laminate. It would be advantageous to have a method whereby such rankings could be done analytically to reduce the sample size required for the experimental tests.

2.8 Summary

The analysis of laminated fiber composites has largely been handled using laminated plate theory, since this provides an adequate description of the behaviour of the laminate for most applications. However these theories still have their limitations, and several methods have been proposed to overcome them. These have all involved increasingly higher order truncations in the functions used to describe the midplane displacements. Such methods allow a better solution to the zero surface

shear stress conundrum, but do not address the problem of the edge effects responsible for delamination behaviour.

The application of the Finite Element Method to laminated fiber composites has generally used a form of plate element to represent the laminate. However these elements are incapable of providing an insight into some of the failure mechanisms that arise due to the nature of their formulation. Standard 3D elements are available that can be used, however they are usually limited to a single ply representation through their thicknesses. Incorporation of a multi-ply element will increase the utility of a Finite Element analysis.

In the majority of cases, the ply properties used in the laminate analysis are obtained from experimental data, thereby limiting the utilization of these materials to lamina for which properties are already known. However various techniques exist which allow the use of a design philosophy in which the final laminated structure can be created from the basic material properties of the constituents themselves, rather than from the more limited knowledge of the ply properties. Though rarely implemented in classical plate theory, the application of these techniques to the Finite Element Method is straightforward.

Several laminate failure criteria are available to determine the overall strength of laminates. Unfortunately their use is generally of an overly conservative nature, in that failure of a single point is taken to constitute catastrophic failure of the laminate. There is generally no account taken of the significant residual load carrying capability after initial failure. The application of a damage variable analysis to these materials has been limited. However the use of the currently available failure criteria, in conjunction with a multi-ply element, allows the use of a more realistic approach to failure.

Studies of the energy absorption characteristics for laminated fiber composites have been undertaken by various investigators, however few of the experimental results have been conclusive. Analytical studies of energy absorption have dealt mainly with the effects of overloads on single fibers embedded in a binder. Various expressions have been proposed to evaluate the energy absorption, however they all require the measurement of a property that is not readily accomplished. The Finite Element Method allows failure to be tracked at the integration point level within an element. This in turn allows a simple evaluation of the energy absorption as a function of damage progression.

3.0 Element Stiffness

3.1 Strain Energy

The finite element solution to an engineering problem represents the behaviour of a structure by discretization into a number of subregions over which simple displacement assumptions may be used. Each subregion is bounded by a set of nodes. The usual form of the element stiffness matrix follows from the displacement based formulation of the finite element equilibrium equations [86]. The elastic strain energy in a loaded element is given by

$$U_e = \tfrac{1}{2} \int \sigma_{ij} \, \epsilon_{ij} \, dVol \qquad (3.1.01)$$

where the integration is performed over the volume of the element. The stresses and strains in an element are related through Hook's law, which may be written as

$$\{\sigma_{ij}\} = [D] \, \{\epsilon_{ij}\} \qquad (3.1.02)$$

The strains within an element are defined in terms of the assumed displacements as

$$\{\epsilon_{ij}\} = [L] \, \{u\} \qquad (3.1.03)$$

where L is a suitable linear operator. However the displacements themselves are usually defined in terms of a set of basis functions valid only within the element. It is customary to write

$$\{u\} = \sum_{i=1}^{k} N_i \{u_i\} \tag{3.1.04}$$

where the u_i represent constant displacements at discrete points or nodes on the element, and the N_i represent the shape functions associated with that node. Therefore the strains may be written as

$$\{\epsilon_{ij}\} = [B] \{u_i\} \tag{3.1.05}$$

Since the u_i are constants, they may be taken outside of the integral sign. The strain energy expression then becomes

$$U_e = \tfrac{1}{2} \{u_i\}^T \left[\int\int [B]^T [D] [B] \, dVol \right] \{u_i\} \tag{3.1.06}$$

It is readily verified that the term in the square brackets represents the element stiffness matrix.

3.2 Shape Functions

In the usual elasticity approach to solving engineering problems an unknown stress function is assumed over the region of interest, and substituted into the compatibility equations. Application of the boundary conditions then determines the necessary constants that allow a correct representation of the solution. The Finite Element Method represents the same function in a piecewise manner by a set of shape functions valid at discrete intervals within the domain. These functions are used in conjunction with constant values at given points in the subdomain to interpolate the unknown function within the element.

There is no mathematical restriction on the type of basis functions used for the interpolation of the unknown. However it has been customary to use polynomial interpolation due to the ease with which these functions may be developed and differentiated. The latter is especially helpful when computing the element strains. Such functions have been used to develop a large number of elements for use in various engineering problems [87].

The approximation of the unknown function may be accomplished through the use of either Lagrange or Hermitian interpolation. In the former a polynomial is sought that passes through a given set of points within

the domain while satisfying the values at those points. In the latter the polynomial must also satisfy the derivative values at those points. For both cases the general form of the polynomial is given by

$$N_i = \sum_{i=0}^{n} \prod_{j=0}^{n} \left[(x-x_i) \; / \; (x_i-x_j) \right] u_i \qquad (3.2.02)$$

where the symbol π denotes a product of the indicated binomials over the indicated range, and i & j are not the same.

Due to the nature of the shape functions, they may be used to interpolate many other variables within the element. They may be used not only in the evaluation of the stiffness matrix, but also in the representation of the applied loading, the evaluation of the mass and damping matrices for dynamic problems, and the stability matrix for buckling problems. It is therefore useful to isolate the evaluation of these shape functions from the requirements of the problem.

To this end these functions are written in a set of natural coordinates that range from -1 to 1. Such coordinates represent a mapping of the physical coordinates into a nondimensionalized system of parent coordinates. The element stiffness matrix may be easily evaluated in this parent (r,s,t) coordinate system, and

then mapped to the physical (x,y,z) coordinate system through the use of an appropriate transformation.

3.3 Strain-Displacement Matrix

The strains in an element are defined in terms of the displacements within the element through the use of a suitable operator. This operator is referred to as Green's 3D strain tensor to second order, and is given by

$$[L] = \begin{bmatrix} (\delta/\delta x)+\tfrac{1}{2}(\delta/\delta x)^2 & \tfrac{1}{2}(\delta/\delta x)^2 & \tfrac{1}{2}(\delta/\delta x)^2 \\ \tfrac{1}{2}(\delta/\delta y)^2 & (\delta/\delta y)+\tfrac{1}{2}(\delta/\delta y)^2 & \tfrac{1}{2}(\delta/\delta y)^2 \\ \tfrac{1}{2}(\delta/\delta z)^2 & \tfrac{1}{2}(\delta/\delta z)^2 & (\delta/\delta z)+\tfrac{1}{2}(\delta/\delta z)^2 \\ (\delta/\delta y)+(\delta/\delta x)(\delta/\delta y) & (\delta/\delta x)+(\delta/\delta x)(\delta/\delta y) & (\delta/\delta x)(\delta/\delta y) \\ (\delta/\delta y)(\delta/\delta z) & (\delta/\delta z)+(\delta/\delta y)(\delta/\delta z) & (\delta/\delta y)+(\delta/\delta y)(\delta/\delta z) \\ (\delta/\delta z)+(\delta/\delta z)(\delta/\delta x) & (\delta/\delta z)(\delta/\delta x) & (\delta/\delta z)+(\delta/\delta z)(\delta/\delta x) \end{bmatrix}$$

(3.3.01)

In the case of a small deflection analysis it is not necessary to use all of the terms in [L] since the derivatives of the u and v displacements with respect to the x, y and z directions are small in comparison to the thickness.

3.4 Element Families

The form of the strain-displacement matrix will depend upon the type of element utilized to represent the domain of the problem. As described in the literature review, extensive use has been made of plate element formulations in the application of the Finite Element method to problems involving laminated fiber composites. Many of these do not include the out-of-plane shearing stresses, and rarely do they include the out of plane normal stress components that may be responsible for edge delamination failures.

Beginning with the general displacement assumptions of Basset and truncating the inplane displacements to third order, the midplane displacement assumptions are given by

$$u = u^{\circ} + z\,\theta_x + z^2\,\Phi_x + z^3\,\Omega_x$$
$$v = v^{\circ} + z\,\theta_y + z^2\,\Phi_y + z^3\,\Omega_y \qquad (3.4.01)$$

where

$$\theta_x = (\delta w^\circ/\delta_x) \qquad \Phi_x = (\delta w^{\circ 2}/\delta_x{}^2) \qquad \Omega_x = (\delta w^{\circ 3}/\delta_x{}^3)$$

$$\theta_y = (\delta w^\circ/\delta_y) \qquad \Phi_y = (\delta w^{\circ 2}/\delta_y{}^2) \qquad \Omega_y = (\delta w^{\circ 3}/\delta_y{}^3)$$

The symbol δ indicates partial derivatives of the associated functions with respect to the indicated variable. The truncation to third order is the minimum required to satisfy the zero shear stress requirement at the top and bottom surfaces of the laminate. The same expressions may be used to represent the through thickness displacement. However the transverse shear strains due to the inplane displacements should be of the same order in z as those determined by the transverse displacement. It is therefore reasonable to assume a second order truncation for w, giving

$$w = w^\circ + z\,\theta_z + z^2\,\Phi_z \qquad (3.4.02)$$

where

$$\theta_z = (\delta w^\circ/\delta_z)$$

$$\Phi_z = (\delta w^{\circ 2}/\delta_z{}^2)$$

The boundary conditions on the surface shears requires that both Φ_x and Φ_y vanish at $z=\pm\frac{1}{2}h$, therefore the displacement assumptions become

$$u = u^\circ + z \left[\theta_x - (4/3)(z/h)^2 \left[\theta_x + (\delta w^\circ/\delta x) \right] + (h/2)^2 (\delta \Phi_z/\delta x) \right] \tag{3.4.03}$$

$$v = v^\circ + z \left[\theta_y - (4/3)(z/h)^2 \left[\theta_y + (\delta w^\circ/\delta y) \right] + (h/2)^2 (\delta \Phi_z/\delta y) \right]$$

$$w = w^\circ + z\,\theta_z + z^2\,\Phi_z$$

Putting these equations into Green's strain tensor and using the constitutive relations for a generally orthotropic lamina then gives

$$\begin{bmatrix} N_{6x1} \\ M_{6x1} \\ P_{6x1} \\ R_{6x1} \\ S_{6x1} \end{bmatrix} = \begin{bmatrix} A_{6x6} & B_{6x6} & D_{6x6} & E_{6x6} & F_{6x6} \\ B_{6x6} & D_{6x6} & E_{6x6} & F_{6x6} & G_{6x6} \\ D_{6x6} & E_{6x6} & F_{6x6} & G_{6x6} & H_{6x6} \\ E_{6x6} & F_{6x6} & G_{6x6} & H_{6x6} & I_{6x6} \\ F_{6x6} & G_{6x6} & H_{6x6} & I_{6x6} & J_{6x6} \end{bmatrix} \begin{bmatrix} \ddot{U} \end{bmatrix} \tag{3.4.04}$$

where

$$[\ddot{U}] = [\ {}^0\epsilon_{3x1}\ {}^0\Gamma_{3x1}\ {}^1\epsilon_{3x1}\ {}^1\Gamma_{3x1}\ {}^2\epsilon_{3x1}\ {}^2\Gamma_{3x1}\ {}^3\epsilon_{3x1}\ {}^3\Gamma_{3x1}\ {}^4\epsilon_{3x1}\ {}^4\Gamma_{3x1}\ ]^T$$

$$[A,B,D,E,F,G,H,I,J]^T = \int_t Q_{ij}\,[1,z,z^2,z^3,z^4,z^5,z^6,z^7,z^8]\,dz$$

The problem with using this plate element formulation is that each node of the element will require at least 30 independent degrees of freedom. The modelling of fiber composite structures using this element will quickly lead to practical computational difficulties due to the excessive core memory requirements. Furthermore, the use of higher order displacement assumptions in the development of these elements does not give significantly better results when compared to CPLA. Due to the above, this element formulation does not offer the appropriate requirements for a cost effective analysis.

The most general form of element family is the solid, of which the 4-node Tetrahedron is the simplest. The displacement functions for this element are linear, resulting in a constant state of strain throughout the element volume. Unfortunately this element is cumbersome to use in the modelling of laminated plates. Other popular elements suited to this task are the 8-node and 20-node Cuboids. The former uses linear displacement assumptions whereas the latter uses displacement assumptions that are quadratic. Writing the displacements in terms of the shape functions then gives the strain-displacement matrix as

$$[B] = [L]\ \{N\}^T\ \{u_i\} \qquad (3.4.05)$$

Clearly [B] consists of first order derivatives of the shape functions with respect to the global coordinates. The matrix may be written in partitioned form, with the number of partitions equal to the number of nodes used to define the element. If deflections are assumed to be small, it is customary to introduce the von Kàrmàn small deflection assumptions. These imply that the derivatives of u & v with respect to x, y & z are small. For the i'th node, a typical partition is given by

$$[B]_i = \begin{bmatrix} (\delta N/\delta x) & 0 & 0 \\ 0 & (\delta N/\delta y) & 0 \\ 0 & 0 & (\delta N/\delta z) \\ (\delta N/\delta y) & (\delta N/\delta x) & 0 \\ 0 & (\delta N/\delta z) & (\delta N/\delta y) \\ (\delta N/\delta z) & 0 & (\delta N/\delta x) \end{bmatrix}_i \qquad (3.4.06)$$

For the case of an 8-node cuboid element, this would yield a constant variation for ϵ_{ii} in the i-direction, and a linear variation perpendicular to it. This is similar to what is obtained from plate analysis, which gives a linear variation of strain through the laminate thickness and a constant strain in the laminate plane. The use of a 20-node cuboid element will yield a linear variation of strain in the laminate plane since the shape functions

will be quadratic, and a parabolic variation in the thickness and width directions.

3.5 Jacobian Transformation

The derivatives of the shape functions are readily given in terms of the parent coordinates, it is therefore necessary to transform these into the global coordinate system in order to obtain the global element stiffness matrix. In terms of the parent rst-coordinate system, the shape function derivatives in the transformed xyz-coordinate system are given by

$$\begin{bmatrix} (\delta N/\delta x) \\ (\delta N/\delta y) \\ (\delta N/\delta z) \end{bmatrix} = [J]^{-1} \begin{bmatrix} (\delta N/\delta r) \\ (\delta N/\delta s) \\ (\delta N/\delta t) \end{bmatrix} \qquad (3.5.01)$$

where [J] is known as the Jacobian operator. This operator relates the transformed coordinate derivatives to the parent coordinate derivatives, and is a measure of the amount of distortion between the two coordinate systems.

Since the displacement interpolations are given by the sum of the products of the shape functions and their respective nodal displacements, the Jacobian operator is given by

$$[J] = \begin{bmatrix} \sum_{i=0}^{n} (\delta N/\delta r)_i \, x_i & \sum_{i=0}^{n} (\delta N/\delta r)_i \, y_i & \sum_{i=0}^{n} (\delta N/\delta r)_i \, z_i \\ \sum_{i=0}^{n} (\delta N/\delta s)_i \, x_i & \sum_{i=0}^{n} (\delta N/\delta s)_i \, y_i & \sum_{i=0}^{n} (\delta N/\delta s)_i \, z_i \\ \sum_{i=0}^{n} (\delta N/\delta t)_i \, x_i & \sum_{i=0}^{n} (\delta N/\delta t)_i \, y_i & \sum_{i=0}^{n} (\delta N/\delta t)_i \, z_i \end{bmatrix} \tag{3.5.02}$$

The evaluation of the [B] matrix is done in the natural coordinates of the basis functions, so the integration of the element stiffness matrix extends over the parent volume. Therefore the differential volume element must be written in terms of the parent coordinates. In terms of these coordinates, the volume integration is given by

$$\int dVol = \iiint \det[J] \, dr \, ds \, dt \tag{3.5.03}$$

where det[J] refers to the determinant of the Jacobian matrix.

3.6 Material Property Matrix

The material property matrix [D] is based upon the engineering constants of the material comprising the element. These elastic constants are determined by performing a series of mechanical tests [88]. In general, these tests involve a measurement of the deformation that a material undergoes when subjected to a known force. This allows the compliance matrix [C] to be readily determined.

The most general form of the compliance matrix for an anisotropic material contains 36 elastic constants [89]. However the deformations for a fiber composite are usually linearly elastic to failure. It is therefore possible to write a strain energy potential function which can be used to show that the compliance matrix must be symmetric [90], thus reducing the number of independent elastic constants to 21.

For the case of orthotropic materials, there are two orthogonal planes of material property symmetry relative to a third mutually orthogonal plane. There is no interaction between the normal stresses and the shearing

strains, or between the shearing stresses and the normal strains. This reduces the number of independent elastic constants to nine. Thus

$$[C] = \begin{bmatrix} (1/E_{11}) & -(\mu_{12}/E_{11}) & -(\mu_{13}/E_{11}) & 0 & 0 & 0 \\ -(\mu_{21}/E_{22}) & (1/E_{22}) & -(\mu_{23}/E_{22}) & 0 & 0 & 0 \\ -(\mu_{31}/E_{33}) & -(\mu_{32}/E_{33}) & (1/E_{33}) & 0 & 0 & 0 \\ 0 & 0 & 0 & (1/G_{12}) & 0 & 0 \\ 0 & 0 & 0 & 0 & (1/G_{23}) & 0 \\ 0 & 0 & 0 & 0 & 0 & (1/G_{31}) \end{bmatrix} \qquad (3.6.01)$$

where

E_{ii} = Elastic modulus in the i-direction.

G_{ij} = Shear modulus in the ij-plane.

μ_{ij} = Poisson's ratio for strain in the j-direction when stressed in the i-direction.

The material property matrix relates the strains in a material to the stresses, and so is the algebraic inverse of the compliance matrix. In terms of the engineering constants, the non-zero elements of the [D] matrix are given by

$$
\begin{aligned}
D_{11} &= [\ (1 - \mu_{23}\,\mu_{32}) / (E_{22}\,E_{33}\,D_n)\ ] \\
D_{12} &= [\ (\mu_{21} - \mu_{31}\,\mu_{23}) / (E_{22}\,E_{33}\,D_n)\ ] \\
D_{13} &= [\ (\mu_{31} - \mu_{21}\,\mu_{32}) / (E_{22}\,E_{33}\,D_n)\ ] \\
D_{21} &= [\ (\mu_{12} - \mu_{32}\,\mu_{23}) / (E_{11}\,E_{33}\,D_n)\ ] \\
D_{22} &= [\ (1 - \mu_{13}\,\mu_{31}) / (E_{11}\,E_{33}\,D_n)\ ] \\
D_{23} &= [\ (\mu_{32} - \mu_{12}\,\mu_{31}) / (E_{11}\,E_{33}\,D_n)\ ] \\
D_{31} &= [\ (\mu_{13} - \mu_{12}\,\mu_{23}) / (E_{11}\,E_{22}\,D_n)\ ] \\
D_{32} &= [\ (\mu_{23} - \mu_{21}\,\mu_{13}) / (E_{11}\,E_{22}\,D_n)\ ] \\
D_{33} &= [\ (1 - \mu_{12}\,\mu_{21}) / (E_{11}\,E_{22}\,D_n)\ ] \\
D_{44} &= G_{12} \\
D_{55} &= G_{23} \\
D_{66} &= G_{31}
\end{aligned}
\qquad (3.6.02)
$$

where

$$D_n = \frac{(1 - \mu_{12}\,\mu_{21} - \mu_{23}\,\mu_{32} - \mu_{31}\,\mu_{13} - 2\,\mu_{13}\,\mu_{32}\,\mu_{21})}{(E_{11}\,E_{22}\,E_{33})}$$

3.7 Lamina Orientation

Laminated fiber composite structures are usually constructed by stacking several unidirectional layers of laminae in a specified sequence of orientations with

respect to a reference system of coordinates. Therefore, in order to perform an engineering analysis the principal direction of material orthotropy must be referenced to a common geometric axis.

From elementary mechanics of materials, the transformation equations required to express the material stresses in a coordinate system inclined to the material axis is given by

$$\{\sigma\} = [T]^T [D] [T] \{\epsilon\} \qquad (3.7.01)$$

where [T] is the transformation matrix relating the strains in the ply principal directions to those in the global reference axis. For the three dimensional case this matrix is given by a fourth order tensor transformation in terms of the direction cosines of the unit vectors in the respective coordinate systems [91]. Since the laminae rotations are confined to the x-y plane [92], the transformation matrix simplifies to

$$[T] = \begin{bmatrix} \cos^2\theta & \sin^2\theta & 0 \\ \sin^2\theta & \cos^2\theta & 0 \\ 0 & 0 & 1 \\ \cos\theta\,\sin\theta & -\cos\theta\,\sin\theta & 0 \\ 0 & 0 & 0 \\ 0 & 0 & 0 \end{bmatrix}$$

$$\begin{vmatrix} -\mathrm{Sin}2\theta & 0 & 0 \\ \mathrm{Sin}2\theta & 0 & 0 \\ 0 & 0 & 0 \\ \mathrm{Cos}2\theta & 0 & 0 \\ 0 & \mathrm{Cos}\theta & \mathrm{Sin}\theta \\ 0 & -\mathrm{Sin}\theta & \mathrm{Cos}\theta \end{vmatrix} \qquad (3.7.02)$$

where θ is the counter clockwise inplane rotation angle from the global reference axis to the material reference axis.

3.8 Numerical Integration

The evaluation of the element stiffness matrix involves integration of a function over the domain represented by the element. From the above discussion, this integral is given by

$$[K] = \int [B]^T [T]^T [D] [T] [B] \det[J] \, dr \, ds \, dt \qquad (3.8.01)$$

An explicit evaluation of this integral is generally impractical. Exact solutions of this equation are obtainable in the parent coordinate system for only the simplest of these expressions. In general, cases may arise where such closed form integration is not possible.

In practice the integrals are evaluated numerically using Gauss quadrature [93], the integration order used generally being dependent upon the degree of the interpolating polynomials used for the element shape functions and the particular matrix to be constructed.

The Gauss technique substitutes the integration by a summation over the domain of the product of a substitute function evaluated at discrete points within the domain and a weighting factor. The number of points at which the function is evaluated is not necessarily the same in all three dimensions of the domain. If W_i represents the weighting factor for a particular point, then the stiffness matrix is evaluated as a triple summation over the domain given by

$$[K] = \sum_{t=1}^{gpt} \sum_{s=1}^{gps} \sum_{r=1}^{gpr} [\, F_{(r,s,t)}\, W_r\, W_s\, W_t \,] \qquad (3.8.02)$$

where

gpr = Number of integration points in r-direction

gps = Number of integration points in s-direction

gpt = Number of integration points in t-direction

$F_{(r,s,t)} = [B]^T\, [T]^T\, [D]\, [T]\, [B]\, \det[J]$

The number of operations required to evaluate this integral is equal to $N_p{}^d$ where N_p is the integration order and d corresponds to the number of dimensions of the

element. It is therefore essential to choose as small a value of N_p as is practical. Zienkiewicz [94] suggests the minimum requirement to be that which would integrate the determinant of the Jacobian operator accurately.

The stiffness matrix for each element of the domain is easily evaluated using this technique by substitution of the appropriate matrices into the above equation.

3.9 Composite Element

For homogeneous isotropic materials the [D] matrix is a constant throughout the element volume. Therefore the evaluation of this matrix is usually performed only once. In the analysis of fiber composite laminates the variation in the material properties through the element domain is done by the assignment of a different [D] matrix for each individual element. Theoretically one can model fiber composite structures by breaking up each ply into the usual finite element mesh, with the thickness of each element representing the thickness of each individual ply.

Practically, this leads to numerical difficulties due to the limitation in the element aspect ratio. The limitation springs from the resulting relative magnitudes of the terms in the element stiffness matrix. Large differences in these magnitudes tend to create problems in

accuracy due to ill-conditioning [95]. The magnitudes of these differences is greatly dependent upon the aspect ratios of the elements used to model the problem.

For the sake of argument, we may set a maximum permitted aspect ratio of 1:20. Since the usual thickness of a fiber composite ply is more or less 0·005 inches (0·013 cm), this limits the physical dimensions of an element to 0·10 inches (0·254 cm) square. A typical problem such as a one square foot plate with 80 plies through the thickness would then require well over a million elements for a moderately accurate solution. If an 8-node cuboid element is employed in the modelling, the problem would require almost three and a half million degrees of freedom. Such a large number of degrees of freedom will tax the core memory requirements of todays supercomputers, and overload the capabilities of current machines. Even if this were not a problem, the large number of degrees of freedom results in an excessive cost in terms of computer time.

One obvious way to overcome this difficulty is to use the method of substructuring [96] in order to reduce the total number of degrees of freedom. The global stiffness matrix is assembled as usual, and then partitioned into four submatrices. These matrices are an external boundary region ($[K_{ee}]$), another representing a region within this

boundary ([K_{ii}]), and two others representing the connection between them ([K_{ei}] & [K_{ie}]). Thus

$$\begin{bmatrix} K_{ee} & K_{ei} \\ K_{ie} & K_{ii} \end{bmatrix} \begin{bmatrix} U_e \\ U_i \end{bmatrix} = \begin{bmatrix} R_e \\ R_i \end{bmatrix} \qquad (3.9.01)$$

The internal degrees of freedom are then condensed out, leaving behind a representation of the model in terms of its overall stiffness and equivalent loads (Fig 1).

$$\begin{aligned} U_i &= K_{ii}^{-1} \left(R_i - K_{ie} U_e \right) \\ \left(K_{ee} - K_{ei} K_{ii}^{-1} K_{ie} \right) U_e &= R_e - K_{ei} K_{ii}^{-1} R_i \end{aligned} \qquad (3.9.02)$$

The condensed set of equations is then solved for the external degrees of freedom, and those results used to obtain the solution in the interior of the structure. In the case of the problem described above, the resulting variable count is approximately two orders of magnitude less than the case without substructuring.

The above procedure is identical to performing Gauss elimination on the internal degrees of freedom and results in a large savings of computer time if repeated solutions are required for the same structure but with different boundary loading. This is not possible if failure occurs at any location in the structure, since the global stiffness matrix must be modified. Any change in the load

response due to material failure requires a reformation of the substructures. The disadvantage is that the unknown function used in the derivation of the finite element equilibrium equations is now represented by a series of piecewise approximations inside the region of interest.

In the case of laminated fiber composite analysis, unless the deflections are known to lie within the elastic limit of the material, it is necessary to evaluate the stresses and strains in the interior region to determine whether or not failure has occurred. This requires the solution of the displacements in the interior of the structure. Since such a priori knowledge cannot be assumed, this method offers no advantages.

It is not possible to use the substructure method at the element level in order to overcome the requirement of reassembly due to material failure. It is feasible to create a super-element from a stack of elements, with each element representing a single ply through the thickness. However the assembly of the structure from this super-element will not yield accurate results since interelement displacement continuity will not be satisfied.

An alternative approach is to represent several plies of the structure within one element (Fig 2). If, for example, ten plies were represented through the element

thickness, the above mentioned problem would require a little over one thousand elements and about four thousand five hundred degrees of freedom (a reduction of over 99%). For the case of a 20-node cuboid element the displacement would be represented by a single quadratic function rather than several quadratics through the thickness.

In the analysis of fiber composite materials, there is a tacit assumption that the material of which any one given ply is composed is the same from one point to another. This implies that the material properties are the same within the ply. It is therefore possible to break the integral at the ply boundaries, and assume a constant [D] matrix within each ply. The overall [D] matrix may be computed by summing the contributions of each ply.

Unfortunately the variation of the material properties within the element need not be caused only by the differences in the ply constituents, their relative volume fractions and the ply orientations with respect to the global reference axis, but also by local material failures. Since the stresses within an element are not necessarily constant throughout its constituent ply volumes, material at different locations will fail at different values of the applied load. This is important

in the prediction of the displacements of the overall structure. Therefore the [D] matrix must be computed at each integration point within any one given ply.

Due to the non-constant nature of the material property matrix throughout the element volume, it is no longer possible to perform the volume integration using a minimum number of Gauss points. Rather, the integration must be performed using several points through the thickness. The procedure adopted is to divide the element thickness into a number of sections equal to the number of plies through the element thickness, with the ply boundaries delineating each section.

The general expression for the element stiffness matrix then becomes

$$[K] = \sum_{n=1}^{p} \left[\sum_{t=1}^{gpt} \sum_{s=1}^{gps} \sum_{r=1}^{gpr} [\, F(r,s,t)\, W_r\, W_s\, W_t \,] \right]_n \qquad (3.9.03)$$

where n is the number of plies through the element thickness. The stiffness matrix is evaluated over each ply volume, and the results summed over the element volume. Since Gauss quadrature is used through the ply thickness, the integration points and weights must be corrected for the nonstandard limits in the thickness direction. If the upper and lower limits of integration

are denoted by L_u and L_l, the new sampling point (S_p) and weight (S_w) are given by

$$S_p = \tfrac{1}{2}\,(L_u-L_l)\;S_p^\circ + \tfrac{1}{2}\,(L_l-L_u) \qquad (3.9.04)$$
$$S_w = \tfrac{1}{2}\,(L_u-L_l)\;S_w^\circ$$

where

S_p° = Sampling point based on interval of -1 to 1.

S_w° = Sampling weight based on interval of -1 to 1.

The values of the sampling points and weights based upon the parent interval of -1 to 1 have been computed and published in the open literature [97].

The modified integration procedure neatly takes care of several problems. It not only allows a smooth variation of the material properties within the ply volume, but also allows a smooth variation of the fiber orientation. This is useful in studies in which the fiber orientation is a function of the position, as in the case of injection molding. Its is also useful in the analysis of thick laminates for which the properties at the center of the thickness may be significantly different from those near the outer surfaces due to fabrication anomalies.

4.0 Damage Analysis

4.1 Introduction

The design of a structure in terms of its load carrying capability is determined by comparing the results of an analysis to some form of failure criterion. The basis of the failure criterion is dependent upon the application, and may be perceived as the separation of critical structural components. However, in general, the failure criterion is usually based upon maximum allowable strains or stresses for the material of which the structure is composed. The allowables represent the limit of elasticity under any possible combination of loads.

Unlike common engineering materials, fiber composites cannot be classified in terms of any one particular failure criterion. It has been common practice to set the laminate failure point in terms of the failure of the first ply for which the load exceeds the capacity of the laminate. In this case the strains or stresses are computed in the lamina principal material axis and substituted into one of the various failure criteria described in the literature review. As mentioned before, this approach is overly conservative, and takes no account of the localized failure mechanisms.

The mechanical modelling for fiber composites as well as other materials is much more developed towards rheological behaviour than towards failure prediction. Among the questions that must be answered in the prediction of material behavior is that of how to model the damage caused by exceeding the various material strengths of a structure under load. The determination of the onset of nonlinearity and degradation of material properties is much easier to determine for a unidirectional test specimen than it is for some general laminate. This is due to the nonlinear behaviour of general laminate configurations from the onset of loading. Furthermore, it would be uneconomical to establish allowable strengths for all possible orientations of laminates that may be utilized.

It is much simpler tc establish strength allowables for each lamina based upon its constituents, their respective weight fractions and the void volume fraction. The resulting strains from the finite element analysis can then be transformed to the laminae axis and used to evaluate the lamina stresses in the principal material directions.

The material properties of the laminae constituents are customarily determined from tests in which the specimens are subjected to a uniaxial state of stress.

This necessitates a logical method of approach to the application of uniaxial strengths to multiaxial loading conditions. There are a number of failure criteria available in the literature that may be used to predict ply failure in a fiber composite laminate.

4.2 Binary Damage Model

Evaluation of the various strength criteria mentioned in the literature review is fairly straight forward with the exception of the Tsai-Wu failure theory. In this case we are dealing with a criterion that involves the use of interaction terms between the normal and shear stresses. In its expanded form, the Tsai-Hill failure criteria is given by

$$\begin{aligned} & F_1 \sigma_{11} + F_2 \sigma_{22} + F_3 \sigma_{33} + F_4 \tau_{12} + F_5 \tau_{23} + F_6 \tau_{31} \\ & \quad + F_{11} \sigma_{11}^2 + F_{22} \sigma_{22}^2 + F_{33} \sigma_{33}^2 \\ & \quad + F_{44} \tau_{12}^2 + F_{55} \tau_{23}^2 + F_{66} \tau_{31}^2 \\ & \quad + 2 F_{12} \sigma_{11} \sigma_{22} + 2 F_{13} \sigma_{11} \sigma_{33} + 2 F_{14} \sigma_{11} \tau_{12} \\ & \quad + 2 F_{15} \sigma_{11} \tau_{13} + 2 F_{16} \sigma_{11} \tau_{31} \\ & \quad + 2 F_{23} \sigma_{22} \sigma_{33} + 2 F_{24} \sigma_{22} \tau_{12} + 2 F_{25} \sigma_{22} \tau_{13} \\ & \quad + 2 F_{26} \sigma_{22} \tau_{31} \\ & \quad + 2 F_{34} \sigma_{33} \tau_{12} + 2 F_{35} \sigma_{33} \tau_{23} + 2 F_{36} \sigma_{33} \tau_{31} \\ & \quad + 2 F_{45} \tau_{12} \tau_{13} + 2 F_{46} \tau_{12} \tau_{31} \\ & \quad + 2 F_{56} \tau_{23} \tau_{31} = 1 \end{aligned} \tag{4.2.01}$$

where the symmetry of the tensor has been used to reduce the number of independent components.

The engineering strengths are related to the strength tensors in the same manner that the engineering constants are related to the components of the elastic compliance matrix. For the case of a uniaxial state of stress in the i-direction, the criterion simplifies to

$$F_i \sigma_{ii} + F_{ii} \sigma_{ii}^2 = 1 \qquad (4.2.02)$$

where summation over the repeated indices is not implied. If S_{iC} and S_{iT} are the measured compressive and tensile strengths respectively in the i-direction, then it can be shown that

$$\begin{aligned} F_1 &= (1/S_{1T}) - (1/S_{1C}) & F_{11} &= (S_{1C}S_{1T})^{-1} \\ F_2 &= (1/S_{2T}) - (1/S_{2C}) & F_{22} &= (S_{2C}S_{2T})^{-1} \\ F_3 &= (1/S_{3T}) - (1/S_{3C}) & F_{33} &= (S_{3C}S_{3T})^{-1} \end{aligned} \qquad (4.2.03)$$

Similarly, if S_{ij} and S_{ji} are taken as the measured positive and negative shear strengths in ij-plane, then the imposition a state of pure shear in the three orthogonal planes gives

$$\begin{aligned} F_4 &= (1/S_{12}) - (1/S_{21}) & F_{44} &= (S_{12}S_{21})^{-1} \\ F_5 &= (1/S_{23}) - (1/S_{32}) & F_{55} &= (S_{23}S_{32})^{-1} \\ F_6 &= (1/S_{31}) - (1/S_{13}) & F_{66} &= (S_{31}S_{13})^{-1} \end{aligned} \qquad (4.2.04)$$

Thus all six linear terms F_i and all six diagonal terms F_{ii} are easily established. In general the magnitudes of the shear strengths in any given plane are the same but of opposite sign, resulting in the disappearance of all three of the shear interaction diagonal terms F_4, F_5 and F_6.

The off-diagonal terms are related to two stress components, and so require the imposition of a biaxial stress state in their determination. The ratio and sign of this biaxial stress state is arbitrary. For the case of the normal stress interaction terms F_{ij}, if the magnitudes of σ_{ii} and σ_{jj} are identical, we have

$$F_{ij} = (1/2\sigma^2) \{ 1 - [(1/S_{iT})-(1/S_{iC})+(1/S_{jT})-(1/S_{jC})] \sigma - [(1/S_{iC}S_{iT})+(1/S_{jC}S_{jT})] \sigma^2 \} \quad (4.2.05)$$

This test is rather expensive to perform. However there may be no need to perform such a test since it has been possible to correlate experimental data with the quadratic normal stress interaction terms set to zero [98]. Nonetheless Tsai [99] has suggested the use of

$$F_{ij} = - 1.0 / (2.0 [S_{iC} S_{iT} S_{jC} S_{jT}]^{\frac{1}{2}}) \quad (4.2.06)$$

as an alternative.

For the case of the remaining normal and shear stress interaction terms F_{ij}, if the magnitudes of σ_{ii} and σ_{jj} are identical, we have

$$F_{ij} = (1/2r^2) \{ 1 - [(1/S_{iT})-(1/S_{iC})+(1/S_{ij})-(1/S_{ji})] r - [(1/S_{iC}S_{iT})+(1/S_{ij}S_{ji})] r^2 \} \quad (4.2.07)$$

However if the material principal axis coincides with the longitudinal axis of the fibers then these terms must vanish. Therefore there is no need to compute them. For the case of a specially orthotropic lamina in the principal material axis it can be shown that the Tsai-Wu failure criterion simplifies to

$$\begin{aligned} &F_1 \sigma_{11} + F_2 \sigma_{22} + F_3 \sigma_{33} \\ &\quad + F_{11} \sigma_{11}^2 + F_{22} \sigma_{22}^2 + F_{33} \sigma_{33}^2 \\ &\quad + F_{44} \tau_{12}^2 + F_{55} \tau_{23}^2 + F_{66} \tau_{31}^2 \\ &\quad + 2 F_{12} \sigma_{11} \sigma_{22} + 2 F_{13} \sigma_{11} \sigma_{33} \\ &\quad + 2 F_{23} \sigma_{22} \sigma_{33} = 1 \end{aligned} \quad (4.2.08)$$

Since this failure criterion is formulated in the principal axis of the laminate, its utility in the global reference axis is contingent upon transformation to the latter. It is instructive to express this failure criterion in laminate coordinates for analysis of failure at free edges and surfaces where selected stress components must vanish. Doing so gives

$$
\begin{aligned}
&F_1\,\sigma_{xx} + F_2\,\sigma_{yy} + F_3\,\sigma_{zz} + F_4\,\sigma_{xy} \\
&\quad + F_{11}\,\sigma_{xx}^2 + F_{22}\,\sigma_{yy}^2 + F_{33}\,\sigma_{zz}^2 \\
&\quad + F_{44}\,\tau_{xy}^2 + F_{55}\,\tau_{yz}^2 + F_{66}\,\tau_{zx}^2 \\
&\quad + 2\,F_{12}\,\sigma_{xx}\,\sigma_{yy} + 2\,F_{13}\,\sigma_{xx}\,\sigma_{zz} + 2\,F_{14}\,\sigma_{xx}\,\tau_{xy} \\
&\quad + 2\,F_{23}\,\sigma_{yy}\,\sigma_{zz} + 2\,F_{24}\,\sigma_{yy}\,\tau_{xy} \\
&\quad + 2\,F_{34}\,\sigma_{zz}\,\tau_{xy} + 2\,F_{56}\,\tau_{yz}\,\tau_{zx} = 1
\end{aligned}
\qquad (4.2.09)
$$

Alternatively, one can transform the strains in the global reference axis to the principal material axis using the inverse transformation. The criteria may then be utilized by evaluating the stresses from these transformed strains.

Binary failure models provide an envelope within which the material is considered to be safe. They in themselves do not provide any means to model material degradation. This requires the use of damage mechanics to model the degradation of the material properties as a function of the applied load.

4.3 Progressive Damage Model

Fiber composites generally fail by microvoid coalescence, interfacial debonding and fiber breakage resulting in a degradation in the mechanical stiffness and strength. The failure is highly dependent upon the direction of the applied load due to the material anisotropy. Therefore in order to use damage mechanics in the prediction of material behaviour, the parameter used

to represent the damage growth must take this into account. One way to do this is through the use of several damage parameters that model degradation of material behaviour by altering the material engineering constants. The change in the engineering constants can be modelled by

$$\begin{aligned} E_{11} &= E_{11}^{\circ}(1-D_{m1}) & G_{12} &= G_{12}^{\circ}(1-D_{m4}) \\ E_{22} &= E_{22}^{\circ}(1-D_{m2}) & G_{23} &= G_{23}^{\circ}(1-D_{m5}) \\ E_{33} &= E_{33}^{\circ}(1-D_{m3}) & G_{31} &= G_{31}^{\circ}(1-D_{m6}) \end{aligned} \qquad (4.3.01)$$

The prediction of the mechanical behaviour also needs to account for the damage growth. This requires a parametric description of the mechanical behaviour. One can use the effective stress approach as outlined in the literature review, with the damage parameter related to the change in the void volume fraction. However it is difficult to obtain a quantitative measure of the volume change.

The overall effect of the evolution of the damage parameter is to introduce nonlinearity in the material behaviour. Experimental studies have shown that this nonlinearity is manifest by a step change in the load deflection curve [100]. Thus we may make the assumption that the material behaviour can be modelled by a piecewise linear function of the damage parameter. This being the

case, the damaged behaviour may be represented by altering the material engineering constants in a similar manner.

The damage parameters may be determined experimentally by use of uniaxial tension tests. In the case of D_{m1}, a single lamina with the fibers oriented parallel to the loading direction will yield a load deflection curve that is monotonic to failure. This is due to the fibers carrying the bulk of the load. Once the fibers fail, the binder would already be saturated with microcracks, and will not be able to sustain the redistributed load. It would be reasonable therefore to assume that this parameter jumps from zero to unity at the failure load. The nonlinearity due to the statistical distribution of the individual fibers would be minor, but easily accounted for if required.

The determination of D_{m2} may be made by loading a single lamina with the fibers perpendicular to the loading direction. The load deflection curve in this case will resemble a discontinuous function with several abrupt changes in the slope. The slope changes are indicative of an increasing number of microcracks that reduce the transverse stiffness to the point of failure. The damage parameter may be computed for the i'th step change as

$$D_{m2i} = [1-(E_i/E^\circ)] \qquad (4.3.02)$$

It is difficult to separate the effects of D_{m2} and D_{m3}. It is quite possible that the latter may be affected by the laminate thickness due to the material constraints away from the surface. However since the individual laminae are assumed to be orthotropic, it may be assumed that the two damage parameters follow an identical evolution law.

The shear damage parameter D_{m4} may be evaluated by a uniaxial tension test on a symmetric crossply laminate with the fibers oriented at an angle of 45° to the loading direction. The resulting load deflection curve will again be similar to that obtained for D_{m2}. In this case the damage growth will be representative of interlaminar delamination as well as microcracking. The slope will again be represented by a discontinuous function, so this damage parameter may be computed in a similar manner as above using the change in shear modulus. Also, the variation of D_{m6} may be assumed to be the same as that of D_{m4}.

The remaining damage parameter D_{m5} may be taken to represent the damage growth in the laminate due to shear applied in a plane perpendicular to the fibers. The damage in this case will be representative of the generation of microcracks and interlaminar delamination as for D_{m4}, however the evolution of this damage parameter

cannot be taken to be the same. This is because of the different constraints due to the fiber orientation. One can assume isotropic damage in this case due to the makeup of the individual lamina in this plane.

4.4 Energy Absorption

For elastic deflections the area under the load deflection curve can be used as a measure of the recoverable energy absorbed by the structure. This energy can also be computed by integrating the strain energy density over the volume.

$$En_S = \tfrac{1}{2} \int \{\sigma\}^T\{\epsilon\}\ dVol \qquad (4.4.01)$$

Since there is more than one ply through the element thickness, it is necessary to perform the integration within each ply and sum over the total volume. This recoverable strain energy will not vary linearly with increasing load due to material failure, so it is necessary to perform the integration at each load step.

Local point failure is characterized by the formation of various defects ranging from microvoid coalescence to through thickness cracks. The formation of these defects results in the lowering of the strain energy density

around the failed point. Defect formation may be modelled by a modified Griffith [101] approach, whereby material failure is treated as resulting in the formation of a strain free volume surrounding the failed point. The strain energy available is equated to the energy of the new surfaces created by the defects.

Consider a structure loaded to a given stress level. If no material degradation has occurred, the elastic strain energy stored in the volume around the integration point is given by the above equation. Two running totals are kept for each ply of each element at each load level; a recoverable total and a nonrecoverable total. If the integration point remains in the elastic region, the strain energy is added to the recoverable total.

If the integration point experiences an overload as defined by one of the failure criteria, the strain energy is added to the nonrecoverable total and the point marked as failed. The corresponding void volume fraction is set to 0·95, which will result in a greatly reduced contribution to the material properties from this point. A value of unity is not used to avoid numerical problems with the global stiffness matrix. Alternatively the elastic properties may be obtained in the usual manner, and then reduced to some insignificant fraction of their

original value. In either case, further contributions from this point to either total are ignored.

Defect formation may also be modelled by using the damage analysis approach. As the load is increased, material failure will result in a jump displacement, giving a new value of strain for the same stress level. The difference in the stored strain energy can be used to compute the energy lost due to failure.

Consider a structure loaded to a given level ${}^1P$. If no material degradation has occurred, the elastic strain energy stored in the volume around the integration point is given by

$$ {}^1En_S = \tfrac{1}{2} \int \{{}^1\sigma\}^T\{{}^1\epsilon\}\, dVol \qquad (4.4.02) $$

Consider now a further increase in the applied load to ${}^2P$. If there is again no material degradation, the stored elastic strain energy will be a function of the load. In this case we have

$$ {}^2En_S = {}^1En_S\ ({}^2P/{}^1P)^2 \qquad (4.4.03) $$

However, if material degradation has occurred a jump displacement will have taken place during the loading. The response of the material will still be linear, but now

with a different set of material constants. The stored strain energy in this case will be given by

$$ {}^{2}En_{S}^{*} = \tfrac{1}{2} \int \{{}^{2}\sigma\}^{T}\{{}^{2}\epsilon\}\, dVol \qquad (4.4.04) $$

The energy lost due to defect formation will then be given by the difference of the last two equations.

$$ {}^{12}En = {}^{1}En_{S}\,({}^{2}P/{}^{1}P)^{2} - \tfrac{1}{2} \int \{{}^{2}\sigma\}^{T}\{{}^{2}\epsilon\}\, dVol \qquad (4.4.05) $$

The process is then repeated for the next load step. In general the lost strain energy for the j'th load step is computed from

$$ {}^{ij}En = {}^{i}En_{S}\,({}^{j}P/{}^{i}P) - (1/2) \int \{{}^{j}\sigma\}^{T}\{{}^{j}\epsilon\}\, dVol \qquad (4.4.06) $$

where i=j-1.

The main drawback in using this approach is that only the stress state at the end of the load increment is known. The location of the jump displacement is not. Also, if the load increment is too large several jumps may be missed. This problem can be alleviated by lowering the

load increment and resolving from the previous known stress state until failure is no longer detected. The load is then incremented by the new value. This will guarantee that the jump occurs at the end of the load step (Fig 3).

In computing the lost energy there is a tacit assumption that the strains in the structure vanish upon unloading. This is not always the case. However since the degraded material constants are known, and since the material is still assumed to be linearly elastic, it is possible to determine the intercept on the strain axis for a zero state of stress. This can then be used to evaluate the elastic strains by taking the difference between the current strains and the intercept strains. This difference can then be used to compute the strain energy for the current load step. Thus, for the j'th load step

$$ {}^{j}En_{S}^{*} = \tfrac{1}{2} \int \{{}^{j}\sigma\}^{T}\{{}^{j}\epsilon - {}^{0j}\epsilon\}\, dVol \qquad (4.4.07) $$

where $\{{}^{0j}\epsilon\}$ are the intercept strains. In the case where the intercept strains are zero, this reduces to equation (4.4.04).

4.5 Structural Failure

Either of the above approaches will give an indication of the failure state throughout the structure at the integration point level. However this approach leads to another problem. Whereas before the traditional approach to failure was overly conservative, this one is overly generous. It is now possible for structures having suffered material overloads to be considered as failed long before total material failure has occurred. Some overall failure limit needs to be defined.

This problem may be overcome by using the ratio of the stored and lost strain energies. As the structure is loaded the total energy lost at each load step is summed. As this happens the recoverable elastic strain energy stored in the structure will diminish. Eventually a point will be reached at which the recoverable energy will be equal to the energy lost. Eventually the structure will have failed to the point where no appreciable strain energy can be stored, and no further degradation is possible.

The ratio of the stored and lost strain energies may be used to determine the limit for structural failure, and will depend to a large extent on the application involved. In the case of energy absorption, a failure limit of V50 is often used. This indicates the velocity at which 50%

of any given projectile type will penetrate the armor. Similarly, for this application a 1:1 ratio of the stored and lost energies can be used to delimit structural failure.

5.0 FEA Code

5.1 Implementation

The end result of this study was to devise a method whereby laminated fiber composites could be ranked in terms of their energy absorption capabilities as a function of the known loading conditions, the laminate constituents, the laminae orientations, their relative abundances and their respective material properties. To this end the above formulation has been incorporated into a special purpose finite element code that can be used to predict the small deflection response of laminated fiber composite structures. The code was written in standard FORTRAN-77 to run on an IBM compatible personal computer, and can easily be altered to run on any machine with a standard FORTRAN compiler by changing the machine dependent parameters. The code has been successfully run on a Digital Equipment VAX 11/730 and a Silicon Graphics 4D/2206TX Work Station.

The FEA code was written in three parts due to the memory limitations of the PC. These parts consist of an input processor, a main analysis section, and an output processor. The first of these sets up the required files for the main finite element analysis. The last extracts

the relevant information from the binary storage files, and writes it to an ASCII file that may be read in the ordinary fashion. The output processor also includes the necessary graphics interfaces.

In addition to the main set of FEA codes, there were three separate programs written in a supporting role. The first (CLPA) was a program implementing the Classical Laminated Plate Analysis to verify the predictions of the FEA code for thin laminates. The next two (GSSM and EMSM) generate the generalized stress strain matrix and the element stiffness & mass matrices from knowledge of the lamina constituents. These two independent programs use the same basic routines as the main code, and may be used to interface the modified element formulation with existing FE codes for a non-linear and/or a dynamic analysis.

5.2 Elements

There are two element families implemented in the code. The Variable 9-Node Quadrilateral (V09Q) may be used to analyze certain problems that are amenable to a 2D examination. The full 3D analysis must use the Variable 20-Node Cuboid (V20C). These elements can be used to define 2D meshes with the number of nodes per

element varying from four to nine, and 3D meshes with the number of nodes per element varying from eight to twenty.

Although there are commercial codes that allow the analysis of fiber composite structures, the elements they employ are invariably modifications of plates or thick shells [102,103,104]. In all cases the material properties must be specified for the entire element at once. This is usually done by the use of separate laminate analysis routines. These routines are rarely provided with the code, requiring the user to generate this piece of information independently.

Both element families model multiple layers of material through the element thickness using the refined integration scheme previously described. The number of nodes used to describe the element geometry is independent of the number of layers through the element thickness, therefore higher order elements may be easily implemented in the code by the addition of the appropriate shape function routines.

5.3 Material

Before the overall element properties are used to describe the element behaviour, knowledge of the individual lamina properties must be known. Although

there are a large number of combinations and permutations when considering the makeup of a laminated fiber composite, there are nevertheless only a few building blocks from which these lamina are constructed. The material properties of these building blocks are fixed, and can be coded into a subroutine as a database. It is then a simple matter to add to the database. This is the approach adopted in the code. All that is required of the user is the binder and fiber of which the lamina is composed, along with their respective weight fractions and the volume fraction of voids.

The lamina properties are determined by another subroutine using the information provided above. These properties are used to evaluate the [D] matrix for any given point within the ply. The [D] matrix is then rotated into the global frame of reference before being incorporated into the overall element stiffness matrix.

5.4 Stresses

The solution of the simultaneous set of algebraic equations produced upon assembly of the element equations and application of the necessary boundary conditions is a vector of nodal displacements. The displacements over the whole structure can be determined by substitution of these nodal displacements into the assumed displacement

functions for the elements of interest. However application of a failure criterion requires a description of the stress field. This may be obtained by multiplying the material property matrix [D] by the strains at the point of interest. The evaluation of the strains is done through the derivatives of the assumed displacement functions.

Theoretically the strains and stresses may be evaluated at any point within the element. Unfortunately their order of convergence is lower than that of the displacements as the finite element mesh is refined. Some authors use the element node locations as the points at which the stresses are computed. However Barlow [105] has observed that the stresses are best computed at selected points based upon the order of interpolation of the displacement functions used to describe the element behavior. These points are usually chosen to be the same as the integration points used in the formulation of the element stiffness matrix.

For homogeneous isotropic materials the stresses are continuous within an element. This is a result of a constant material property matrix throughout the element volume. However in the case of the current composite element the [D] matrix is a function of the thickness coordinate, and is not necessarily constant even within

each ply. It is therefore necessary to compute the strains at each location of concern and use the appropriate [D] matrix at that location to obtain the stresses. There are two methods that may be employed.

The first method is to compute the strain-displacement matrix [B] within the ply of interest at the ply integration points, and use this to evaluate the strains. The second method is to evaluate the strains at those integration points based upon a homogeneous isotropic element, and then use some form of extrapolation to evaluate the strains for the individual plies.

In the case of laminated fiber composites the interlaminar stresses are of vital importance in the determination of laminate failure. The stresses at the ply boundaries will control the delamination mode of failure for the laminate. Consequently the locations of the evaluation points may be chosen to be the Gauss coordinates in the longitudinal and transverse directions and the ply boundaries in the thickness direction. An additional set of points may be chosen located at the midpoint of each ply face. These points may be referred to as semi-Gauss points.

Although the node locations are not the best place to compute the stresses in terms of accuracy, sometimes

comparison of results with other references may require this to done. In the case of the composite element, the ply corner and edge locations corresponding to a single element may be chosen. Since each option has its advantages, all three are implemented in the FEA code.

5.5 Failure Routines

There are four models of failure coded into the program that may be used to determine material failure. The first three of these are the binary models of Rankine, Hoffman and Tsai-Wu. The stresses at each evaluation point are computed in the principal axis of the lamina, and compared to the strengths computed from the lamina constituents. A failed point may be marked by setting its associated void volume fraction to 95%. This will avoid the numerical difficulties that may be encountered in the solution of the global stiffness matrix.

The progressive damage model is the fourth criteria that may be used. In this case the variation of each damage parameter must be specified as a function of the load level. This is best obtained from experiments on coupon specimens. The variation is tracked for each parameter at each evaluation point as the material is loaded, with the appropriate parameter used to modify the

elastic constants of the lamina when the material property matrix is computed.

The binary damage models described above are usually implemented in commercial codes in 2D since only these kinds of elements are used. All models used in the FEA codes described here have been expanded to cover 3D stress distributions. Since it is not always possible to use one failure criterion for the entire laminate, each of the above may be individually specified for any one given ply.

Before any of the above criteria can be utilized, it is necessary to evaluate the laminate strengths as a function of the constituents. This is done by the same subroutine that computes the lamina properties. Since these strengths are referred to the lamina principal axis, the strains from the FE analysis are rotated into this reference frame before using the point [D] matrix to evaluate the stresses.

5.6 Damage Tracking

Tracking damage progression with applied loading is an important ability in the analysis of fiber composite laminates. The onset of damage occurs at a specific applied load level which is generally not known

beforehand. In an actual experimental test the load is applied gradually, and material failure monitored as a function of the applied load. This can be easily simulated in an FEA code.

The program allows the load vector to be incremented in steps. Once the element stiffness matrices have been computed and assembled, the displacements are solved for some initial value of the applied load. These are used to compute the stresses, which in turn are used in the failure routines described above. If no failures have occurred, the load vector is incremented and the process repeated. If failure has occurred within an element, the location is marked, and the affected element stiffness matrix is regenerated with the relevant modification in the ply properties. The global stiffness matrix is then reassembled, and a new solution found for the same load vector. The process is repeated until there are no further failures for that load vector. The load vector is then incremented to the next value, and the process repeated. In this way it is possible to track the progression of damage in the structure.

6.0 Verification

6.1 One Element Example

The FEA code described in the previous chapter was written from the bottom up, with each subroutine being tested on its own before being integrated into the main code. Numerical verification of the algorithms was done using various textbook examples. The main parts of the code tested were the element stiffness routines, the boundary condition routines, the equations solver routines, the stress evaluation routines and finally the failure criteria routines. Numerical verification of the integrated code was done by comparison with theory and with a previously available general purpose code (INDAP) [106].

The first problem solved was taken from Grandin [107]. This was a single 4-node quadrilateral with two nodes fixed and concentrated loads applied at the remaining two nodes (Fig 4). Although the material of the element was the same through the thickness, ten plies were used to test the integration scheme. The results obtained from the FEA code using the new composite element were in excellent agreement with those from the text.

6.2 Patch Test

The use of any element formulation is contingent upon the verification of the element's ability to reproduce the observed behaviour of the structure it is used to model. Before such verification studies can be undertaken, it is necessary to prove that the element will converge to an acceptable solution as the mesh model is refined. Confirmation of element convergence is guaranteed by passing what is generally known as the patch test [108]. This test requires that a patch of elements be able to reproduce all of the constant states of stress when subjected to the appropriate boundary and loading conditions. The requirement arises from the condition that as the mesh model is refined, the size of the elements in the mesh will be small enough that the stress variation within the element will be negligible. This test provides a necessary and sufficient condition to guarantee monotonic convergence under the required conditions.

The test involved a patch of sixteen 4-node quadrilaterals [109] to determine the validity of the new formulation as well as its implementation (Fig 5). Constant states of stress for σ_{xx}, σ_{yy} and τ_{xy} were correctly reproduced with the appropriate boundary and loading conditions as required. Following this, a pure

bending moment was applied as shown in figure 5, and the stresses in the middle of elements #5 to #8 were evaluated and compared with those obtained from beam theory. The deflected shape is shown in figure 5, and a graphical comparison of σ_{xx} is given in figure 6. The agreement between the FEA analysis and beam theory was within 3%.

6.3 Convergence Test

The patch test provides for a guarantee that a given element formulation will converge to a solution, but not that it would converge to the right solution. In order to confirm the convergence of the modified element formulation, the problem of a laminated bar was investigated (Fig 7). The bar was 1 inch (2·54 cm) square in crossection and 8 inches (20·32 cm) long. It was composed of two equal thickness layers of aluminium and steel, with the top layer being steel. At one end of the bar all nodes were fixed in all directions, while a uniformly distributed load of 1000 psi (6·89 MPa) was applied to the opposite end, in a direction away from the fixed end and parallel to the long axis of the bar.

The element formulation described above was tested using various 2D and 3D elements. In each case, from one to eight elements were used, with each mesh refinement included in the old mesh. Table 1 compares the strain

energy convergence for the various elements and meshes. Figure 7 illustrates the computed deformation, with the dotted lines representing the undeformed mesh. All deflections have been magnified by a factor of 1000.

The upper part of the table gives results for the modified elements using from one to eight elements along the length, and one element to represent the thickness. The lower part of the table gives results from a separate code (INDAP) using one element per ply through the thickness. The LB designation refers to the Laminated Bar mesh. The next two numbers refer to the number of nodes per element, and the final letter indicates the use of either a quadrilateral (Q), or a cuboid (C) element. The results were obtained on a Zenith ZF-158 with an 8087 math coprocessor using Lahey F77, and verified of a Silicon Graphics 4D/2206TX Work Station.

The same results were obtained using the modified element formulation with two elements used to represent the thickness. All elements indicated good convergence (Fig 8) in that the difference in the stored elastic strain energies for the last two cases was of the order of 5%.

As is apparent from the deformed mesh, the resulting deflection along the middle of the bar was a combination

of extension and bending, the latter due to the coupling introduced by the unbalanced construction. A rough estimate of the horizontal deflection of the loaded end was determined by assuming an equivalent modulus for the bar and applying Castigliano's Theorem [110]. The vertical deflection of the loaded end at the midplane was evaluated by assuming an equivalent flexural rigidity [111] and applying the Second Moment-Area Theorem [112]. The stored elastic strain energy was determined using energy methods [113].

A comparison of the results from the FEA code with those obtained from theory is given in Table 2. The sixteen element models (LB09Q8x2 & LB20C8x2) were used to compare the results of the FEA code with INDAP. Only one ply was assigned to each element for these cases. The results of the two codes were found to be identical. The eight element models (LB09Q008 & LB20C008) were used to obtain a comparison of the composite element results with the normal elements used in other codes. In this case each element was assigned two plies through the laminate thickness. Again, the results were in good agreement in that the variations were less than 1%.

6.4 Reinforcement Interactions

Fiber composite laminates can display some rather unorthodox behaviour under certain loading conditions that is at variance with normal homogeneous materials. For instance, a strip of homogeneous material subjected to uniaxial tension will exhibit an extension in the direction of the applied force, and a contraction due to Poisson effects in the width and thickness directions. In addition, an anisotropic material will also undergo shearing deformation in planes parallel to the coordinate planes.

Consider the case of an off-axis laminated strip subjected to a uniform normal stress along its length (Fig 9). If the ends are free to displace, then the inplane shearing stresses result in shearing strains that cause the strip to distort into the shape of a parallelogram. However if movement of the ends of the strip is constrained in such a manner as to prevent lateral and rotational displacement (simulating clamped ends), additional shearing forces and bending couples will be induced. These induced loads will result in an S-shaped deformation pattern that has been experimentally verified by Pagano & Halpin [114] using a nylon reinforced rubber composite with various length to width ratios.

To verify this type of behaviour, a laminated strip consisting of four plies of a Kevlar/Epoxy composite was modelled using a 20 element mesh with a length to width ratio of 4:1. The strip was fixed at one end, and a uniform prescribed longitudinal displacement was applied to the other end. The character of the resulting deformation response (Fig 10) is similar to that given by the analytical solution provided in the above reference. The mesh deflections shown in Figure 10 are magnified by a factor of 1000.

6.5 Lamina Coupling

One of the unique aspects of fiber composite behaviour is the coupling that arises out of unbalanced constructions and the effect of the free edge on the delamination of laminated plates [115]. The bending and stretching coupling caused by the unbalanced construction of the laminated bar described above is evident. However to better illustrate this, the case of an unsymmetric layup of a four ply square plate was investigated (Fig 11). At one of the plate edges all nodes were fixed in all directions, while a uniformly distributed load of 1000 psi (6·89 MPa) was applied at the opposite edge in a direction away from the fixed edge and parallel to the plate surface. The plate was represented

by a 25 element mesh using the variable 20-node cuboid. The plate was 5 in (12·7 cm) on a side and 1 in (2·54 cm) thick. The layup sequence used was (00,-05,+05,00).

The deflection of the loaded plate illustrates the bending and stretching coupling phenomenon arising from unsymmetrical laminate constructions (Fig 12). The undeformed mesh is represented by the dotted lines. The displacements in the figure have been magnified by a factor of 1000. Similar behaviour was found by Ashton et al [116] for a ±30 degree layup (Fig 13).

The twisting behaviour arises from the unbalanced moments produced by the nonuniform through thickness shear stress distribution (Fig 14). Application of an off-axis tensile load results in the fibers tending to line up with the loading direction. This realignment is restricted by the presence of the surrounding plies, so a shearing stress is created in each off-axis ply. The direction of this shearing stress is reversed in the two off-axis plies, and since each is on the other side of the midplane, a torque results that tends to twist the laminate.

In spite of the fact that the fiber orientations are symmetric with respect to the load direction, it is impossible to pull on this kind of a laminate without

bending and/or twisting it at the same time. Neither can such a laminate be subjected to a moment without inducing extensional deformations. This behaviour has important implications from the standpoint of construction, in that for certain applications the lamina orientation angle must be tightly controlled to avoid unwanted behaviour in balanced symmetric laminates. Of particular importance is the use of laminated composites in high performance aircraft. For example, the wing torque box of the F-15 Eagle uses a Boron/Epoxy laminated skin bonded to Graphite/Epoxy ribs and supported by two main spars of titanium [117]. High positive G-loads induce high tensile stresses on the bottom surface, and high compressive stress on the top surface. If the construction is not properly balanced, the skin will tend to debond in flight.

6.6 Tensile Behaviour

The safe design of engineering structures takes into account the limitations of the materials used in making up the elements of the structure. These limitations are generally related to some form of failure criteria that the constituent materials must be able to meet, multiplied by a safety factor that is dependent upon the application. The failure criteria used in the design process are based upon the experimentally determined properties of the

materials used. Even though multi-axial loading conditions may prevail in the finished structure, the criteria are still based upon the results from uniaxial tension or compression tests. These mechanical tests form the basis of the design efforts, and so must be carefully implemented.

The situation for structures of laminated fiber composites is complicated by the fact that the material properties may be dependent upon not only the orientation of the test specimen with respect to the applied load, but also with the direction of the load application. This requires a logical approach in the application of the chosen failure criteria to multi-axial loading conditions. The selection of the specimen shape and testing methodology must take into account the manner in which the material will be actually utilized. It is important that the design of the specimen be such that neither it nor the test fixture will have an influence on the reproducibility of the test results. Yet the test method itself has to be simple to use.

In the case of orthotropic materials, the test method must take into account the peculiarities of their behaviour, otherwise major inaccuracies may result during reduction of the raw data. For instance, the statistical variability in the individual fiber strengths results in a

hump when the tensile strength is determined as a function of the specimen thickness. The apparent decrease in the tensile strength for small specimen thicknesses is due to the presence of surface defects [118]. The decrease for large thicknesses is due to the increased probability of encountering defects in the greater crossectional area of larger specimens. This scale effect is anisotropic, and is largest in the direction in which the greatest dimensional change occurs.

The use of standard test methods such as those recommended by ASTM overcomes some of the problems associated with the reproducibility of test data. The relevant standard for the tensile strength of unidirectional crossplied composite specimens is ASTM D3039. This method gives recommended specimen dimensions for several tensile coupons, and sets a limit on the size of the test specimen that is dependent upon the lamination type.

When specimens of this nature are tested, they are fitted with bonded fiberglass or aluminum end tabs in an attempt to lower the longitudinal stresses near the ends and minimize the end effects. ASTM D3039 recommends the use of bonded glass/epoxy end tabs with a 5 degree taper. The tapered section of the tabs is usually placed outside of the jaws, with the flat area inside the grips. However

it is easier and cheaper to manufacture end tabs without any taper. Also, the specimen extension is usually measured by a clip gauge having a gauge length of from ½ to 1 inch (1·27 to 2·54 cm). Since several specimens are usually required for a good statistical result, they are cut from one sheet onto which the end tabs are co-cured. To cut down on costs, these specimens may also be cut to a shorter length. The end result is that the actual test specimen may not conform exactly to the ASTM standard. The variations may be minor, and it is often argued that they have little effect on the overall result.

The growth of damage in a fiber composite tensile specimen is strongly dependent upon the loading history it is subjected to. There are two kinds of tensile testing machines in use. The oldest machines are screw driven, and subject the specimen to a constant rate of extension. Tests done on these machines are referred to as displacement controlled. The newer servo-hydraulic machines are capable of applying a monotonically increasing load to the specimen. Tests done on these machines are referred to as load controlled. Although both kinds of tests will give the same failure load, the tensile behaviour will be different.

Consider the case of a $(0,90)_S$ fiber composite tensile specimen subjected to a displacement controlled

test. Ideally, as the specimen is loaded, a uniform state of stress is produced along its length. As the failure load is attained, the specimen fails catastrophically along its entire length. In reality however, this is not what happens. What is generally found is that as the failure load is approached, dips in the load-displacement curve begin to appear. The load drops and rises several times as the inner 90 degree plies fail, and then continues to rise at a different slope.

This behaviour is due mainly to the constraints applied to the specimen ends. Immediately outside of the jaws, the longitudinal constraint is relaxed, however the lateral constraint still has some effect on the deformation. Close to the jaws, as the specimen extends along its length, Poisson contraction in the width direction is prevented from taking place. This in turn results in a higher stress in the direction of the applied load at the location of the constraints. These end effects diminish as the distance from the ends is increased. The result is a limit on the minimum size of specimen that can be used for a valid tensile test.

The size and shape of the coupon specimens used in tension tests is designed to give a constant state of stress along a specified gauge length, within which the extension of the test piece is measured. It is imperative

that the stress be constant within the gauge length, otherwise the results will not accurately reflect the material properties.

Outside of the gauge length, the stress distribution becomes nonuniform due to the constraints imposed upon the ends of the specimen. These constraints are brought about by the requirement to grip the test piece. In most cases the ends of the specimen are clamped by a compressive force applied by the jaws into which the specimen is inserted. Therefore movement is restricted in the width and longitudinal direction within the jaws.

Clearly the longitudinal stress distribution is not uniform throughout the full length of the specimen. Therefore as the load is increased, points closer to the ends will fail first, resulting in a drop in the load. As the applied displacement is increased, points closer to the center of the specimen will fail, resulting in another load drop. This will continue until the 90 degree plies fail completely.

Figure 15 shows a photomicrograph of the crossection of a $(00,90)_S$ laminate with a crack through the 90 degree plies. The outer fibers lie parallel to the plane of the paper, and the inner fibers perpendicular to it. The thick dark lines between the 0 degree and 90 degree plies

are resin rich areas. There is also a resin rich area between the two 90 degree plies in the middle of the laminate. The crack in the 90 degree plies runs vertically all the way from top to bottom. The vertical white lines are defects in the photograph.

Since the 90 degree plies will no longer be contributing to the specimen stiffness after failure, the load-displacement curve will have a different slope. From simple mechanics of materials, this new slope will be given by

$$M_f = M_i \frac{(n_{00} E_{00})}{(n_{00} E_{00}) + (n_{90} E_{90})} \qquad (6.6.01)$$

where

M_i = Initial slope

n_{00} = Number of 0 degree plies

n_{90} = Number of 90 degree plies

E_{00} = Elastic modulus of 0 degree plies

E_{90} = Elastic modulus of 90 degree plies

Analysis of the stress distribution brought about by the constraints using elementary mechanics is futile, since these methods assume a constant state of stress in the first place. Elasticity methods using the stress function approach may yield good results, however the expressions utilized can become fairly complicated. The

finite element method provides an avenue that overcomes these objections.

Verification of this behaviour was done by modelling a tensile specimen using a mesh of from 7 to 22 elements. The specimen consisted of a 4-ply Glass/Epoxy Laminate. Each element was one inch (2·54 cm) square and 0·2 inches (0·51 cm) deep. The first and last elements of the mesh model were given the properties of aluminum. One end of the specimen was fixed in all directions, and a uniform prescribed displacement applied to the other end. The Tsai-Wu criterion was used as the failure model.

The longitudinal stress distribution for one of the middle plies shows the expected variation (Fig 16). Evidently a specimen length of less than 5 inches (12·70 cm) is inadequate for a reliable evaluation of the tensile strength. The distribution of the same stress through the specimen thickness (Fig 17) indicates that this stress is lower in the middle plies than in the outer plies. Nevertheless, the middle plies fail first due to their lower strength in the direction of the specimen length. A specimen modelled with 12 elements was used to verify the load-displacement behaviour (Fig 18). The expected load drops and change in slope were observed.

The load drops observed in a displacement controlled test are replaced by displacement jumps in a load controlled test (Fig 19). When failure occurs at a specific point, the load is redistributed, and carried by the surrounding unfailed material. The total applied load remains constant due to the nature of the test. Since material failure constitutes a lowering of the overall laminate stiffness, a jump in the displacement trace occurs.

The above examples verify the expected behaviour of the modified element in a qualitative manner. Quantitative verification requires knowledge of the makeup of the fiber composites used in the experiments in terms of their respective volume fractions and relative abundances. Unfortunately, the exact type of binder and/or reinforcement is usually not provided. What is provided is the lamination sequence, the generic type of binder, the generic type of reinforcement and an overall stiffness of the laminate.

Nevertheless it is possible to infer the volume fraction ratios of the components from tensile tests if sufficient information is available. Whitney et al [119], performed experimental tests to determine the behaviour of $(0_m, 90_n)_s$ laminates under tension. Though they do not provide load-displacement traces, their stress-strain

curves indicate that the tests were done under load control. Using their data for a $(0_1,90_3)_s$ laminate along with the initial stiffness provided and the assumption of 0·2% voids, it was determined that their specimen was made up of 65% by weight of fiber. Table 3 compares the results of an analysis using both CLPA and the FEA code with those from the above reference.

The FEA analysis indicated a stiffness drop after failure of the 90 degree plies of 45%. This is identical to the drop predicted by CLPA, and compares well with the drop determined from the graph given in the above reference, which was 42%. The above reference also reports a stress-strain curve for a $(0_2,90_2)_s$ laminate. However in this case no displacement jump is reported. Only a knee in the stiffness response is noted. In contrast, a finite element analysis of this laminate indicated the presence of a displacement jump similar to but of significantly less magnitude than for the $(0_1,90_3)_s$ laminate. The drop in stiffness for this laminate was found to be 22%, which is again the same as that predicted by CLPA. The corresponding drop from the above reference is 27%.

The lower part of the table compares the failure stress and strain from the FE analysis with those obtained from the curves of the above reference. The results for

the failure strains show good agreement for both laminates. The failure stress for the $(0_{1},90_{3})_{s}$ laminate also shows good agreement, however that for the $(0_{2},90_{2})_{s}$ laminate indicates a difference of about 18%.

Experimental tests on fiber composite specimens generally yield from a five to fifteen percent variation in terms of replication of the data. These variations are caused by changes in a number of parameters. For instance, changes in the cure temperature and pressure may affect the degree of compaction of the fibers and the rate of extraction of the volatiles from the curing process as well as the final properties of the binder. The extraction of volatiles is also affected by the laminate thickness and by the type of bleeder and release film used. Strength and stiffness properties can be affected by small changes in the fiber orientation and contiguity for hand layups.

Another consideration in the duplication of the data is the dimension of the specimens. It is evident from the above that past a certain point, the tensile results will depend upon the length of the specimen. The same is true for variations in the specimen width [120]. Furthermore, Whitney et al do not indicate exactly how their measurements for strain were made. There are two common ways to do this. One method uses a bi-axial

dual sensor strain transducer to measure the extension along a given gauge length. Another uses a bonded electrical resistance strain gauge. The latter method requires correction factors that are ignored by the standard ASTM test methods. This can result in significant reinforcement error [121]. When considering these factors along with the realization that the binder material was unknown, the failure strengths predicted by the FEA code show good agreement with those from the reference.

7.0 Element Capabilities

7.1 Introduction

The derivation of the classical theory of laminated plates considers only the inplane stresses. There is no account taken of the through thickness stress σ_{zz}, nor of the out-of-plane shearing strains τ_{yz} and τ_{zx}. Accordingly, the classical approach is unable to provide predictions of some of the stresses that actually lead to laminate failure. Also, CLPA is incapable of predicting certain types of behaviour due to the nature of it's formulation. Some of these have to do with the deformations at the edges of angle ply laminates, and the existence of through thickness stresses. The use of a 3D finite element analysis overcomes many of these limitations, as will be described below.

7.2 Interlaminar Stresses

The extensional stresses predicted by classical lamination theory are unaffected by the stacking sequence used in the make up of the laminate. In contrast, the strength of symmetric angle ply laminates subjected to inplane loading have been observed to show a dependence upon the laminate stacking sequence [122]. In particular,

delaminations have been observed to begin at the free edges [123], with progressive delamination being the failure mode in fatigue. Pagano and Pipes [124] have postulated that the interlaminar normal stress at the free edge is responsible for this behaviour.

To verify this prediction, a $(0,90)_s$ laminate was modelled using 25 elements and loaded on one edge (Fig 11). The finite element solution indicates a through thickness expansion at the loaded edge (Fig 20). The deflections in the figure have been magnified by a factor of 1000, with the original mesh shown by the dotted lines. This is caused by the differential strains in the middle and outer laminae due to the mismatch in the moduli.

Due to the higher modulus of the 0 degree plies parallel to the loading direction, the upper and lower surfaces of the laminate undergo a smaller extension than the two middle plies. Thus the inner plies are subjected to a lower stress in the load direction than the outer plies. Equilibrium considerations require a bending moment on each side of the midplane that is of equal magnitude but opposite sign. Far from the free edge these bending moments have no effect. However as the free edge is approached, compatibility considerations require the deformation shown in figure 20.

Poisson effects result in a contraction of the laminate perpendicular to the direction of the applied load. Since the 90 degree fibers of the two middle plies lie in the direction of the compressive stress, these plies will undergo a smaller compression than the outer plies due to their higher stiffness. The consequent deformation of these edges will also result in a through thickness expansion of the laminate (Fig 21), though of much smaller magnitude than that of the loaded edge.

The distribution of the interlaminar normal stress along the length and width of the laminate is not uniform close to the free edge (Fig 22). Far from the free edge this stress shows a uniform distribution in each ply. As the loaded edge is approached, this stress becomes compressive before increasing to a large value. A similar behaviour occurs in the width direction. Thus the interlaminar normal stresses arise all around the edges of the laminate. For the $(0,90)_s$ laminate, these stresses have a positive sign along the free edges.

Advanced laminated fiber composites generally consist of a multitude of plies stacked on top of each other. The plies are held together by resin rich areas between them that are formed when the laminate is cured. These resin rich areas typically exhibit a lower strength than the bulk of the composite. A positive interlaminar stress in

these areas will tend to delaminate the plies much earlier than the occurrence of a failure due to overload in the plane of the laminate. Reversing the stacking sequence results in a reversal of the interlaminar stress, thereby mitigating against laminate failure due to delamination.

The longitudinal and transverse stress computed at the middle of the laminate agree with those from CLPA. Therefore the stress distributions referred to above indicate that the effect of the free edge is significant only for a distance of from one to two laminate thicknesses. For an unloaded edge, the deviation from CLPA is insignificant after a distance of one laminate thickness. In the case of a loaded edge, CLPA is invalid at a distance less than two laminate thicknesses from the edge.

7.3 Edge Deformations

The concept of Zero-Based design allows one to build into a laminate the desired stiffness properties to match the loads expected in an application. If a desired longitudinal to transverse stiffness ratio is required, this can be accomplished using various numbers of 0 and 90 degree plies. If, on the other hand, isotropic behaviour is required, one must use a balanced construction of plies with a layup sequence of either

$(-45,+45)_S$ or $(0,-120,+120)_S$. These will result in quasi-isotropic behaviour over most of the laminate.

However the deformations at the edges are not symmetric either with respect to the loading direction, or perpendicular to it. Consider a $(-45,+45)_S$ balanced symmetric construction subjected to a uniform distributed load on opposite edges. If all four plies were free to deform, the inner plies would form a parallelogram with the loaded edge making some positive angle with respect to its original position. However the constraints imposed by the outer plies mitigates against this deformation from taking place. The outer plies would deform to the same angle, but of opposite sign. Here too, the constraints from the inner plies would inhibit this kind of deformation. There is no twisting due to the midplane symmetry.

The edge deformations of a $(-45,+45)_S$ laminate were investigated using the mesh of figure 11, but with the loading applied to the opposite edges in the x-direction. As expected, the resulting edge deformations exhibited symmetry about an axis lying 45 degree off the loading direction. The deformation of the loaded edge exhibits a concave curvature on one side of the laminate, and a convex curvature on the other side (Fig 23). The mesh

deflections shown in figure 23 have been magnified by a factor of 500, and are not predicted by lamination theory.

The surface displacements of such a symmetric angle-ply laminate have been experimentally determined by the utilization of a Moire technique by Pipes & Daniels [125]. A plot of these displacements from the FEA analysis indicates the same characteristic deformation pattern (Fig 24). Reversing the order of the layup sequence results in a mirror image of the deformations and stresses.

Although the shearing stresses on both sides of the midplane arising from the constraints are of equal magnitude in all plies, the moment of these stresses is greater for the outer plies than for the inner ones. Hence the through thickness deformation is not uniform across the laminate width. The resulting through thickness stresses are positive on one side of the laminate, and negative on the other (Fig 25).

7.4 Plate Deformations.

The deformation patterns of square plates with various lamination sequences have been investigated analytically using the Finite Element Method by a number of researchers [126,127]. Indeed, the square clamped

plate has become somewhat of a standard to check plate problems [128,129,130]. However these investigations have all used plate elements. As with CLPA, these elements use an averaging technique through the laminate thickness that tends to mask certain behaviour.

Consider a square 8-ply $(0_2,90_2)_s$ laminate with the 0 degree plies lying parallel to the x-axis (Fig 26). The effective moment of inertia of the crossectional area about the centroidal axis in the xz-plane for this laminate will be larger than that in the yz-plane. This is due to the 0 degree plies being further away from the midplane than the 90 plies. Hence the overall laminate bending stiffness will be larger in the xz-plane. It follows then that the deflected shape contours of a face loaded crossply plate will show two axis' of symmetry.

Application of a uniform distributed load, in the negative z-direction, on the top face of such a plate results in the expected surface deformation (Fig 27). The mesh deflections in figure 27 have been magnified by a factor of 100. A trough forms in the direction of the 0 degree plies due to the higher bending stiffness in this direction.

The longitudinal and transverse stresses through the thickness of the laminate indicate large jumps in these

values at the ply boundaries (Fig 28). Both σ_{xx} and σ_{yy} go from tensile at the bottom surface to compressive at the top surface, and reach their maximum values at these locations. Therefore one would expect initial failures to be located at the top and bottom surfaces of the laminate.

The initial failures can be further localized by examining the distribution of the same stresses for these two plies. Doing so indicates that the highest value of σ_{xx} occurs at the x-coordinate limits in the middle of the clamped edge (Fig 29). The highest value of σ_{yy} occurs at the y-coordinate limits, also in the middle of the clamped edge (Fig 30). Initial failure would therefore occur in either one of these locations depending upon the variation of the individual lamina strengths. Increasing the applied load till the onset of failure confirms these predictions.

7.5 Energy Absorption

Laminated plates used in the energy absorption role are generally subjected to loading perpendicular to the lamination plane. It is therefore often necessary to determine the failure characteristics under such loading. Energy absorption for fiber composites is usually related to some form of impact parameter such as the peak force or the maximum deflection [131,132]. Such parameters are

used to rank materials in terms of their energy absorption capabilities before detailed trials are conducted. However the response to a monotonic load test may also be used to determine the initial ranking. Such a quasistatic test may be easily simulated using the finite element method. Both the failure progression and the relative energy absorption characteristics can be explored for various lamination sequences.

Consider a clamped 25 element square plate modelled as in figure 26, but with a uniformly distributed load applied over the center element in the negative z-direction. To investigate the effect of the lamination sequence, each element of the 5x5 grid was composed of a 70% weight fraction of Kevlar fibers embedded in an epoxy binder with a 2% void content. This would give a volume fraction ratio of fiber to binder of 66:32. The applied load was increased in steps to allow the failure progression to be tracked. The Tsai-Wu model was used to determine material failure.

The surface displacements and the stress distributions have the same character as previously described (Fig 31). The first indication of failure (Fig 32) occurs at an applied load of 9.1 ksi (62.7 MPa). The square symbols in figure 32 represent the strain energy dissipated at each load step

due to material failure. The solid line indicates the accumulated energy dissipated up to a particular load step. The stored strain energy at this point is 1510 in-lb (170·6 J). Again the initial failure occurs in the predicted location (Fig 33), and subsequent failures occur in the inner plies along the x-axis of the laminate.

The top surface of the plate is represented in figure 33 by a shaded square, under which is given the applied load. The lighter colored areas in each shaded square represent the location of an element in which at least one integration point through the thickness has failed due to an overload. The direction of the 0 degree fibers is from left to right. There are three main energy release points before total failure of the plate at 11·0 ksi (75·8 MPa). The final value of the total energy absorbed after initial failure is 2980 in-lb (336·7 J), which indicates a good residual energy absorption capability past the initial failure point.

Evidently the entire plate does not fail at once due to the directional variation of the internal stresses cause by the lamination sequence. One can try to change this by equalizing the bending stiffness in the two inplane directions. One way to do this is by relocating one pair of 90 degree plies to the outer surfaces. Doing so modifies the stress distribution (Fig 34), resulting in

a σ_{yy} for plies 1 & 8 that is about the same magnitude as σ_{xx} for plies 2 & 7.

The initial failure locations still lie in the outer plies in the middle of the clamped edges, but now they are located at the limits of the y-coordinates. A plot of the surface deformations confirms the change in the bending stiffness, with a slight trough appearing perpendicular to the previous direction. The initial failure load for this lamination sequence was 10·5 ksi (72·3 MPa), and the stored strain energy at this point was 1750 in-lb (197·8 J). However there was only one major energy release point (Fig 35), and the total absorbed energy after failure was actually less, being 2380 in-lb (268·9 J).

The increase in the initial failure load was due to the altered stress distribution throughout the laminate. More of the load is reacted by the stresses in the inner plies, so the stresses in the outer plies are lowered for the same value of applied load. Thus the applied load can be increased to a higher value before the onset of failure. Unfortunately when failure does occur the higher values of the redistributed stresses result in a quicker spread of the failure locations throughout the laminate (Fig 36). The applied load moves through a

smaller distance before catastrophic failure, resulting in a lower energy transfer.

As mentioned above, quasi-isotropic behaviour can be obtained by using two families of lamination sequences, these being $((+45_n,-45_n)_m)_s$ and $((0_n,+120_n,-120_n)_m)_s$. The order of the plies is irrelevant to the inplane behaviour so long as they are of equal thickness. These two lamination sequences can be used to approach a nearly equal bending stiffness in the two inplane directions. Initial failures for these sequences occur at greater values of the applied load, and occur away from the constrained edges (Fig 37). The failure patterns indicate an axis of symmetry along the ply layup directions. This is clearly evident when a greater number of elements are used in the model. Figure 38 indicates the accumulated energy absorption for each of the above laminates as a function of the applied load. The number at the end of each curve is the stored elastic strain energy prior to catastrophic failure.

Another interesting phenomenon associated with these layup sequences was the warping of the plate surface (Fig 39). The mesh deflections in the figure have been magnified by 100, and are not predicted by lamination theory. The warping is due to the creation of unbalanced shearing forces through the laminate thickness.

In order to use laminated fiber composites as energy absorbers, it is important to use a layup sequence that will result in as high an energy absorption as possible. In addition, the residual energy absorption capability after initial failure should also be maximized to prevent catastrophic failure before the damaged plate can be either repaired or replaced. A comparison of these is presented in Table 4. Increasing the load at which initial failure takes place is a secondary consideration. These factors would tend to suggest that the first layup sequence is best suited to the energy absorption role.

8.0 Conclusions & Recommendations

8.1 New Capabilities

The use of thick laminated fiber composites in primary structure requires a more thorough analysis than simple 2D plate theory is capable of. The Finite Element Method is well suited to this task due to its ease of application to complex geometries. Unfortunately such application has been limited due to the large memory requirement needed to represent a structure with the available 3D element formulations.

Most commercially available finite element codes for laminated fiber composites require that a separate lamina analysis be performed to evaluate the element stiffness matrices. In many cases the codes do not allow the lamina properties to be separately computed, but require the results of experimental testing. The method of implementation of the modified element does away with the requirement of a separate preprocessor for the individual plies. The element allows a realistic modelling of the material property variation throughout each ply volume as these properties change with the progression of material failure.

The geometrical description of the 3D element formulation described above is independent of the number of plies through the element thickness. Therefore the addition of plies through the thickness does not require a corresponding increase in the number of degrees of freedom required to represent the element. Solution of the types of plate problems described in the last two chapters are not practical using currently available 3D elements due to computer memory and time limitations. The use of the modified integration scheme allows a drastic reduction in the number of degrees of freedom required for a given problem. A plate element had been considered during the early course of the research, however it was found to be impractical due to the large number of degrees of freedom required. Also, the literature review indicated that the use of higher order displacement assumptions in the plate element formulation did not significantly increase the accuracy of the results.

Classical theory represents plate displacements in terms of the midplane values. The inplane strains exhibit a linear variation through the thickness, and are limited to constant values in the plane of the laminate. In contrast, the modified element allows a linear variation of the inplane strains in the plane of the laminate, and a parabolic variation of these strains

through the thickness. It is therefore possible to resolve the dilemma of a non-zero surface shear stress that is produced by the classical theory. Also, the Finite Element Method is just as easily applied to complex geometries as it is to simple ones. The same is not true for classical plate theory.

Plate elements are incapable of giving insight into some of the failure mechanisms since the through thickness normal stresses and/or the out-of-plane shearing stresses are not generally included in their formulation. The modified element allows the prediction of the edge deformations and stresses that lead to observed delamination behaviour at the edges. Currently available 3D elements only allow these kinds of deformations at the mesh level. The modified element allows these deformations to be observed at the element level, since full coupling behaviour is simulated within the modified element. Qualitatively, the element reproduces the observed edge deformations for symmetric and unsymmetric laminates. The variation of the interlaminar normal stress is properly modelled. This can be used to predict the change in the delamination behaviour with lamination sequence.

The edge deformations of symmetric balanced laminates can be inferred through the use of Moire techniques.

However plotting the results from the FE code actually allows a 3D visualization of the deformation. Such visualizations have not yet been reported in the literature. The warping of the plate models used in the damage progression and energy absorption studies has not been previously reported, nor have any predictions been made with regard to them. Damage progression studies reported in the literature have been limited to C-scans of individual square plates subjected to ball drop tests. Failure progression with the loading conditions described above has not been previously investigated.

The initial failure locations in the damage progression studies are properly predicted. The modified element has been used to accurately predict the tensile behaviour of two specific laminates. An investigation into the longitudinal stress distribution indicates that ASTM Standard Test Method D3039 allows a specimen size that may be too small to accurately evaluate the tensile strength of $(0_n,90_n)_s$ laminates.

The modified formulation of the element stiffness matrix allows a variation of the material properties throughout the element volume. Classical theory as well as current plate elements allow this kind of variation only through the thickness. The modified element allows a smooth variation of the properties within the plies

themselves, whereas classical theory and current plate elements restrict the materials properties to constants within each ply. As a consequence of the variation of material properties allowed by the modified element, damage progression can be tracked throughout the element volume at the integration point level rather than at the ply level as is done in classical plate analysis. This in turn provides a method whereby the energy absorption due to material failure may be tracked for different lamination sequences, and used as a comparison for ranking purposes.

8.2 Limitations

There are several restrictions on the implementation of the modified 3D element. Large displacement and large strain analysis are precluded. Therefore the plate results are restricted to deformations that are less than 10% of the plate thickness. However this can be overcome by inclusion of the large strain and large displacement matrices in the element stiffness formulation. The modified integration procedure is not affected. The code itself allows only quasistatic loading conditions. However the element mass and stiffness formulations can be incorporated into another code by the inclusion of a subroutine in the latter. This subroutine can call the

existing routines to compute the modified stiffness and mass matrices.

The element formulation described above uses readily available shape functions that allow a cubic implementation of the two variable node elements. Such an implementation does not satisfy the zero shear stress condition at the upper and lower surfaces of the laminate unless at least two elements are used through the thickness. Since the modified integration technique is independent of the number of degrees of freedom used to describe the element, implementation of a higher order element is a straight forward matter. A fully quartic implementation will allow the resolution of the non-zero surface shear stress dilemma encountered using simple plate theory.

Although the modified formulation significantly lowers the core memory requirement for a given static problem, the individual element stiffness matrices take a longer time to compute. However since fewer elements are required, the overall solution times are not significantly different. Also, any averaging technique used to condense a problem invariably results in a loss in accuracy, and this is no exception. However this is balanced by the fact that the modified element allows the solution of problems that would otherwise be deemed impractical to

solve without it. For example, the plate problems described in the last chapter required about 2½ hours of computer time on a Silicon Graphics 4D/2206TX Workstation for a static solution if 100 elements were used in the model. For the 25 element meshes used to investigate the damage progression, the average solution times were about 3 hours. Such problems could not be solved at all on this computer using the currently available formulations due to the significantly higher memory requirements.

8.3 Summary

Problems involving lamina coupling, edge and surface deformations were solved. Some results away from the edges were compared to predictions from classical plate theory and found to be in excellent agreement. The longitudinal interlaminar normal stress distribution was found to exhibit the behaviour hypothesized in the literature. Other results were found to agree with those observed experimentally, such as the deformations resulting from tensile loading of an off-axis specimen with clamped ends. In addition, the code was used to predict the tensile behaviour of a particular laminate. The ability to back calculate the specimen composition parameters has also been demonstrated, and an explanation for the specimen size limitation has been verified. The

quantitative predictions were found to agree well with experimental observations in the literature.

The 3D composite element formulation described above includes all coupling effects, and allows for a smooth variation of material properties throughout the element volume. This has been used to predict the damaged response of various laminated fiber composites. The FEA code developed as part of this effort includes three binary damage models and one progressive damage model, all of which use 3D failure criteria. The material properties for a range of fibers and binders are provided within the code, as well as a lamina analysis capability, for ease of use.

The Finite Element Method has been used to predict the coupled small deflection response of undamaged and damaged laminates, the edge deformations and stresses of symmetric and unsymmetric laminates, and the material failure locations. It has also been used to track damage progression and to rank specific laminates subjected to quasistatic loads.

The main reason for using an analytical method as opposed to an experimental one was the expense and complication of the experiments. Proper testing requires a facility costing of the order of one million dollars,

and only allows one to determine the material ranking in terms of energy absorption. Ball drop tests are used to determine parameters related to energy absorption such as the peak force or the maximum deflection. Nevertheless these too are used only to rank materials.

Such tests require a large group of specimens of each type to obtain statistically valid results. The difficulties in the manufacture of thick laminates further complicates the issue. The research proposes a different method of ranking using finite element analysis. The results from this analysis may be used to screen laminates for tests on a reduced number of samples.

The finite element method can be viewed as a tool used in the solution of complex problems that are not amenable to analysis by standard engineering techniques. Its application to the analysis of laminated fiber composites has been limited by the models used in the analysis. The composite element described above is an attempt at improving this situation.

Tables

Mesh	Element Family				
	LB04Q	LB08Q	LB09Q	LB08C	LB20C
1x1	0.17159	0.21319	0.21477	0.18394	0.23478
2x1	0.17970	0.21619	0.21780	0.19559	0.24020
4x1	0.19053	0.21891	0.21937	0.20953	0.24030
8x1	0.20138	0.21981	0.22003	0.22412	0.24429
4x2			0.21965		
8x2			0.22038	0.22699	0.24460

Table 1 : Strain Energy Convergence Results.

	U (10^4)	W (10^3)	Energy (in-lb)
Theory	4.000	2.950	0.246
LB09Q8x2	4.370	2.579	0.220
LB20C8x2	4.850	2.894	0.245
LB09Q008	4.384	2.577	0.220
LB20C008	4.868	2.885	0.244

Table 2 : Comparison of Composite Element Results.

	$(0_1,90_3)_s$			$(0_2,90_2)_s$		
	Ref	CLPA	FEA	Ref	CLPA	FEA
E_{11i} $(10^{-3}$ psi)	2.37	2.44	2.44	3.60	3.42	3.42
E_{11f} $(10^{-3}$ psi)	1.37	1.33	1.33	2.62	2.66	2.66
%Drop	42.2	45.6	45.4	27.2	22.3	22.2
σ_{fail} $(10^{-3}$ psi)	8.75		9.15	15.6		13.2
ϵ_{fail} (10^{+3})	3.44		3.75	4.53		4.96

Table 3 : Comparison Of Results For Tension Test Analysis.

	Initial (in-lb)	Final (in-lb)	Residual
$(0_2,90_2)_s$	1510	2980	1.97
$(90_1,00_2,90_1)_s$	1750	2380	1.36
$((+45,-45)_2)_s$	1470	1800	1.22
$(00_1,+120_2,-120_2,00_1)_s$	1580	1750	1.11

Table 4 : Comparison of Energy Absorption For Clamped Plate.

Figures

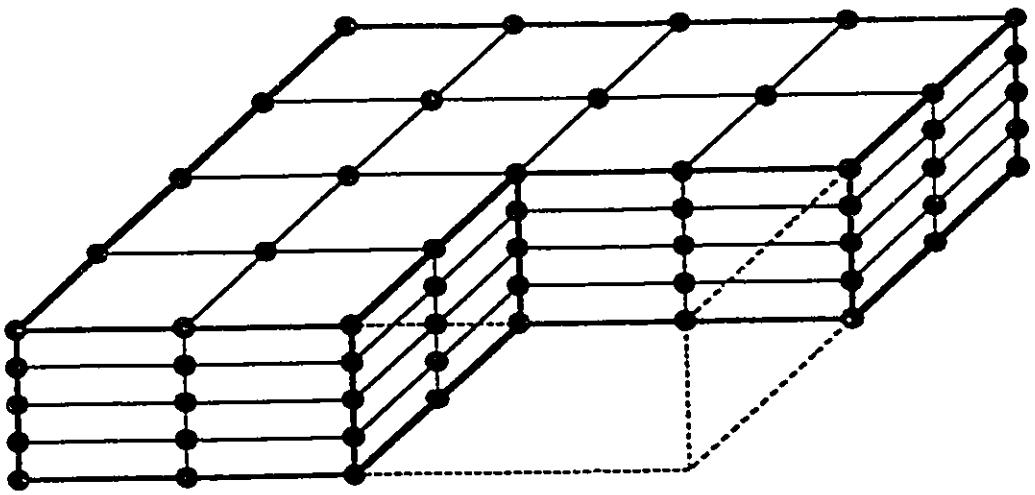

Assembled Structure

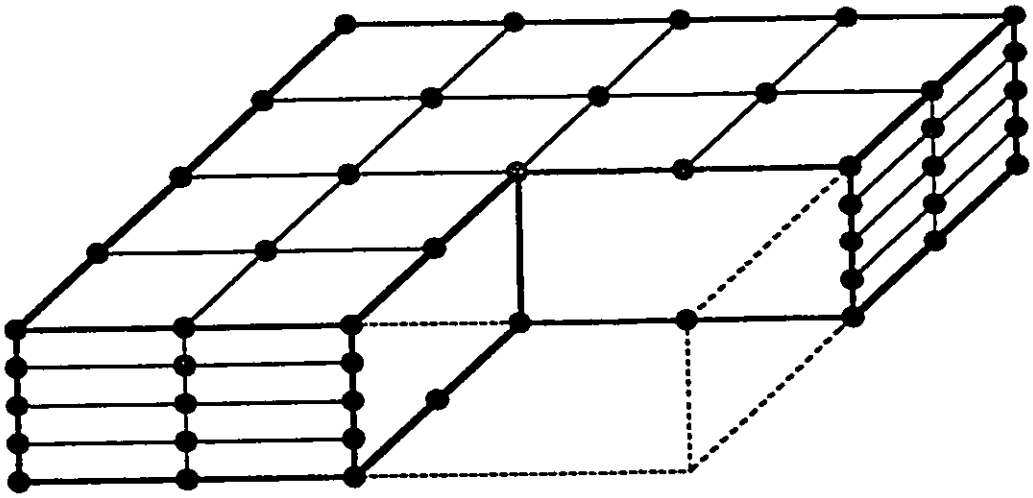

Structure After Condensation

Figure 1 : Substructure Illustration

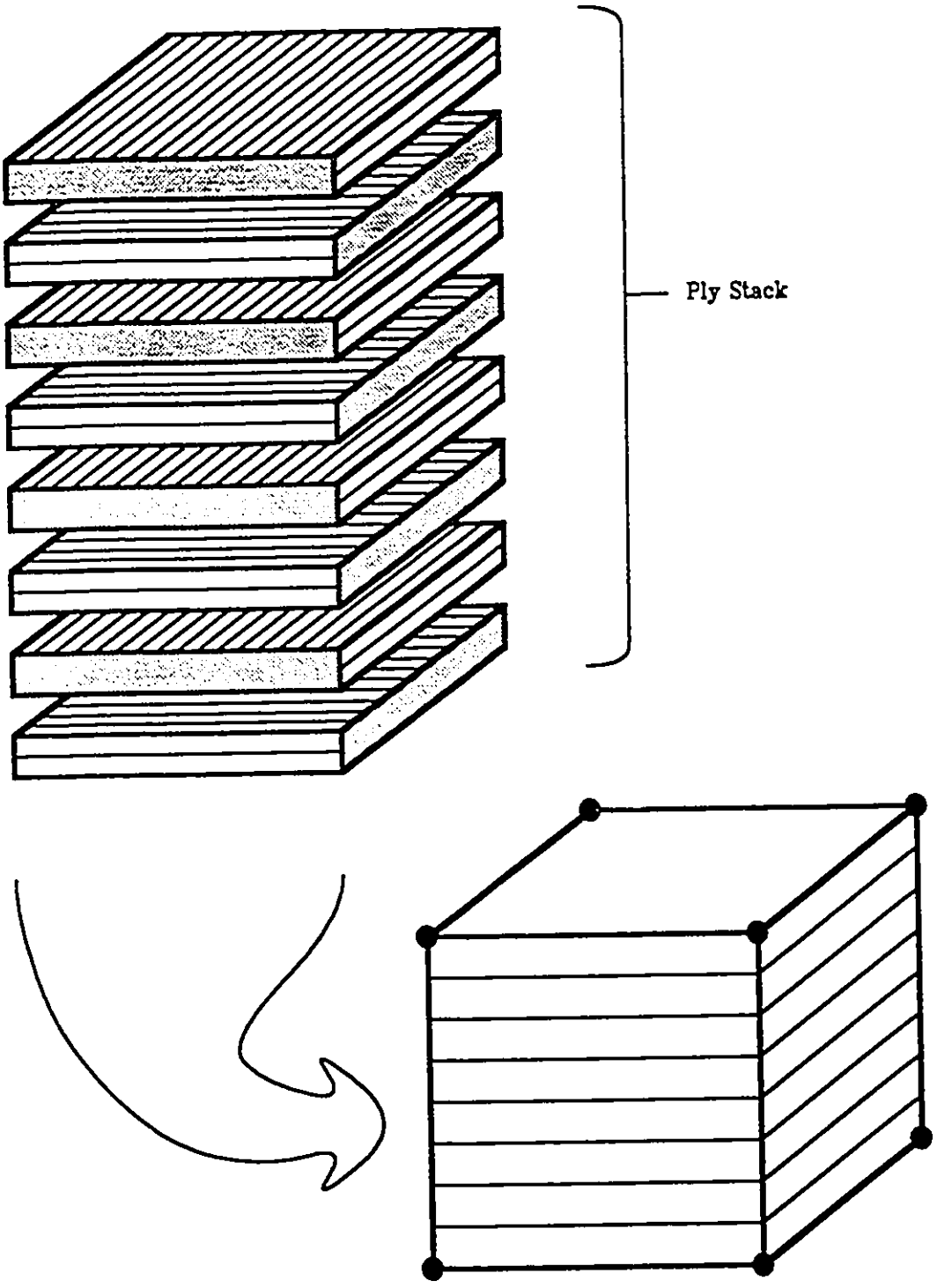

Figure 2 : Composite Element Geometry

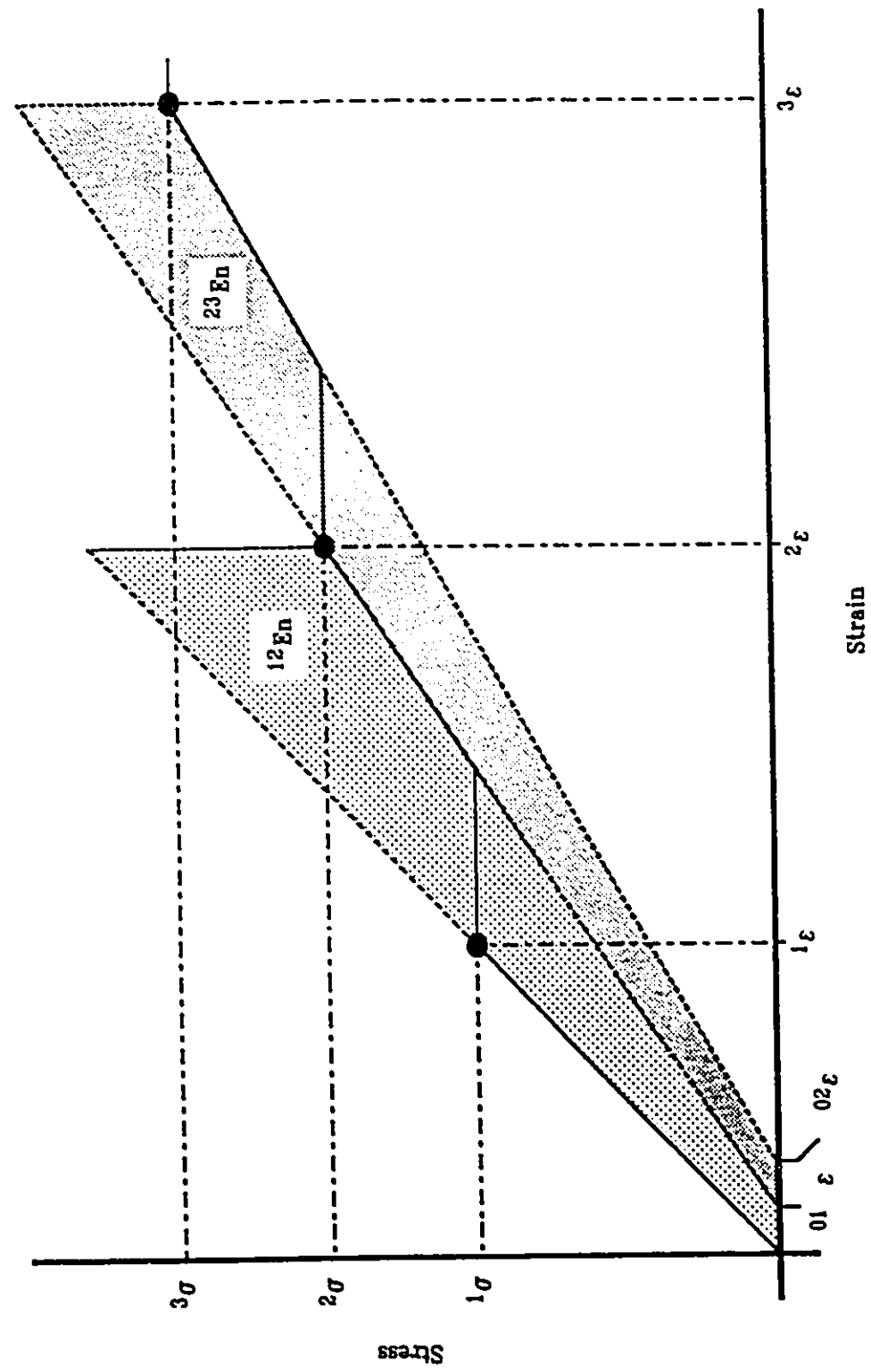

Figure 3 : Energy Lost Due To Defect Formation

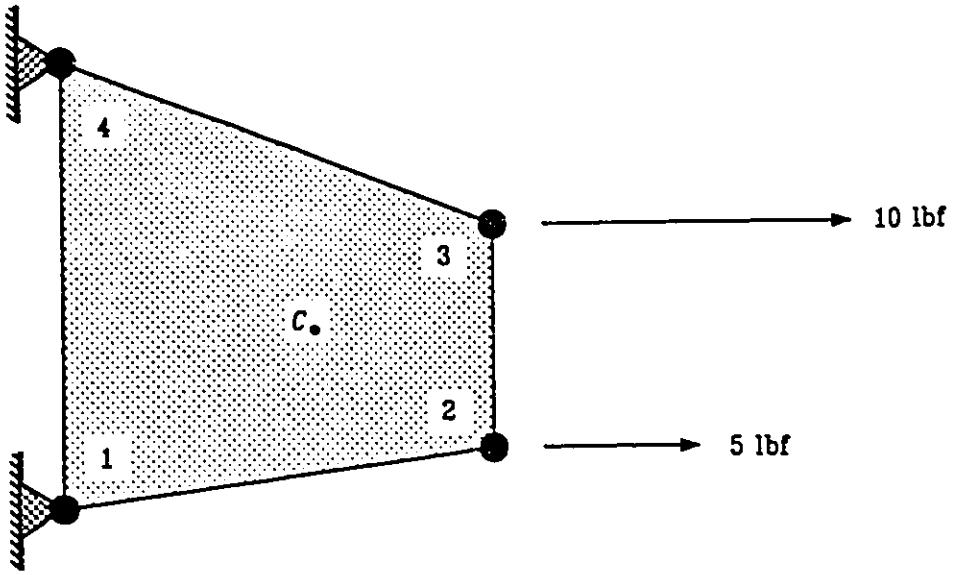

Textbook Solution

$$u = \begin{Bmatrix} +4.8 \\ 0.0 \\ +6.4 \\ -1.6 \end{Bmatrix} (\text{x}10^{-6}\ \text{in})$$

$$\sigma = \begin{Bmatrix} 30.0 \\ 4.2 \\ 0.0 \end{Bmatrix} (\text{ksi})$$

Composite Element Solution

$$u = \begin{Bmatrix} +4.81 \\ +0.04 \\ +6.36 \\ -1.56 \end{Bmatrix} (\text{x}10^{-6}\ \text{in})$$

$$\sigma = \begin{Bmatrix} 30.00 \\ 4.19 \\ 0.00 \end{Bmatrix} (\text{ksi})$$

Figure 4 : Single 2D Element Test For 4-Node Composite Quadrilateral

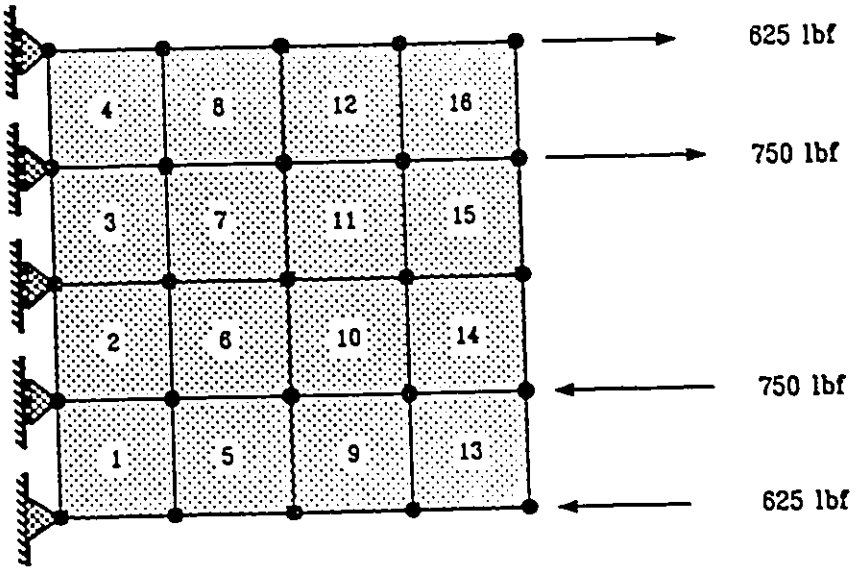

Sixteen Element Model

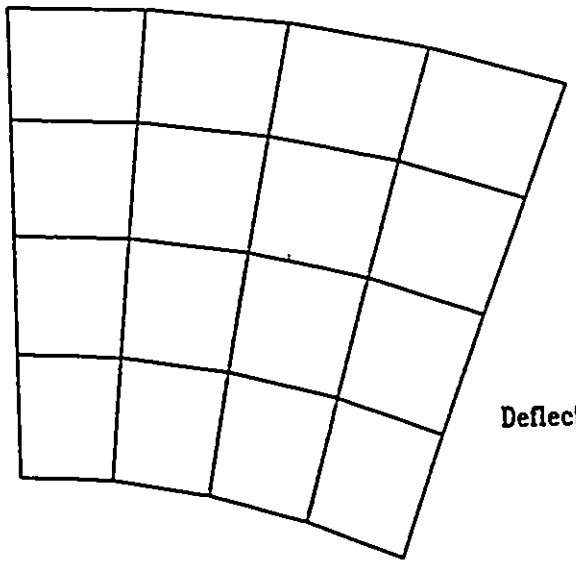

Deflected Mesh

Figure 5 : Patch Test

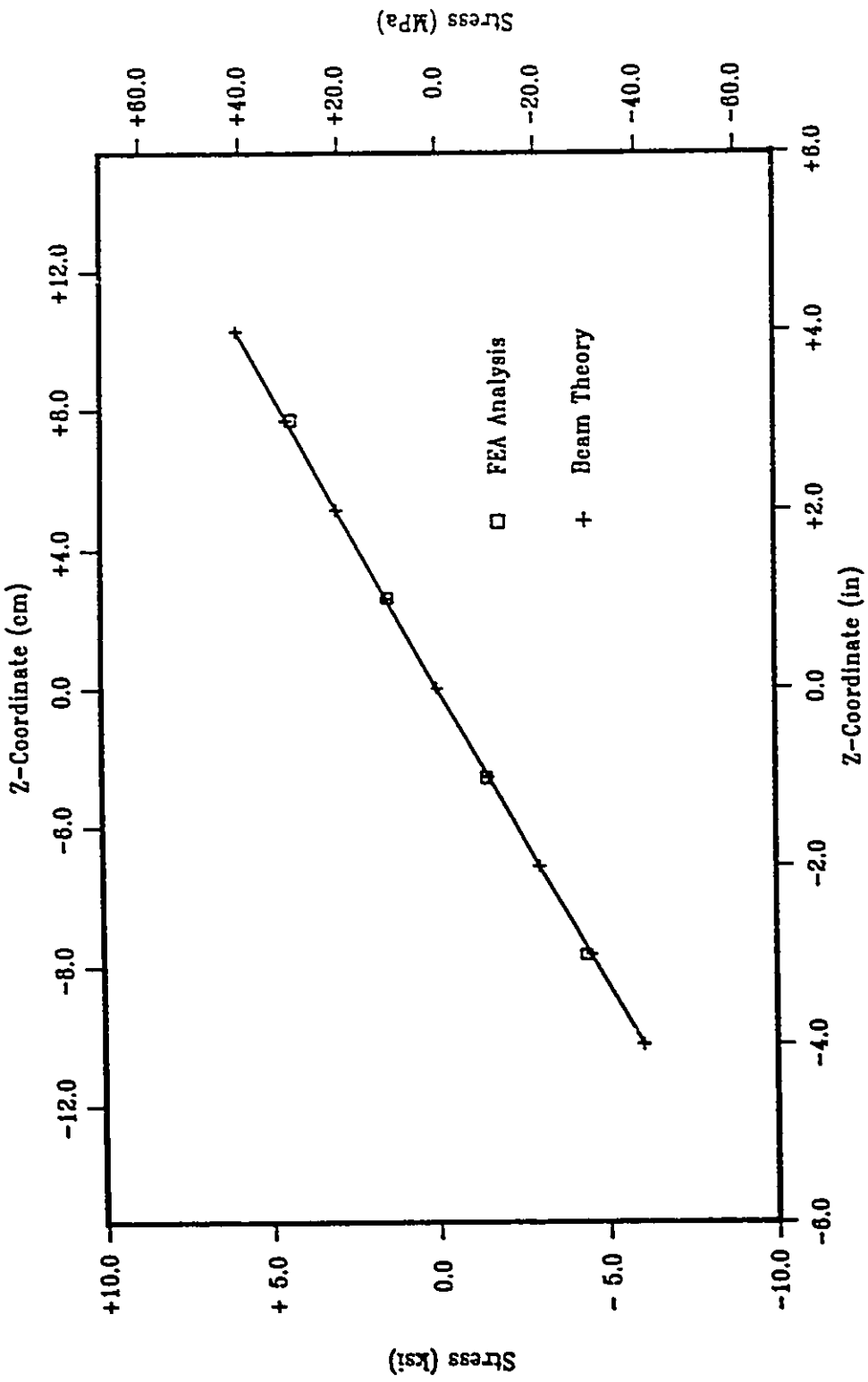

Figure 6 : Comparison Of Stresses At Element Centers

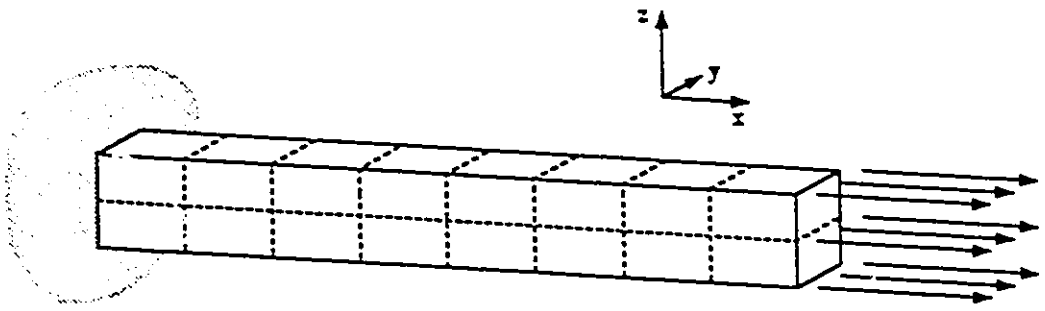

Sixteen Element Model

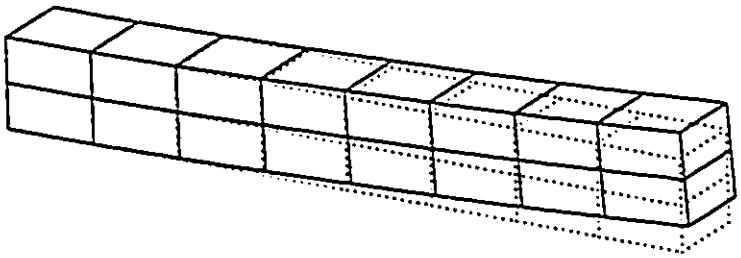

Deflected Mesh

Figure 7 : Laminated Bar Convergence Test

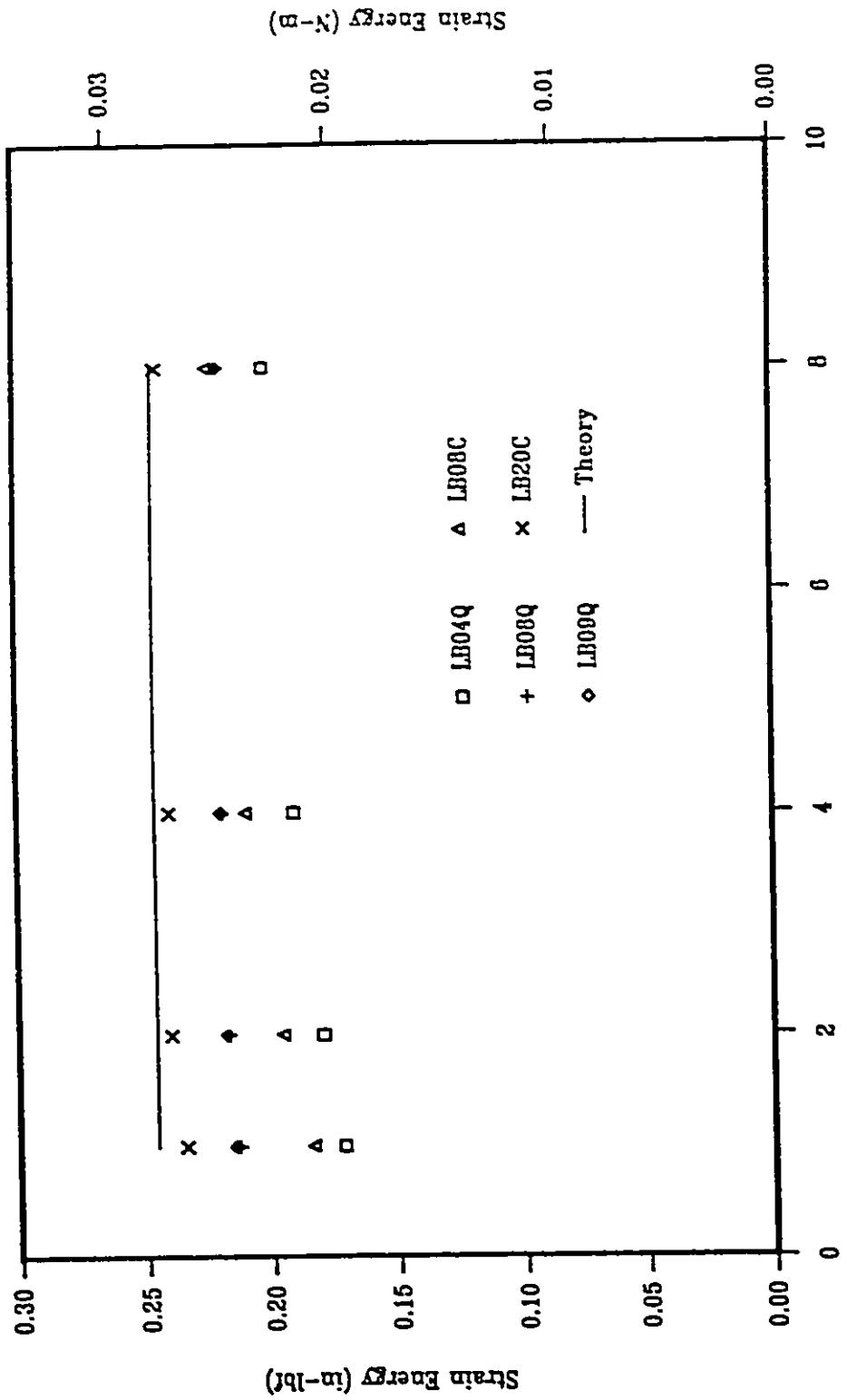

Figure 8 : Modified Element Convergence Results

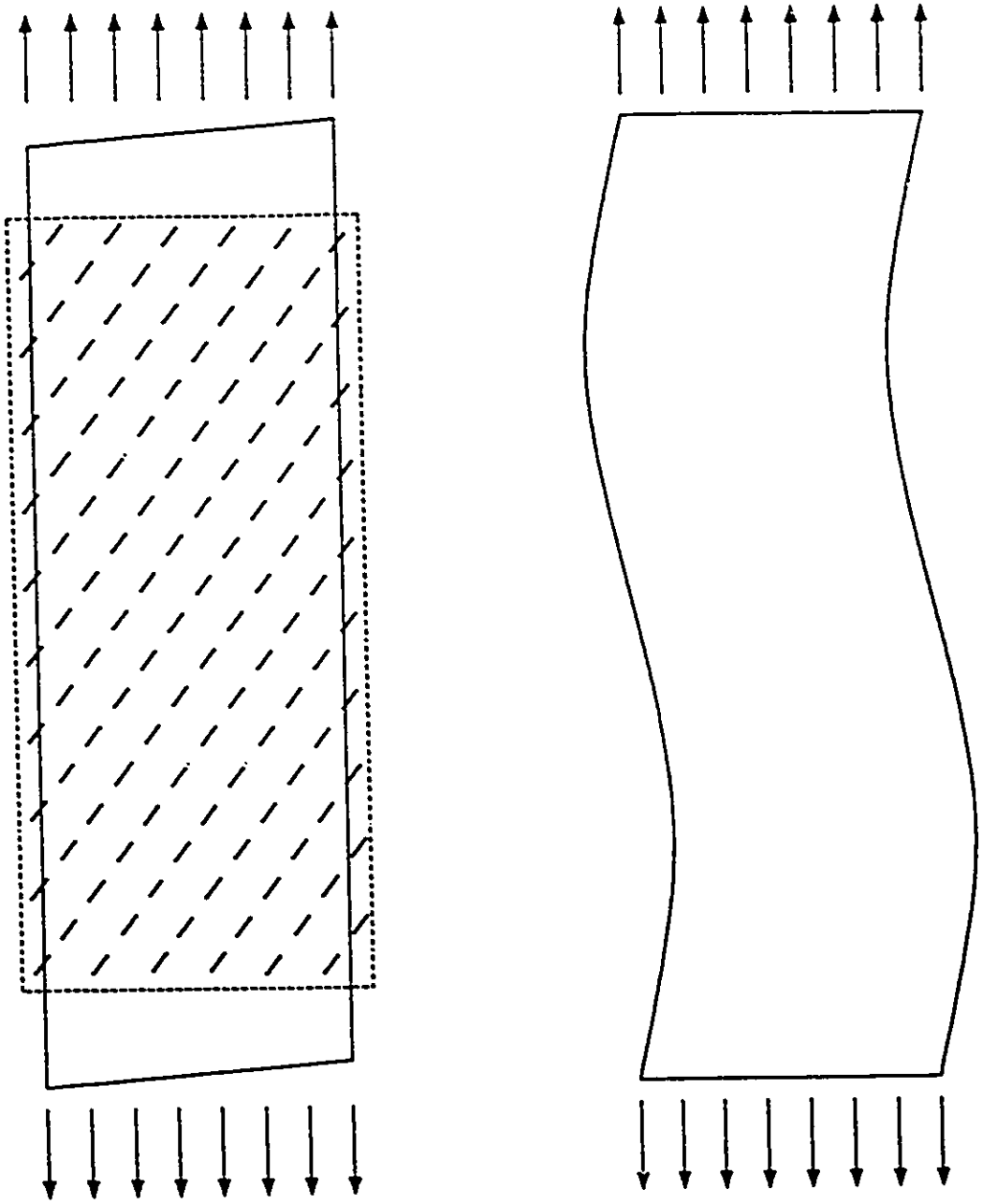

Figure 9 : Off-Axis Laminated Strip Deformation

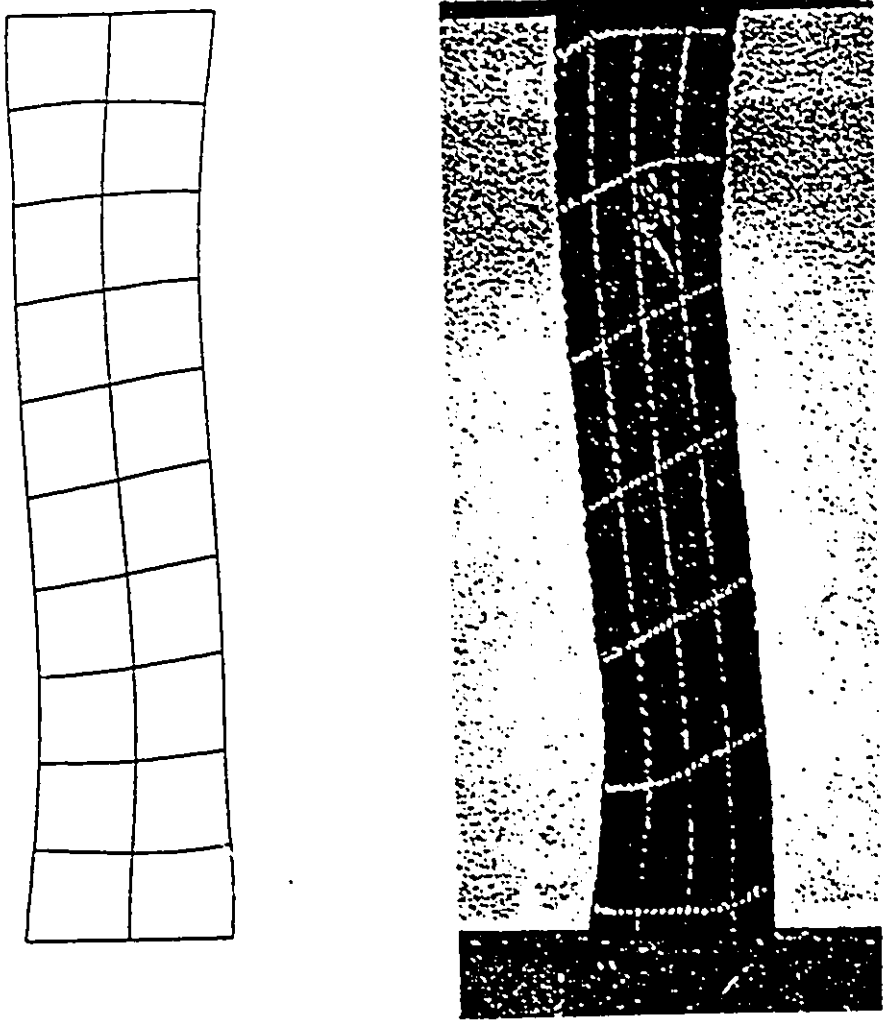

Finite Element Result

Experimental Result
(After Pagano & Halpin)

Figure 10 : Deformed Shape Of Off-Axis Laminated Strip

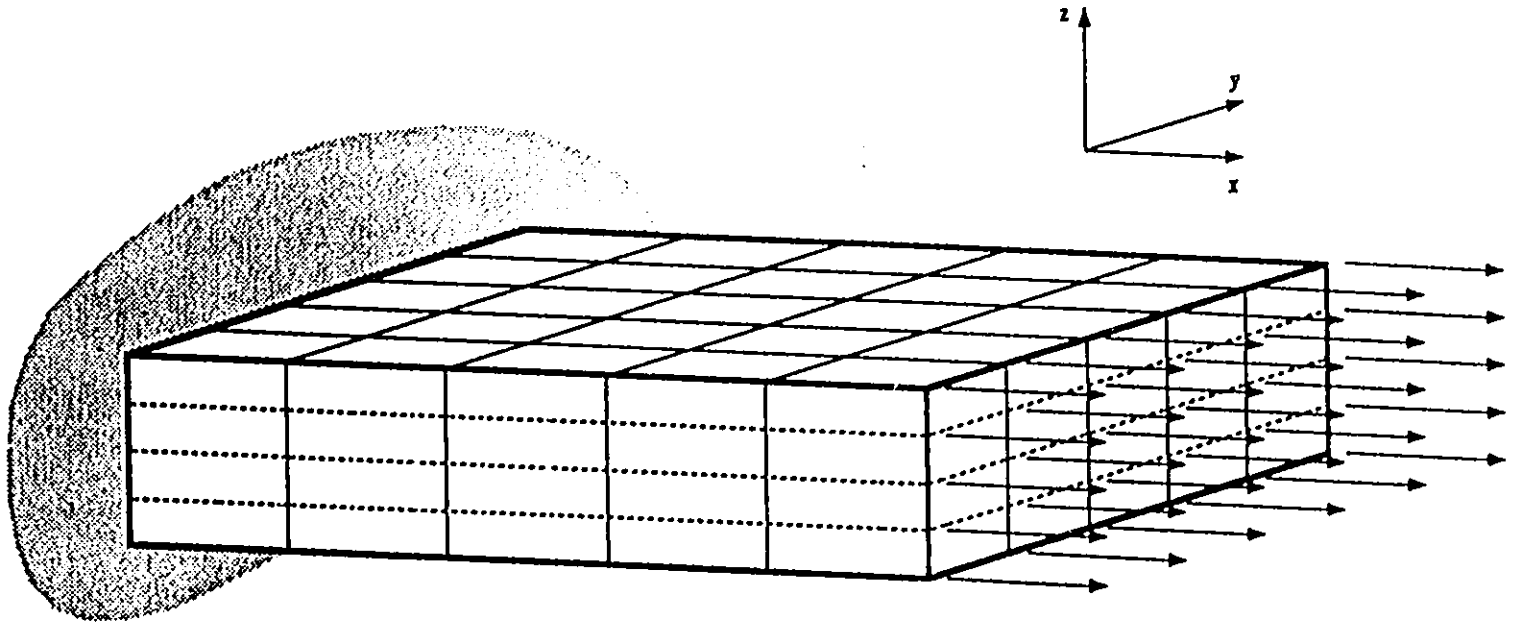

Load = 1000 psi (6.89 MPa)

Ply Constituents : PRD49 (70%wf)

: Epoxy (30%wf)

Figure 11 : Laminated Plate Boundary Conditions And Loading

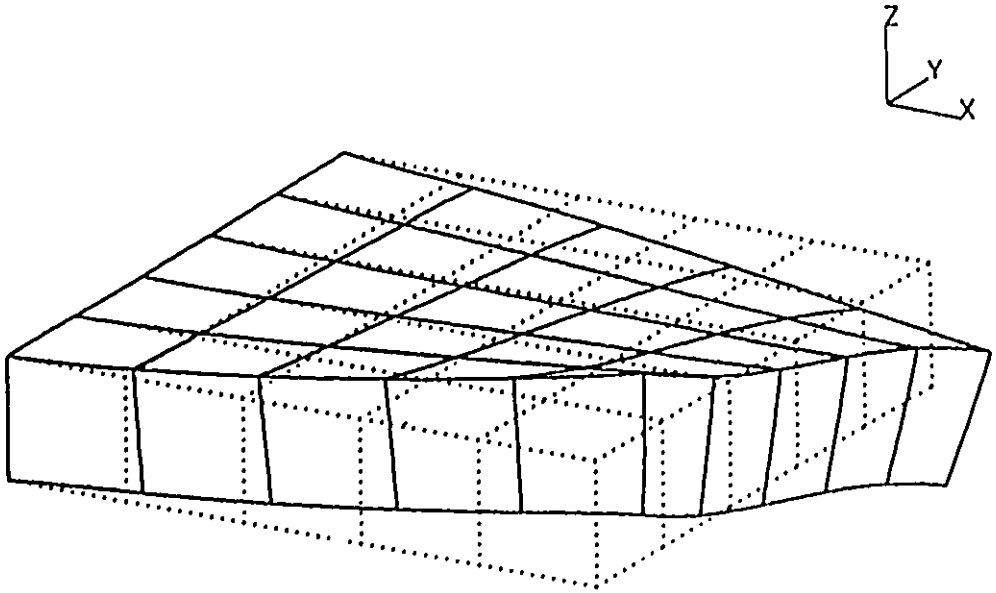

Figure 12 : Twist Deformation Of Laminated Plate

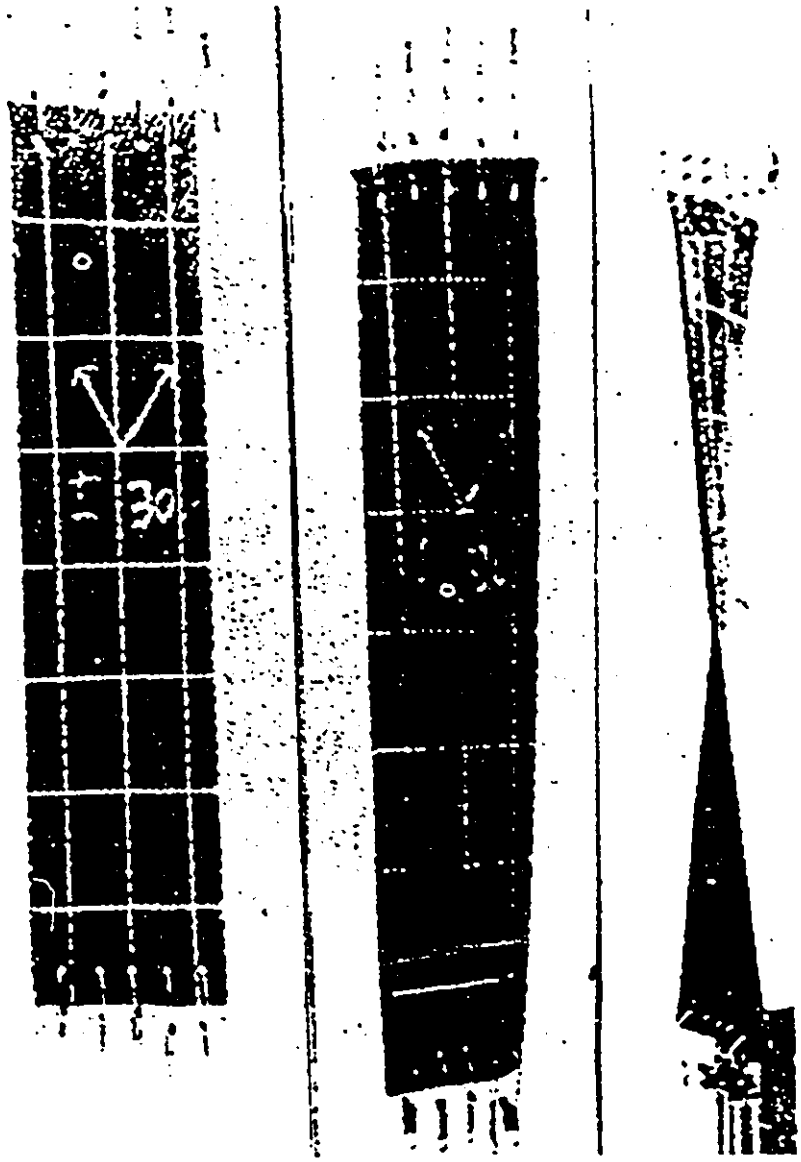

(After Ashton, Halpin & Petit)

Figure 13 : Experimental Confirmation Of Twist Deformation

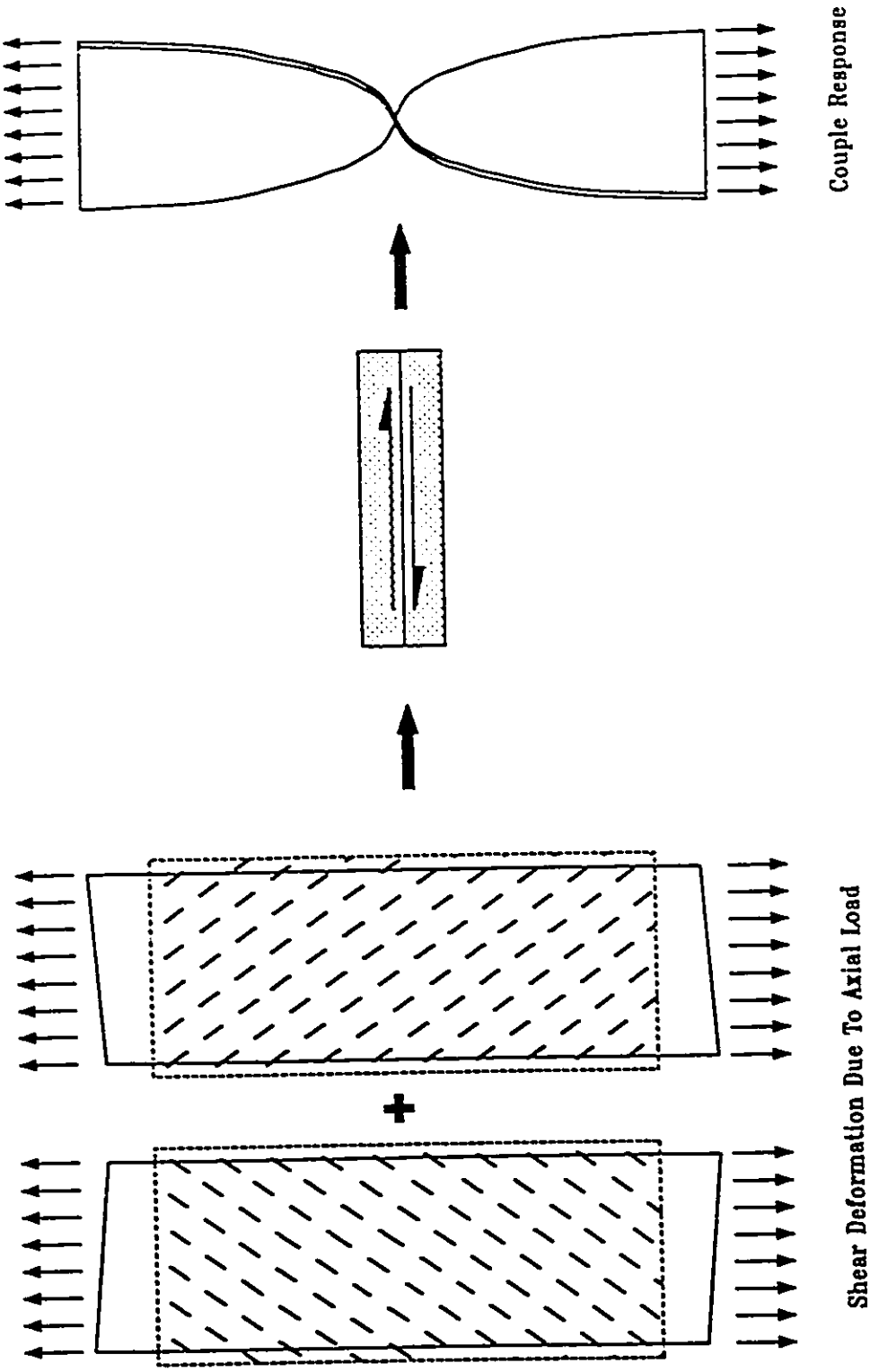

Figure 14 : Moment Generation Due To Applied Load

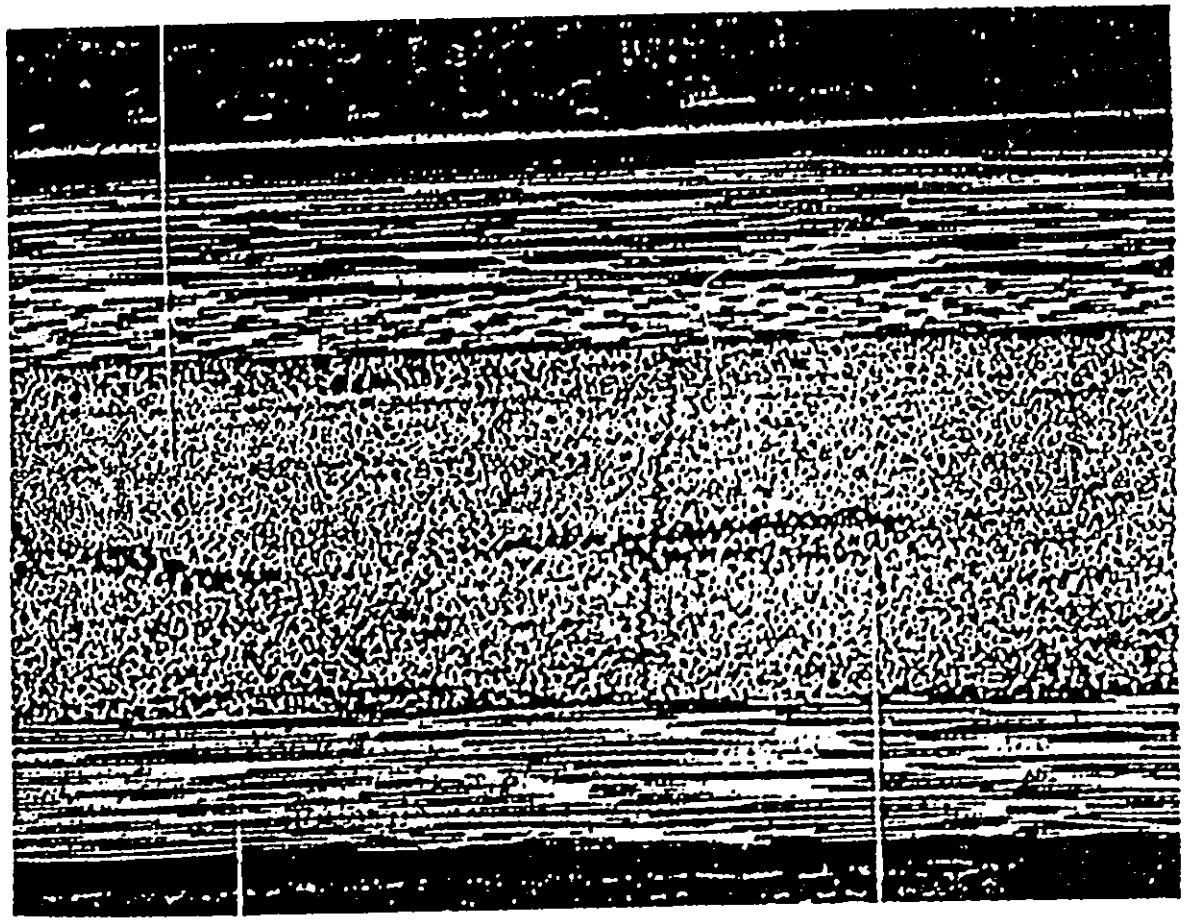

Figure 15 : Through Thickness Crack In 90-Degree Ply (After Whitney, Browning & Grimes)

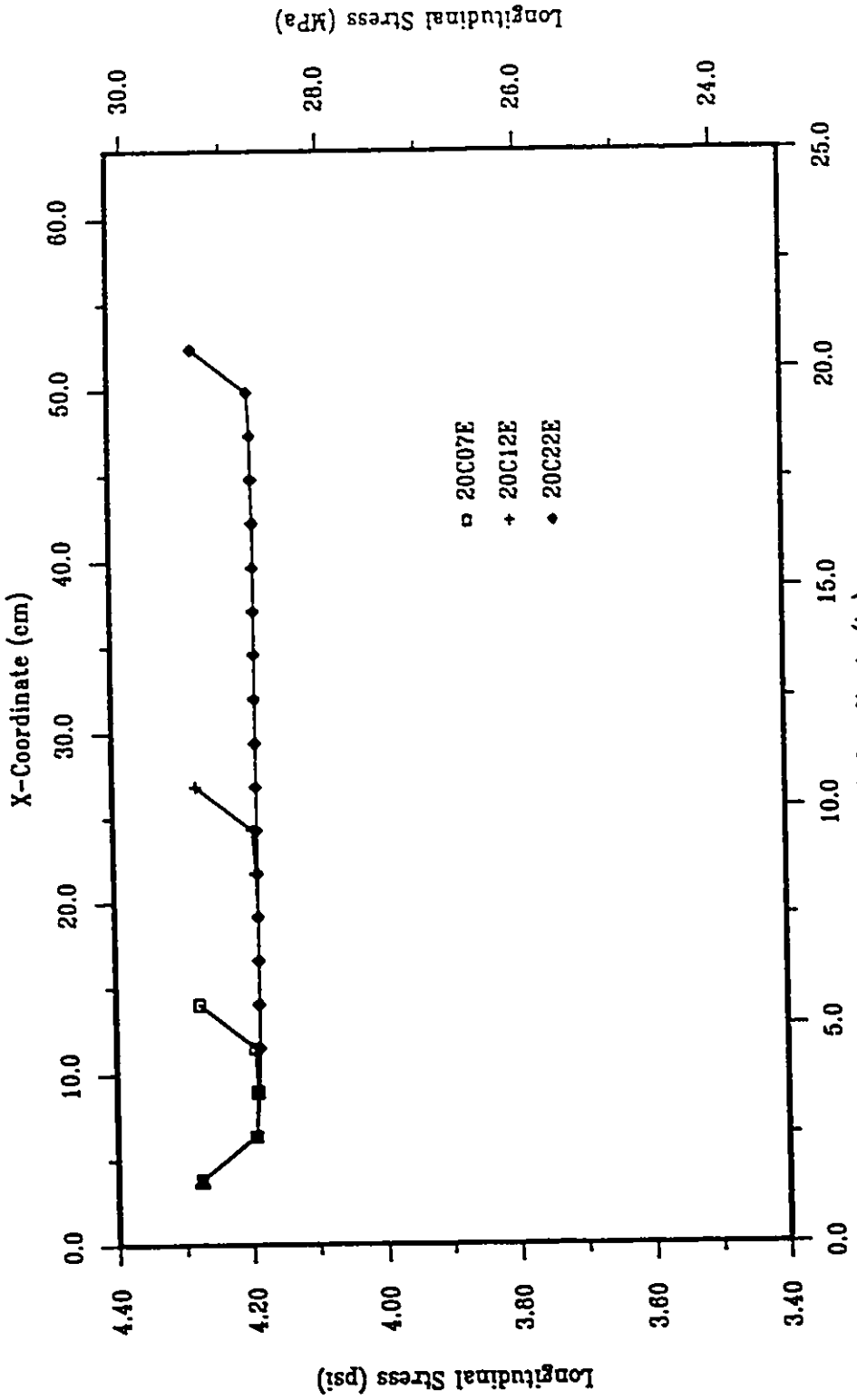

Figure 16 : Longitudinal Stress Variation For Tensile Specimens

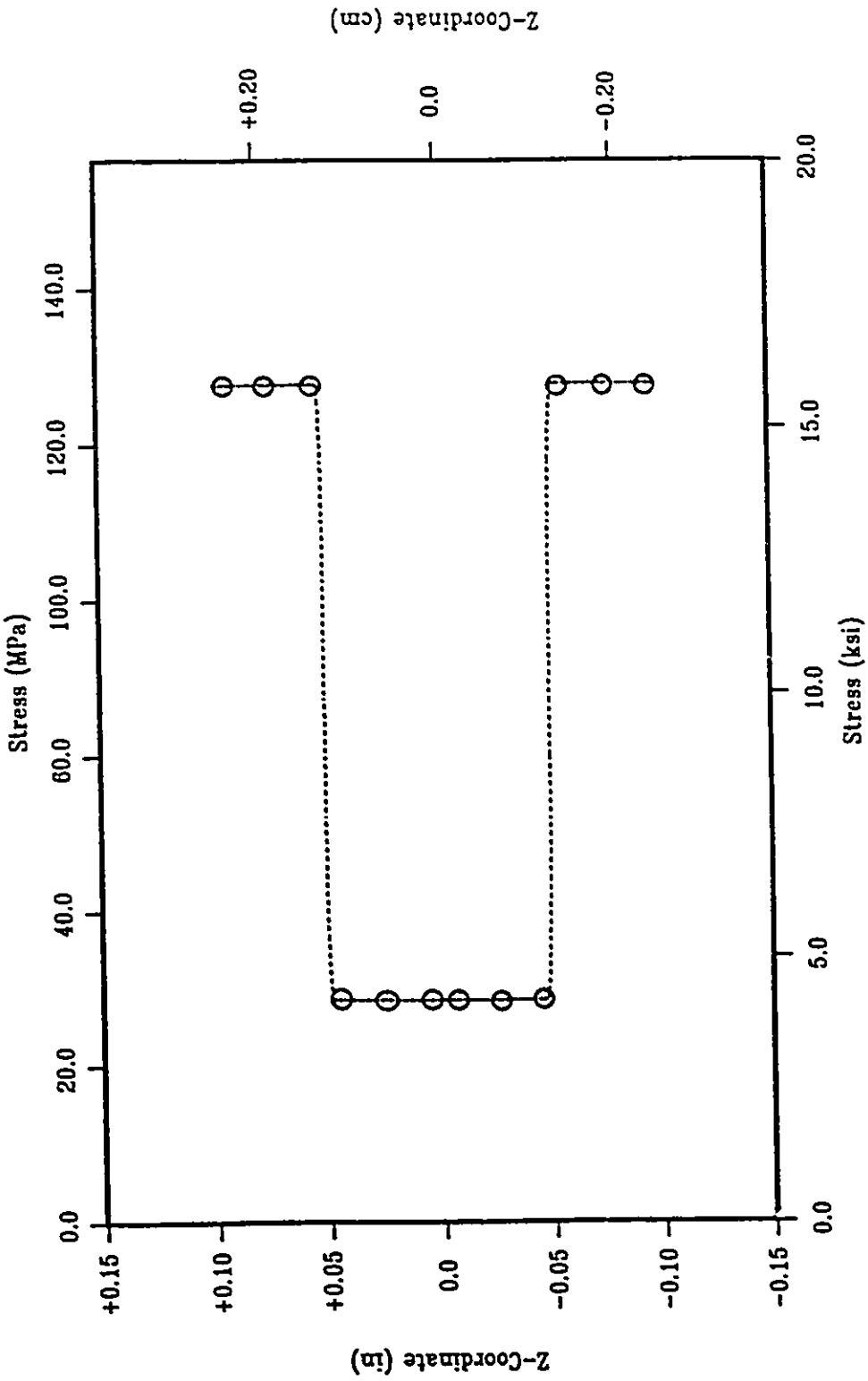

Figure 17 : Variation Of Longitudinal Stress Through Thickness

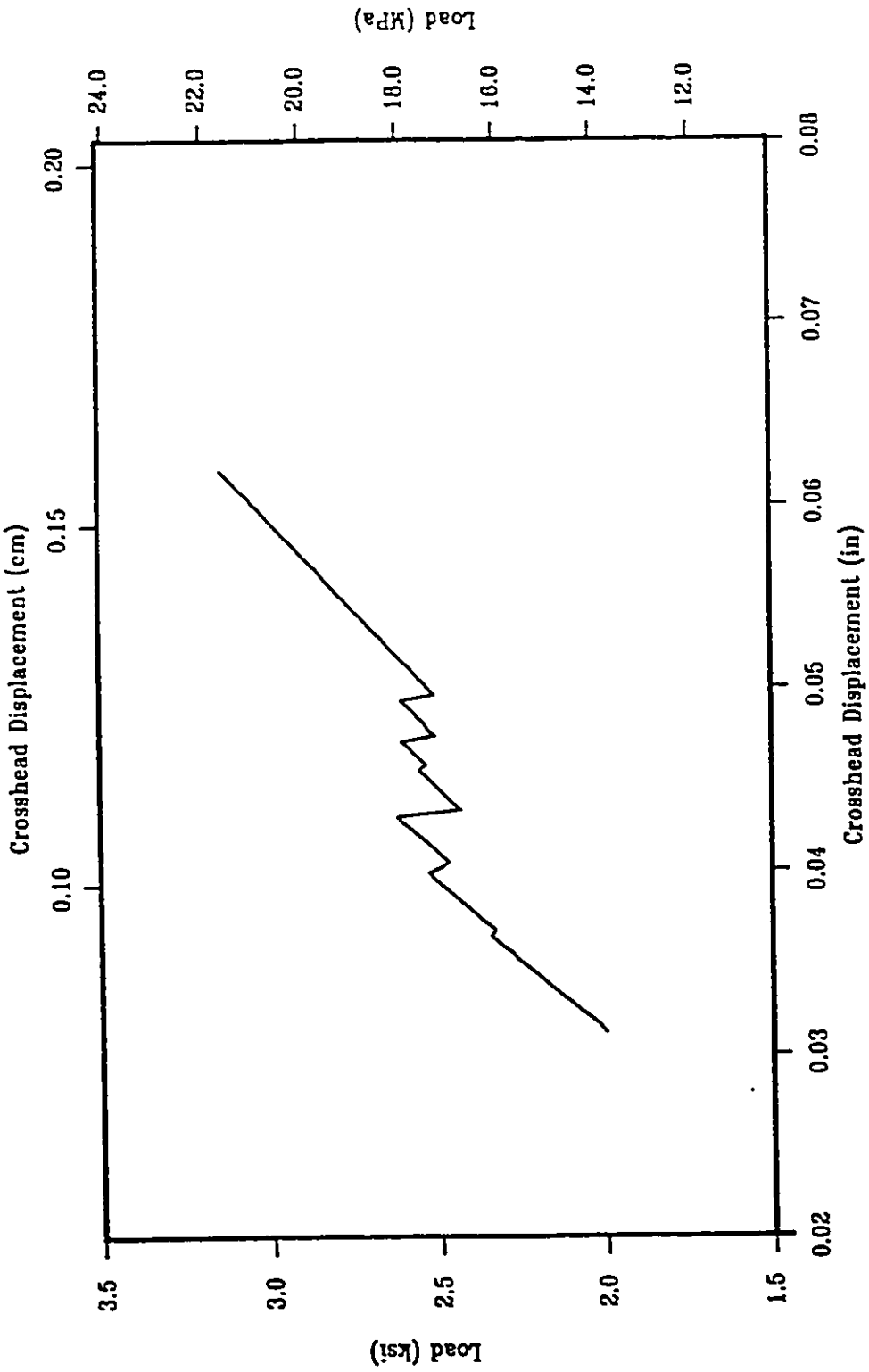

Figure 18 : Load Displacement Behaviour For Displacement Controlled Test

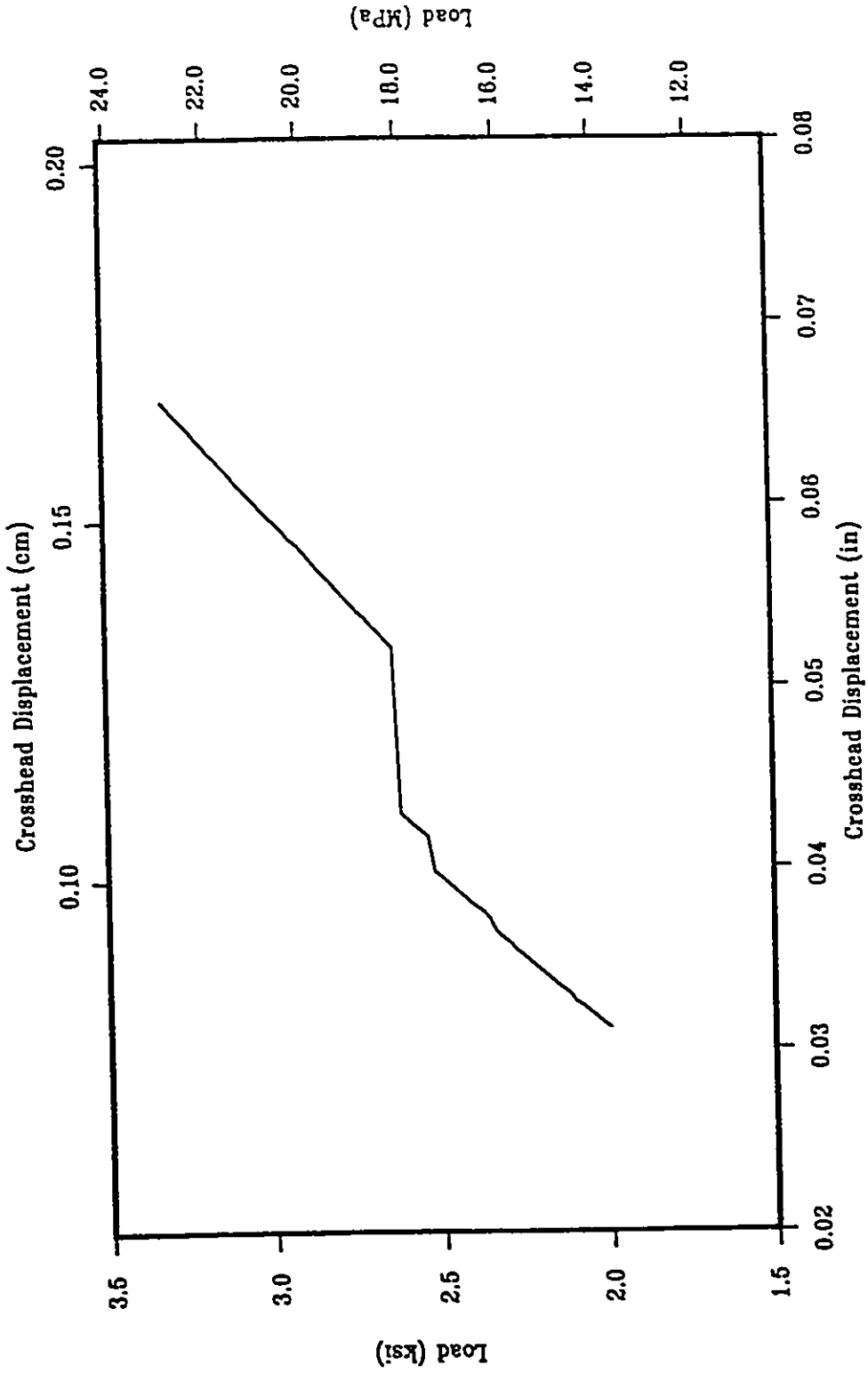

Figure 19 : Load Displacement Behaviour For Load Controlled Test

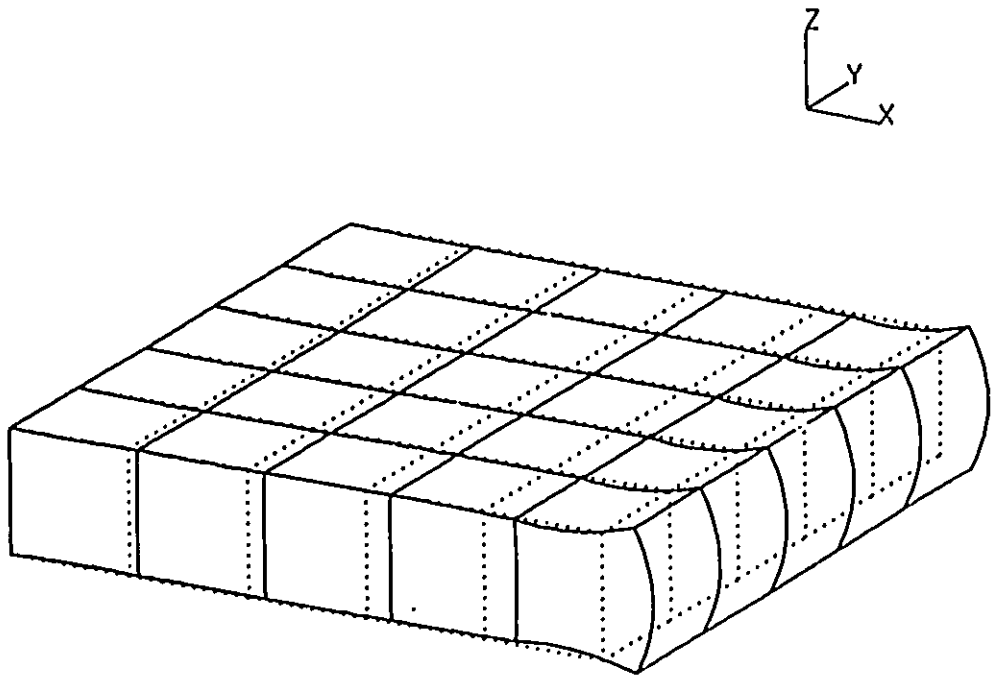

Figure 20 : Edge Deformation Of Crossply Laminate

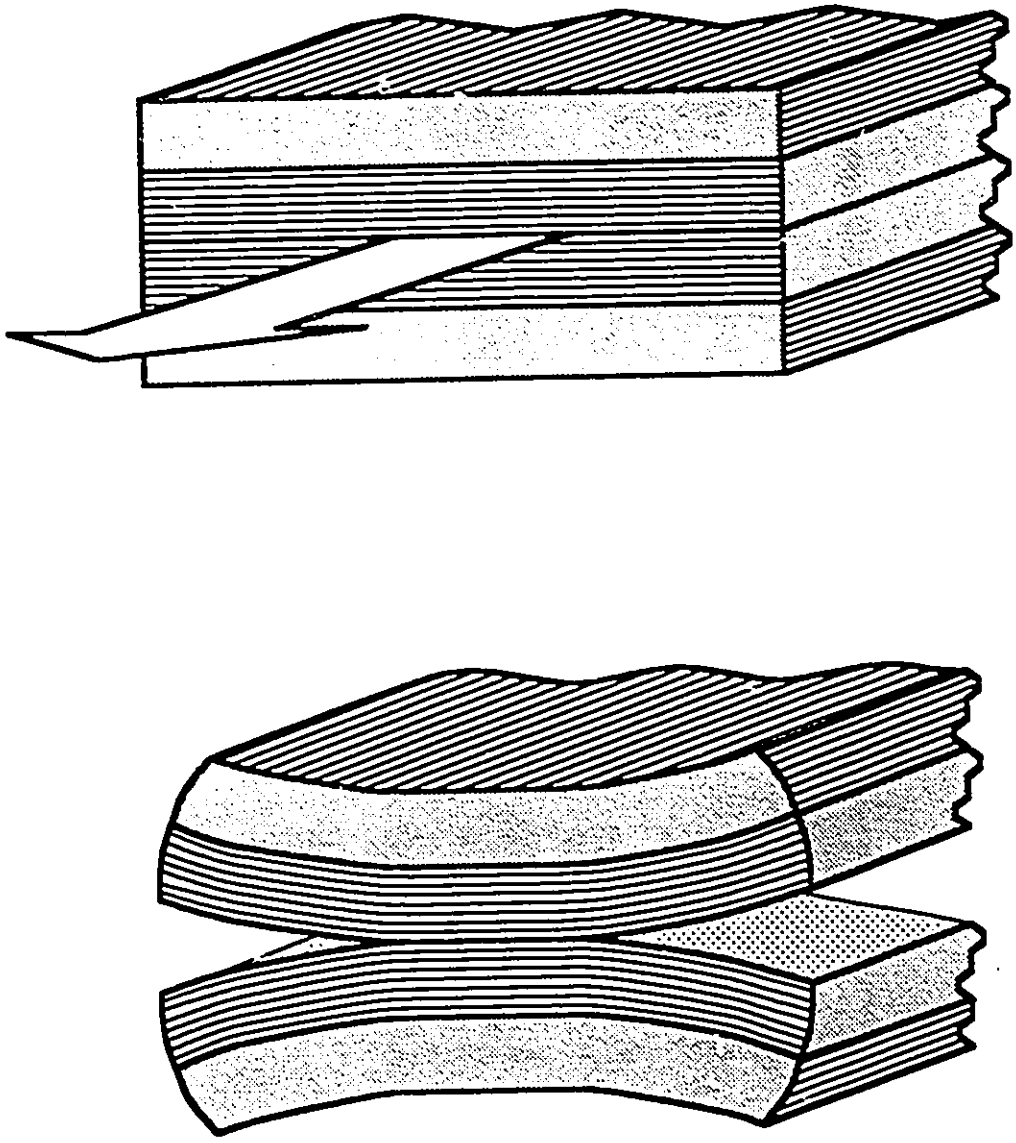

Figure 21 : Deformation Of (0,90) Crossplied Stacks

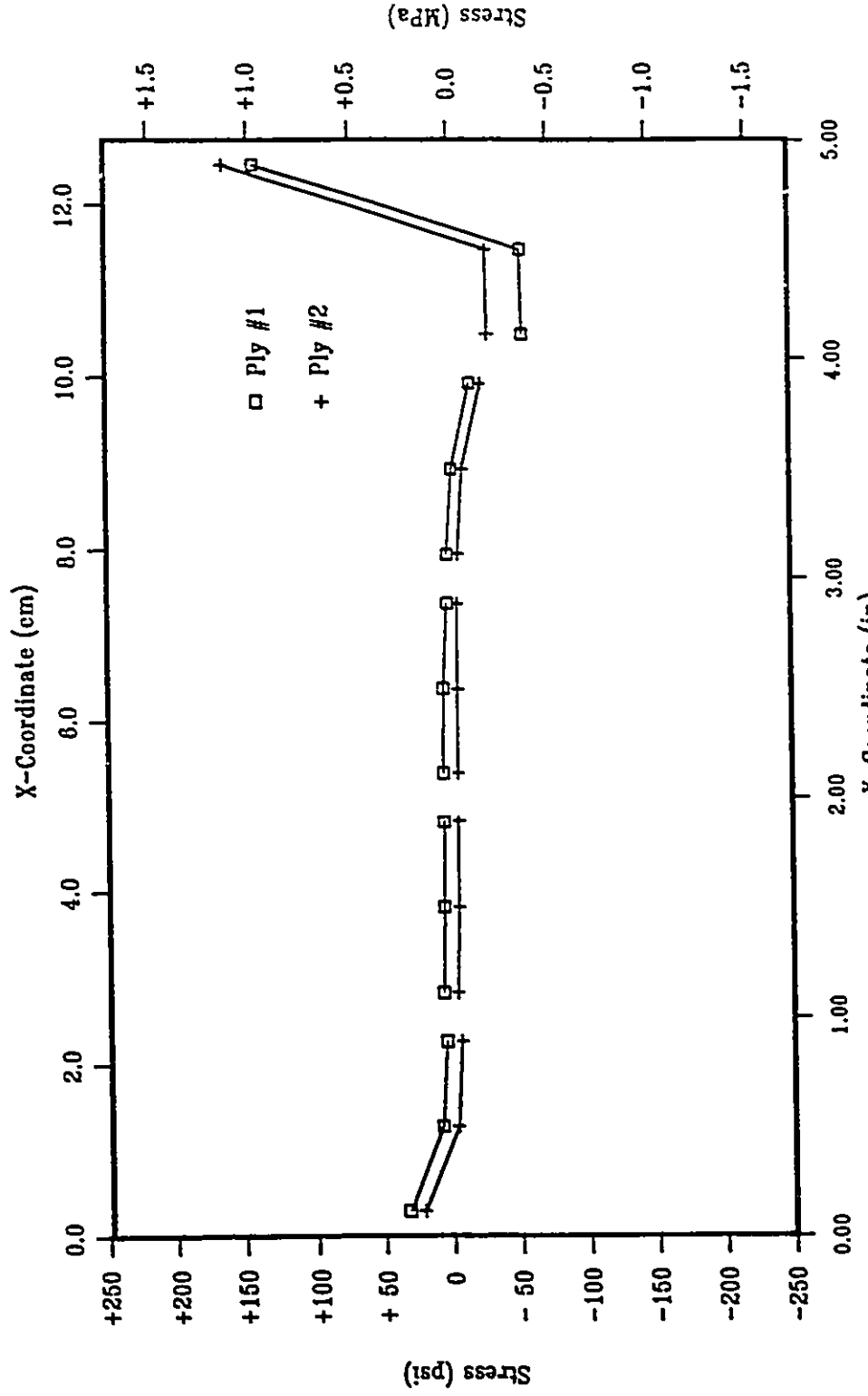

Figure 22 : Interlaminar Normal Stress Along Length

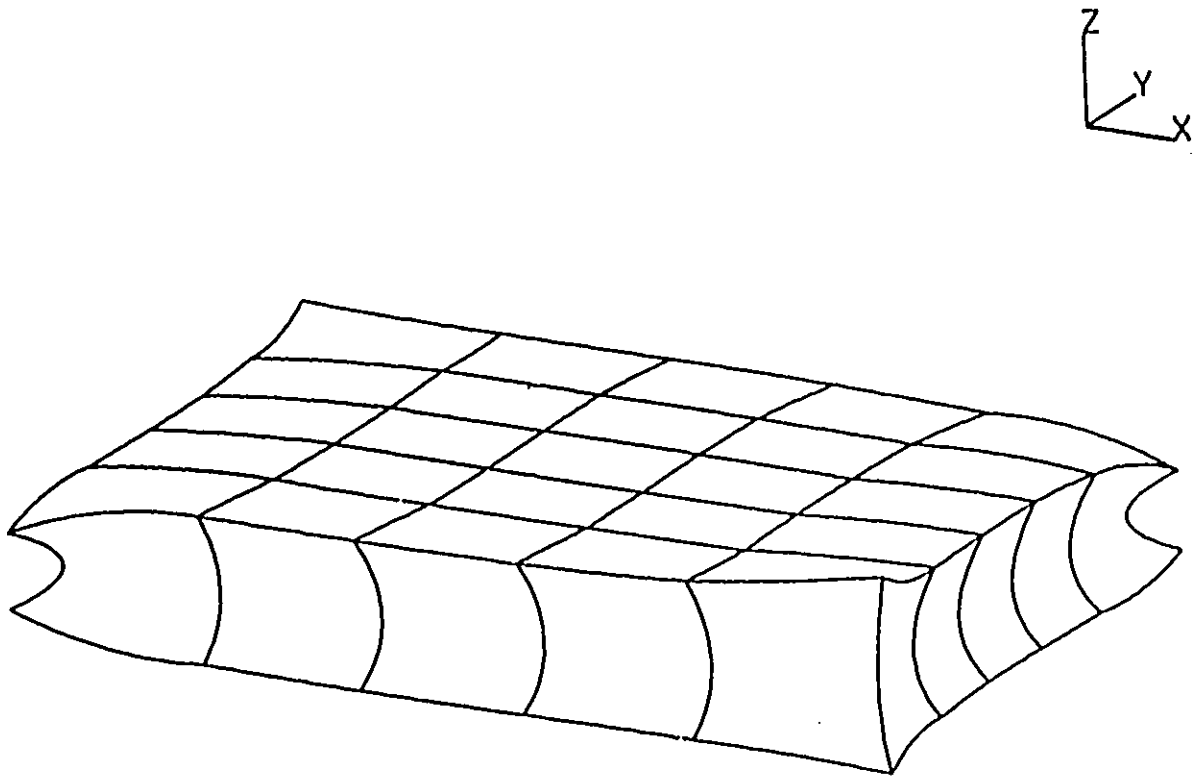

Figure 23 : Edge Deformations Of Unsymmetric Laminated Plate

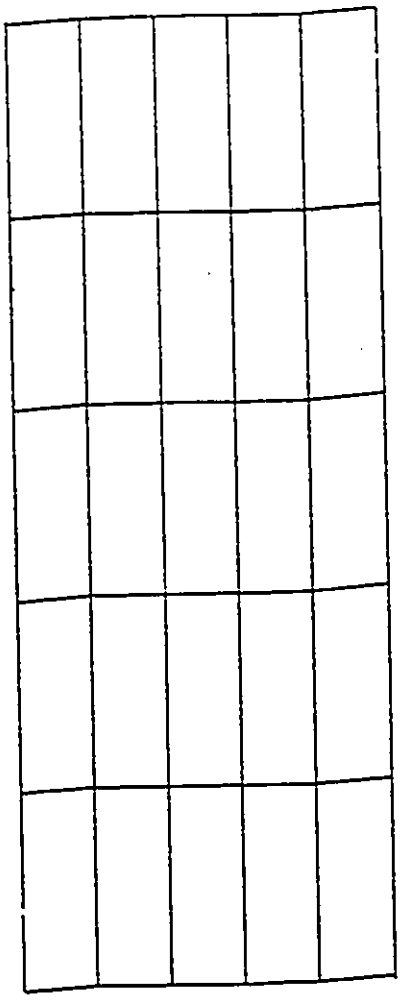

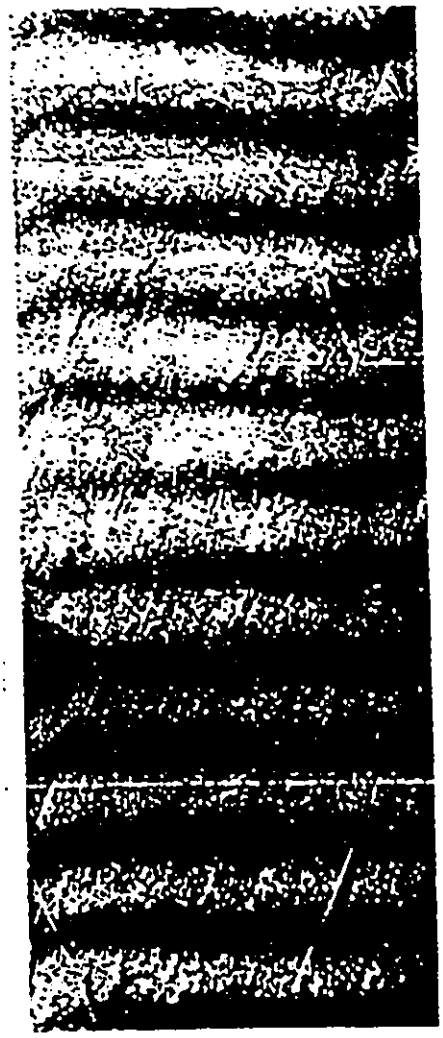

Finite Element Results

Experimental Results
(After Pipes & Daniels)

Figure 24 : Experimental Confirmation Of Surface Displacements

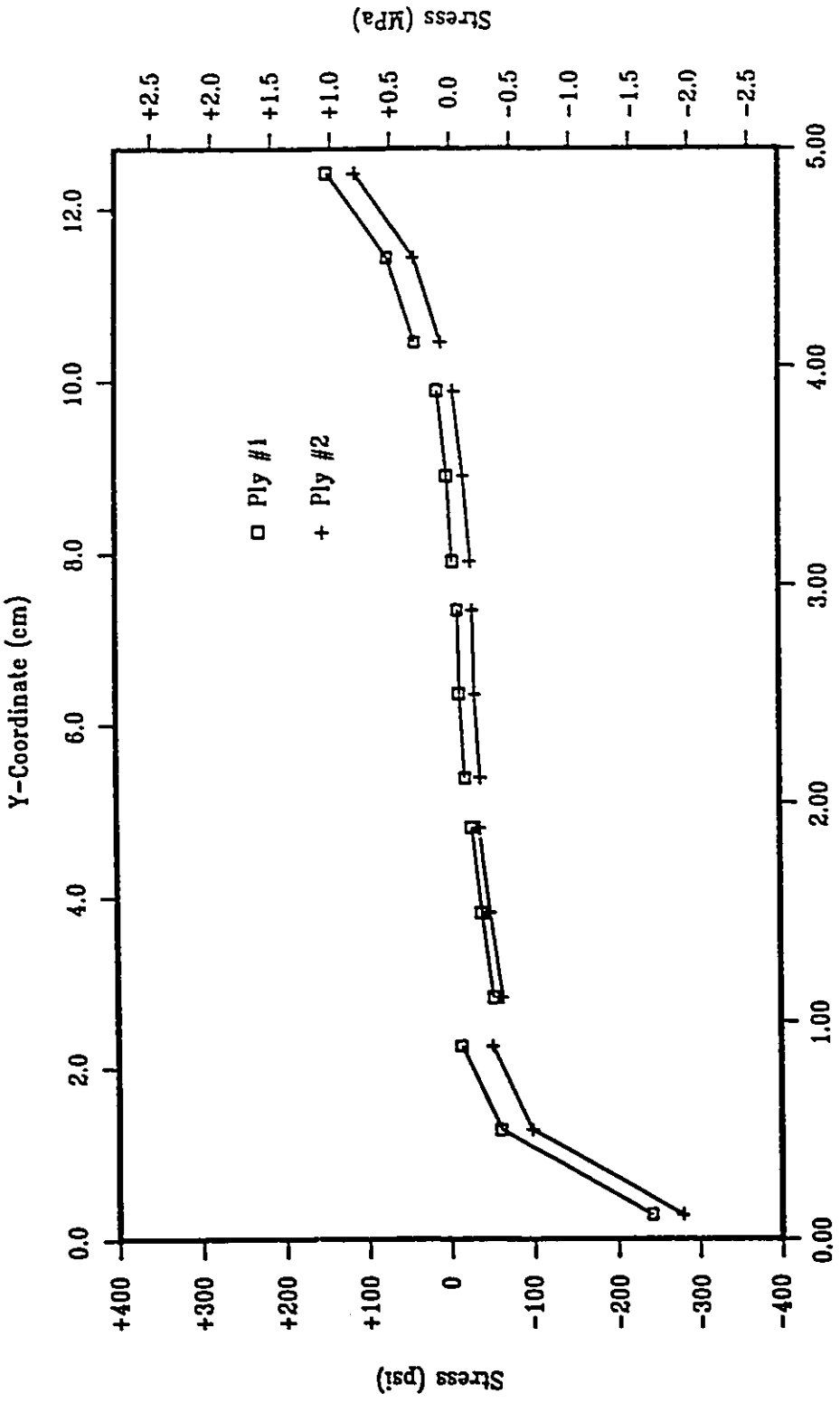

Figure 25 : Interlaminar Normal Stress Distribution Along Loaded Edge

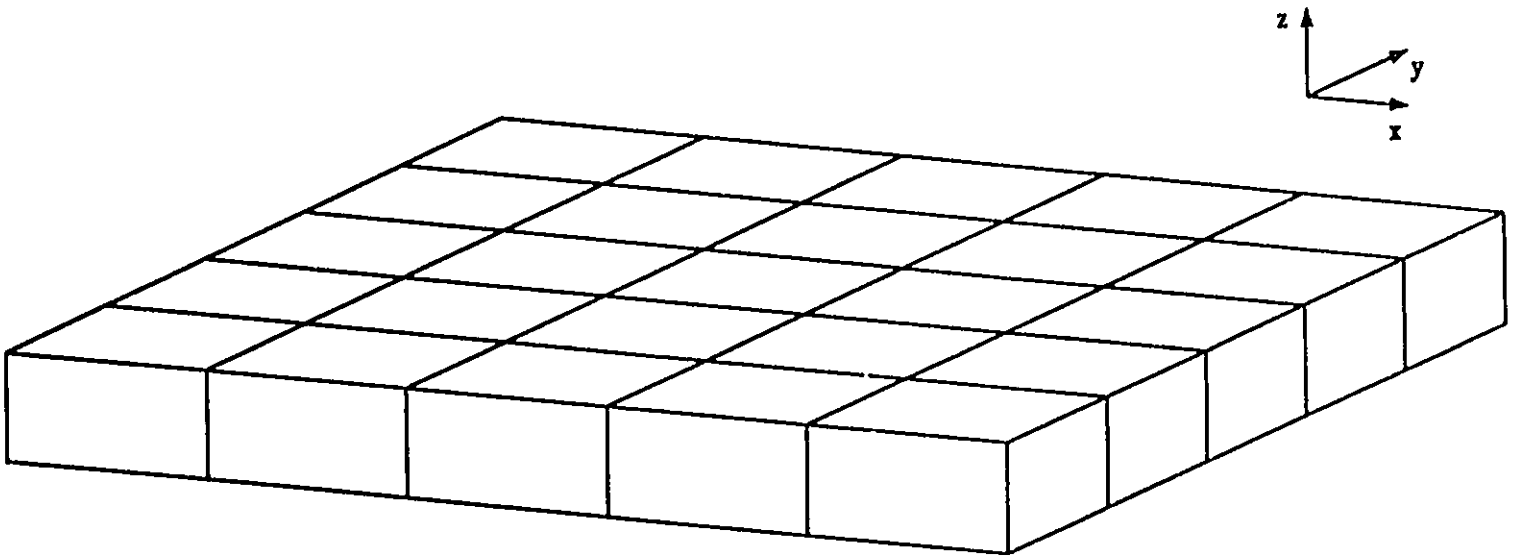

Length = 10 in (25.4 cm)

Width = 10 in (25.4 cm)

Thick = 1 in (2.54 cm)

Load : 1) Uniform On Entire Positive Z-Face

2) Uniform On Z-Face Of Center Element

Figure 26 : Clamped Square Laminated Plate

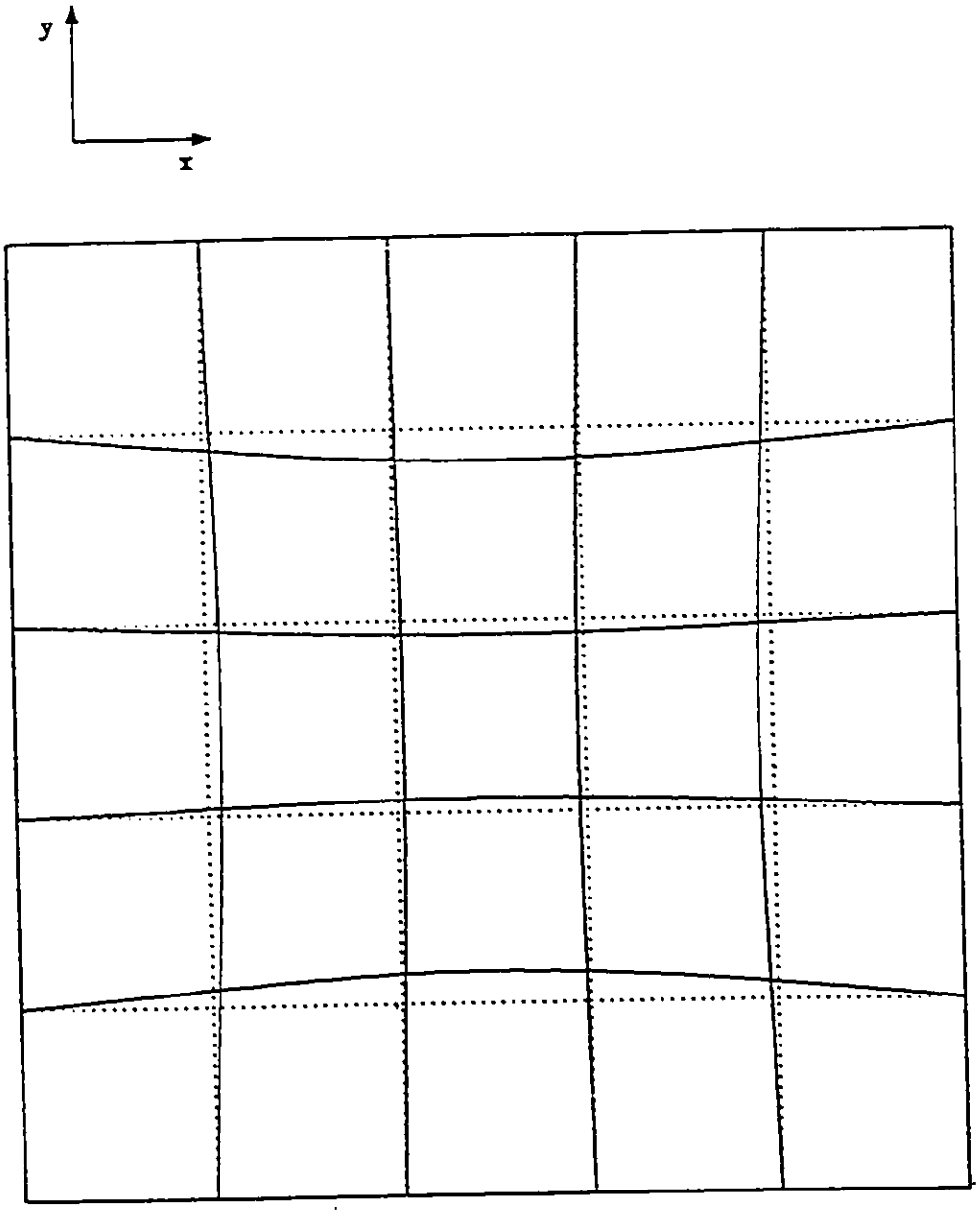

Figure 27 : Surface Deformation Of $(0_2,90_2)_s$ Clamped Plate

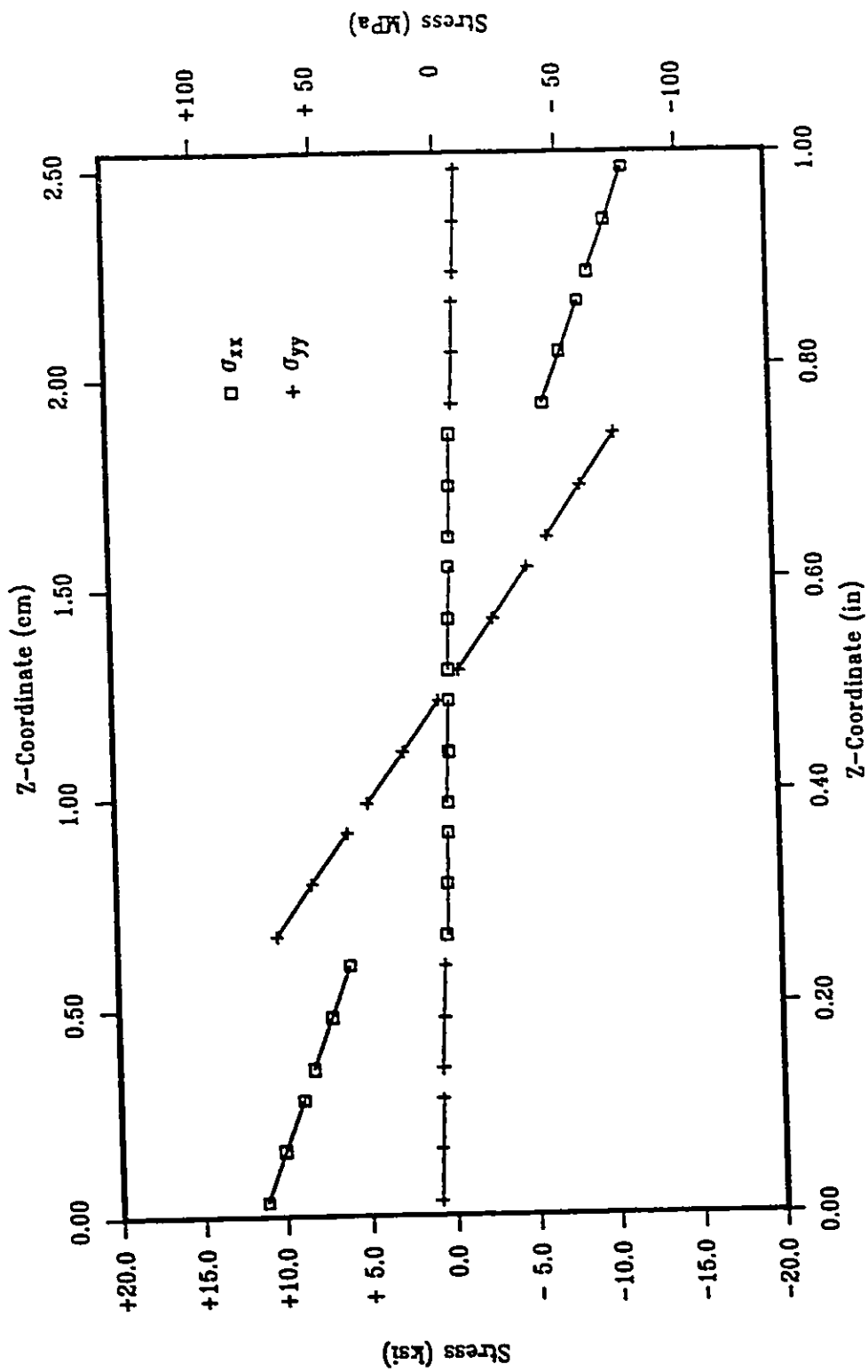

Figure 28 : Stress Distribution Through Plate Thickness At Center

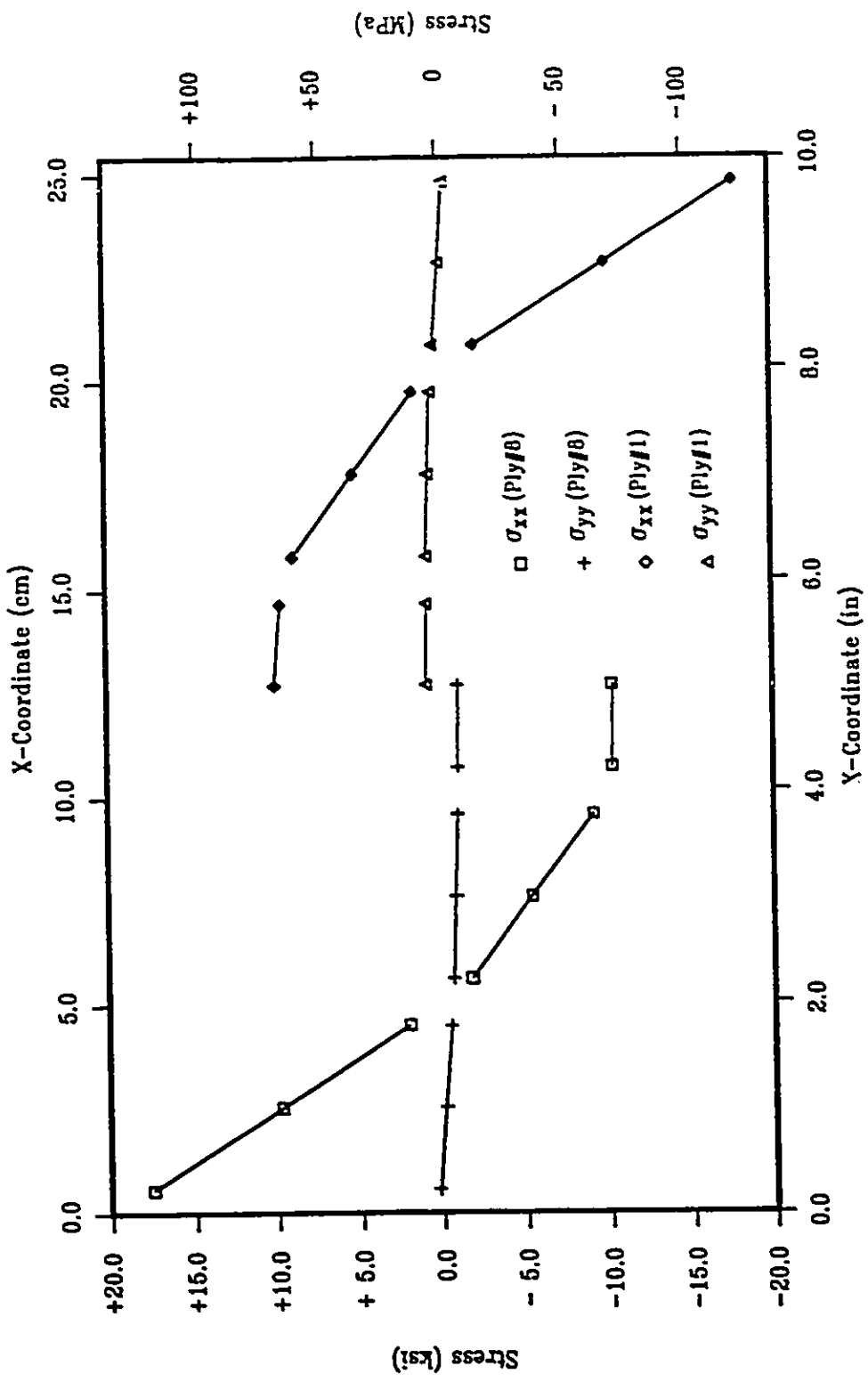

Figure 29 : Stress Distribution Along Length For Top And Bottom Plies

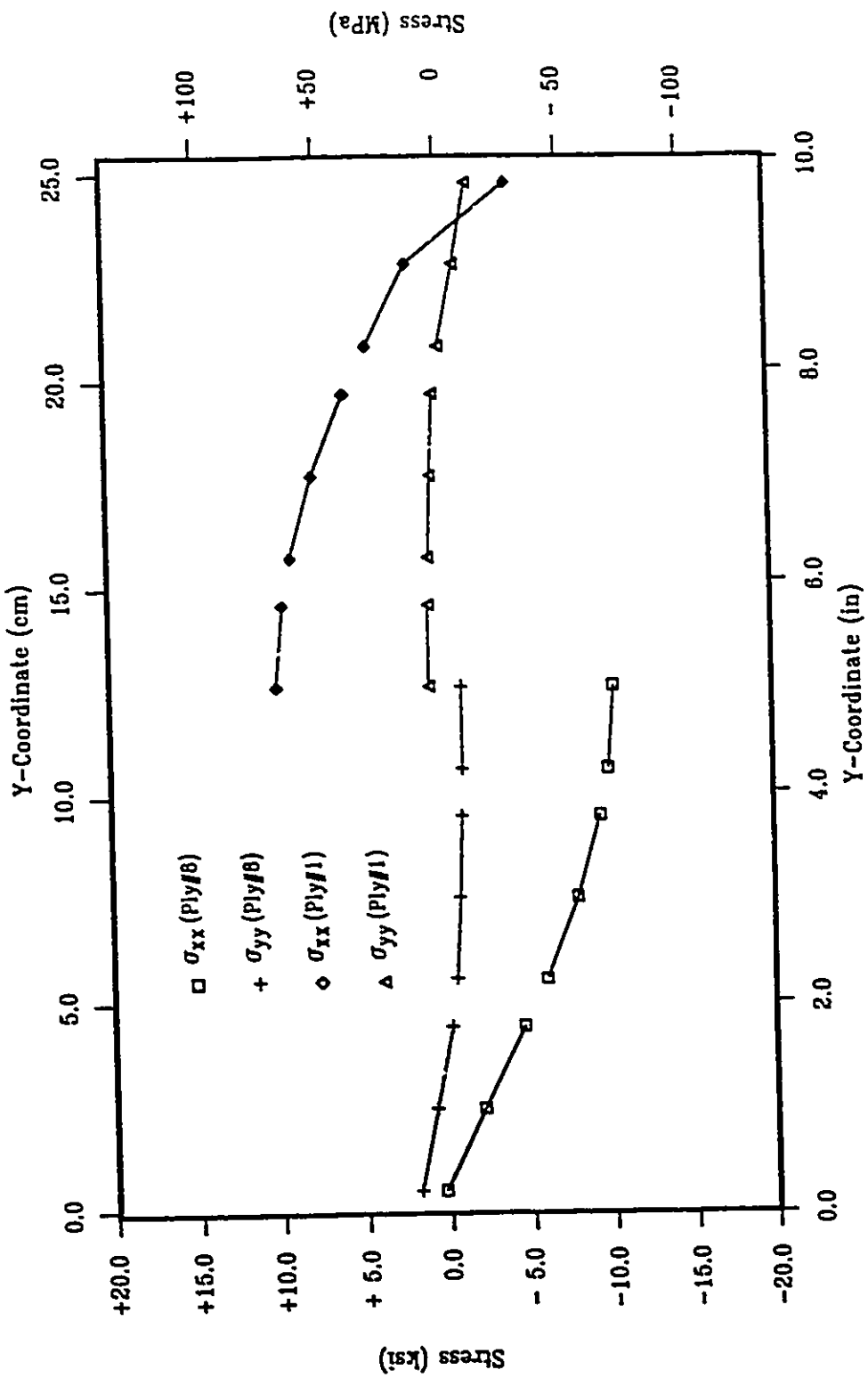

Figure 30 : Stress Distribution Along Width For Top And Bottom Plies

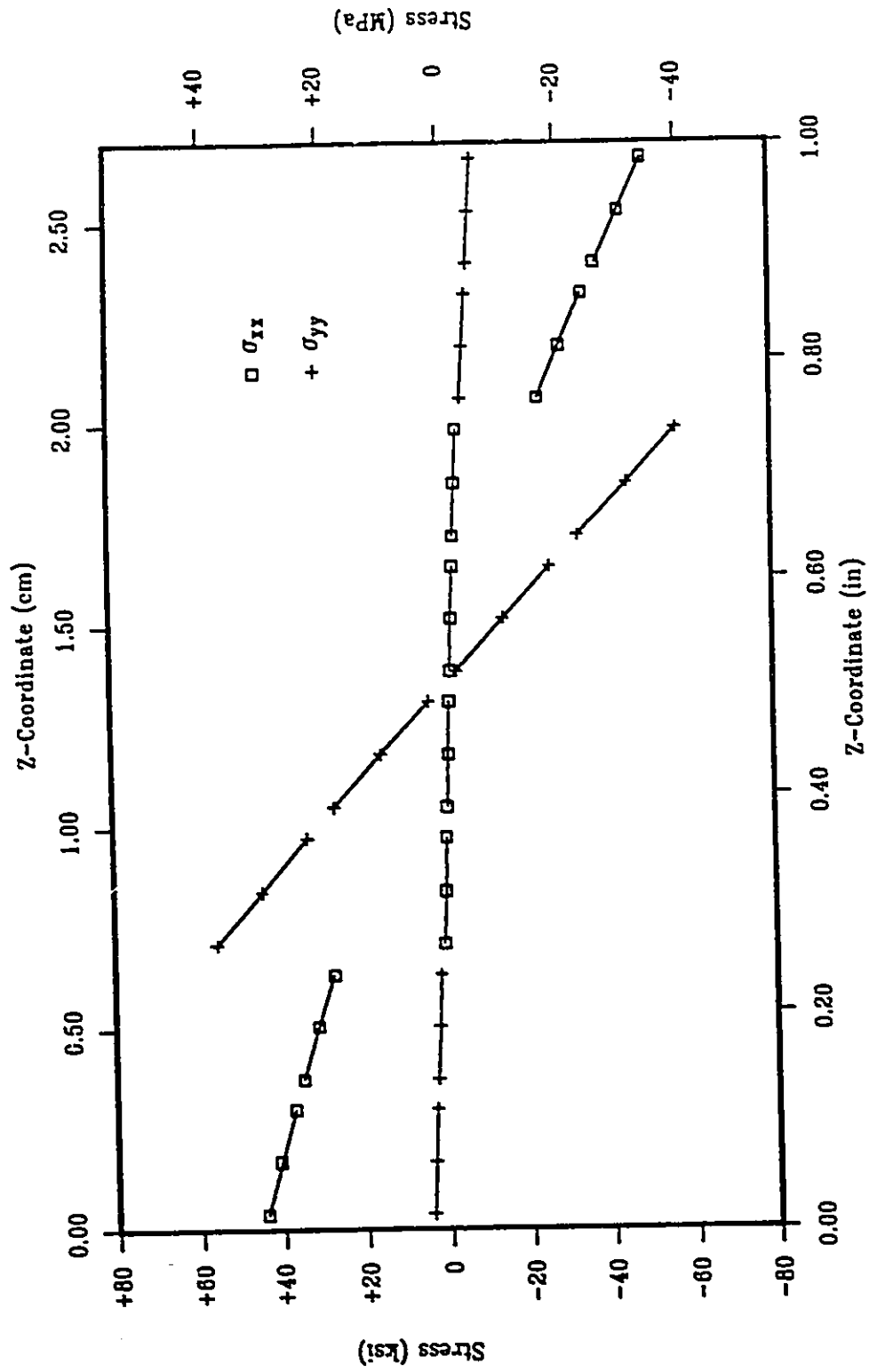

Figure 31 : Stress Distribution For $(0_2,90_2)_s$ Clamped Laminated Plate

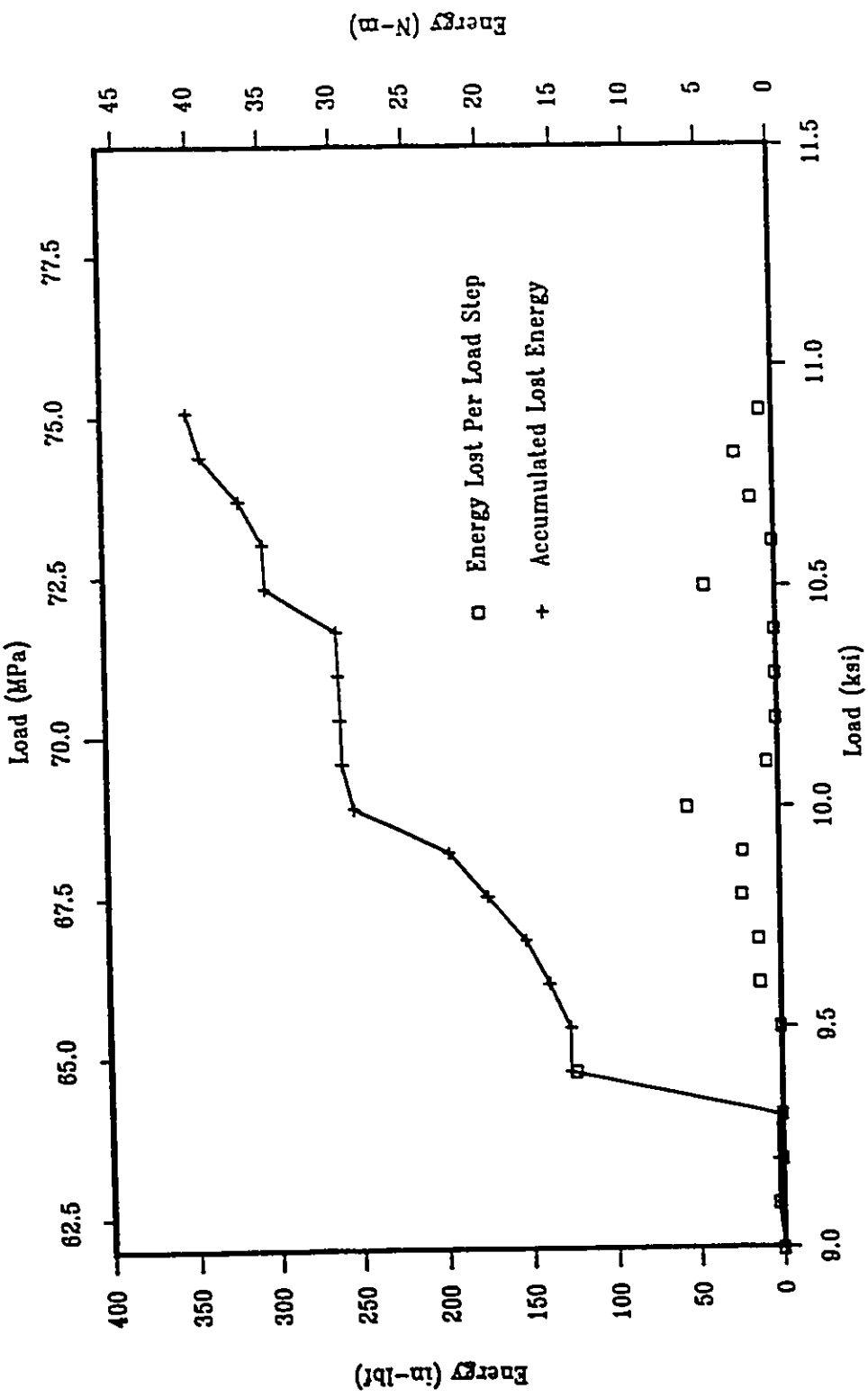

Figure 32 : Energy Absorption For $(0_2,90_2)_s$ Clamped Laminated Plate

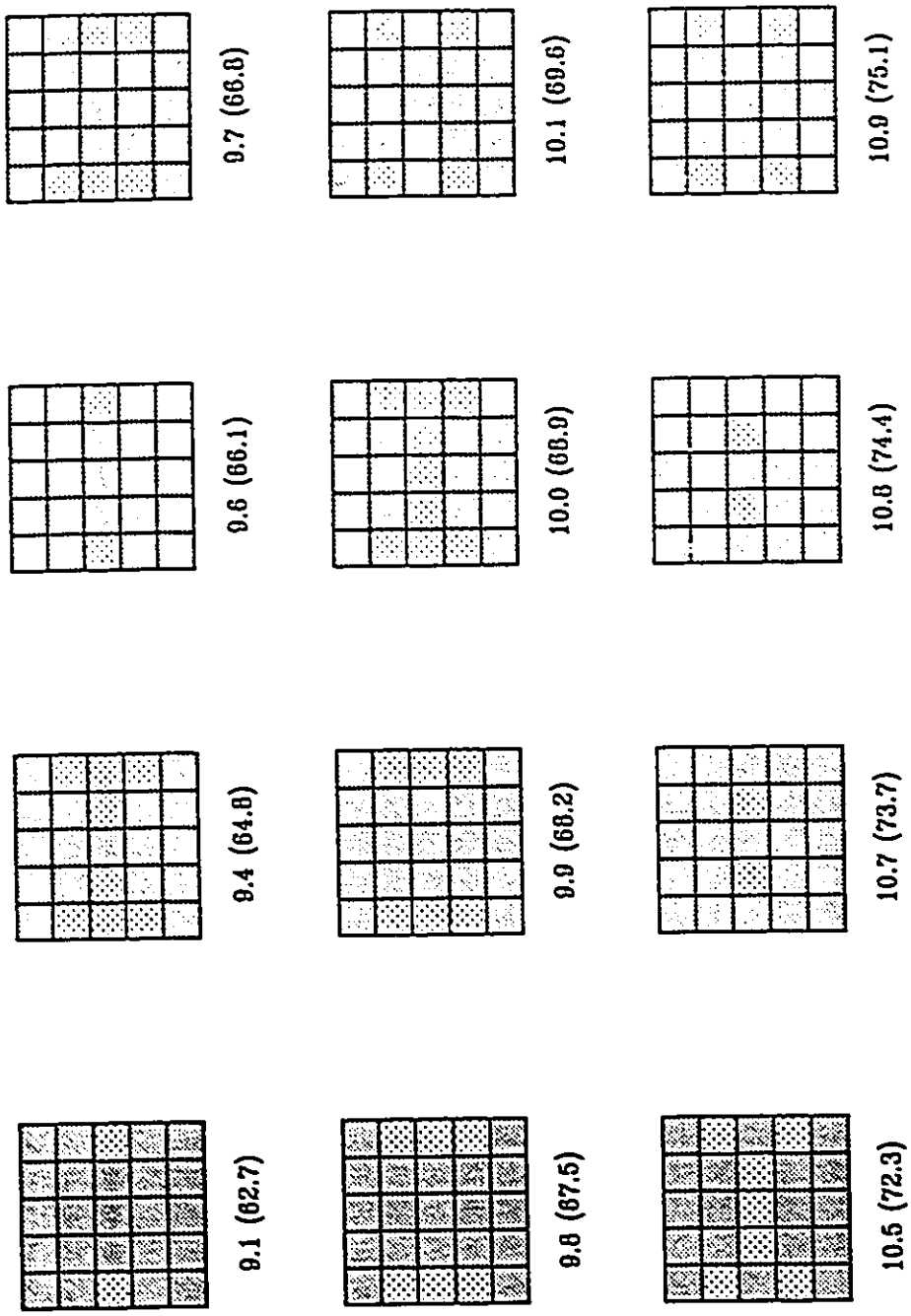

Figure 33 : Element Level Failure Display For $(0_2,90_2)_s$ Clamped Plate

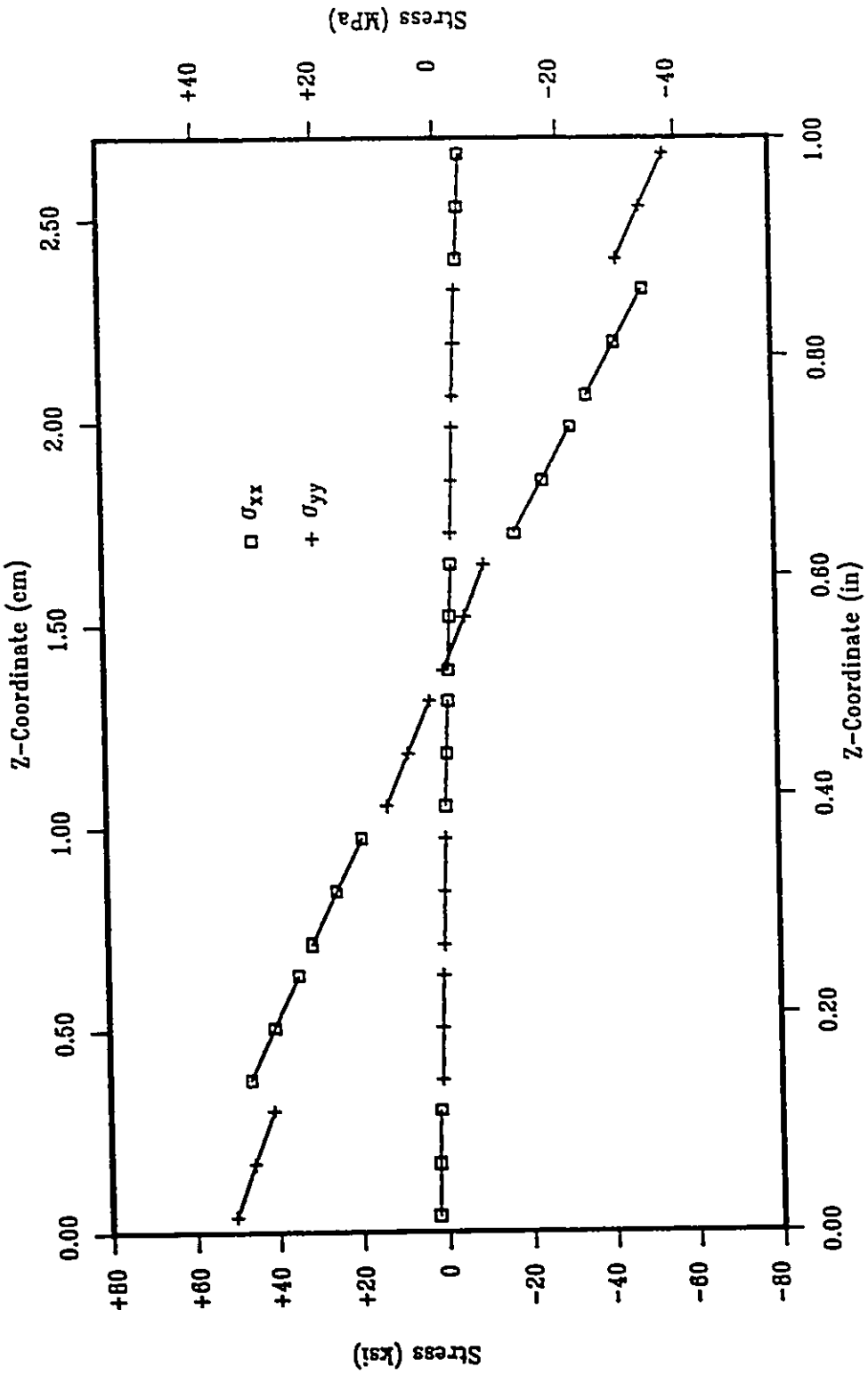

Figure 34 : Stress Distribution For $(90_1,0_2,90_1)_s$ Clamped Laminated Plate

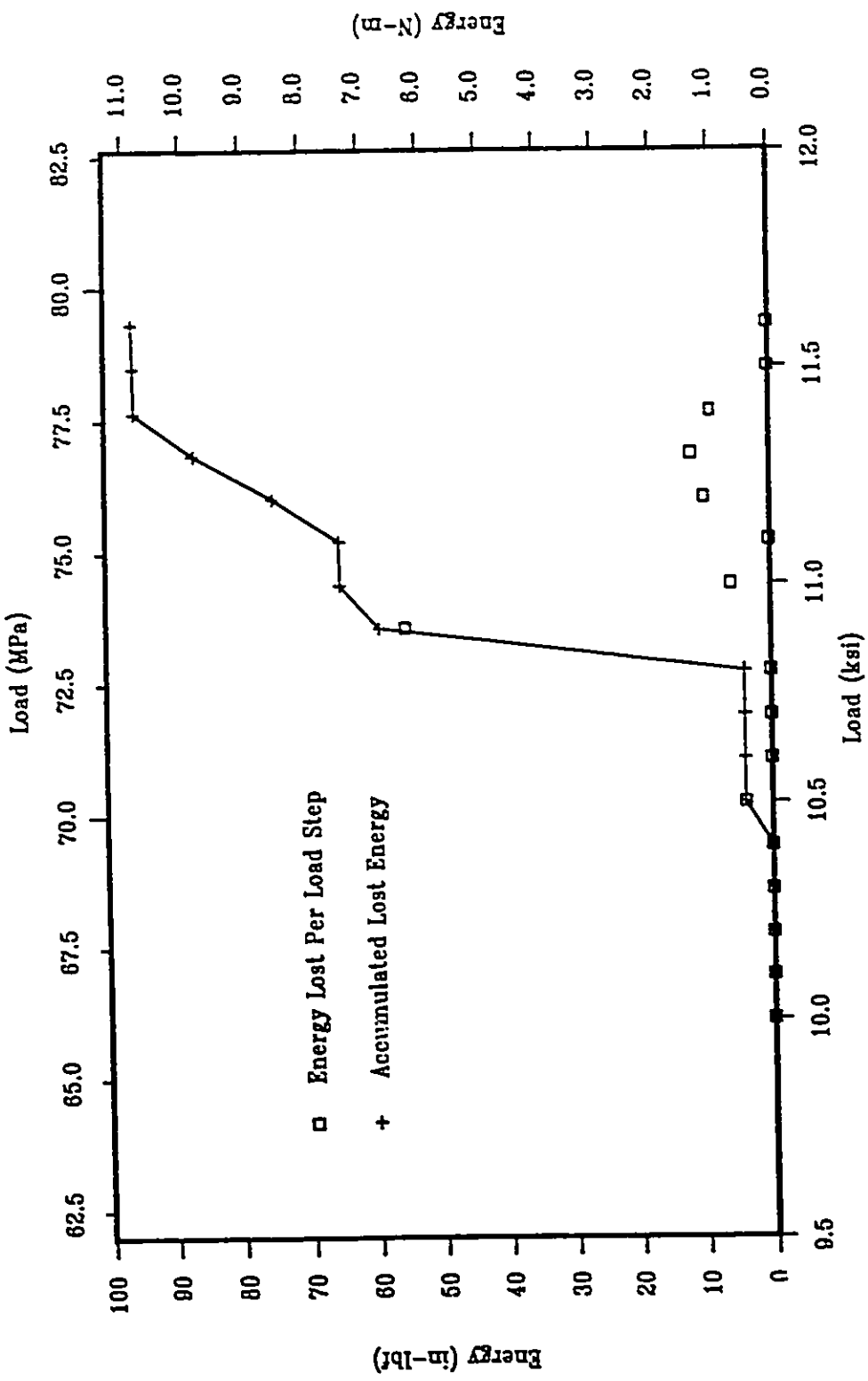

Figure 35 : Energy Absorption For $(90_1,0_2,90_1)_s$ Clamped Laminated Plate

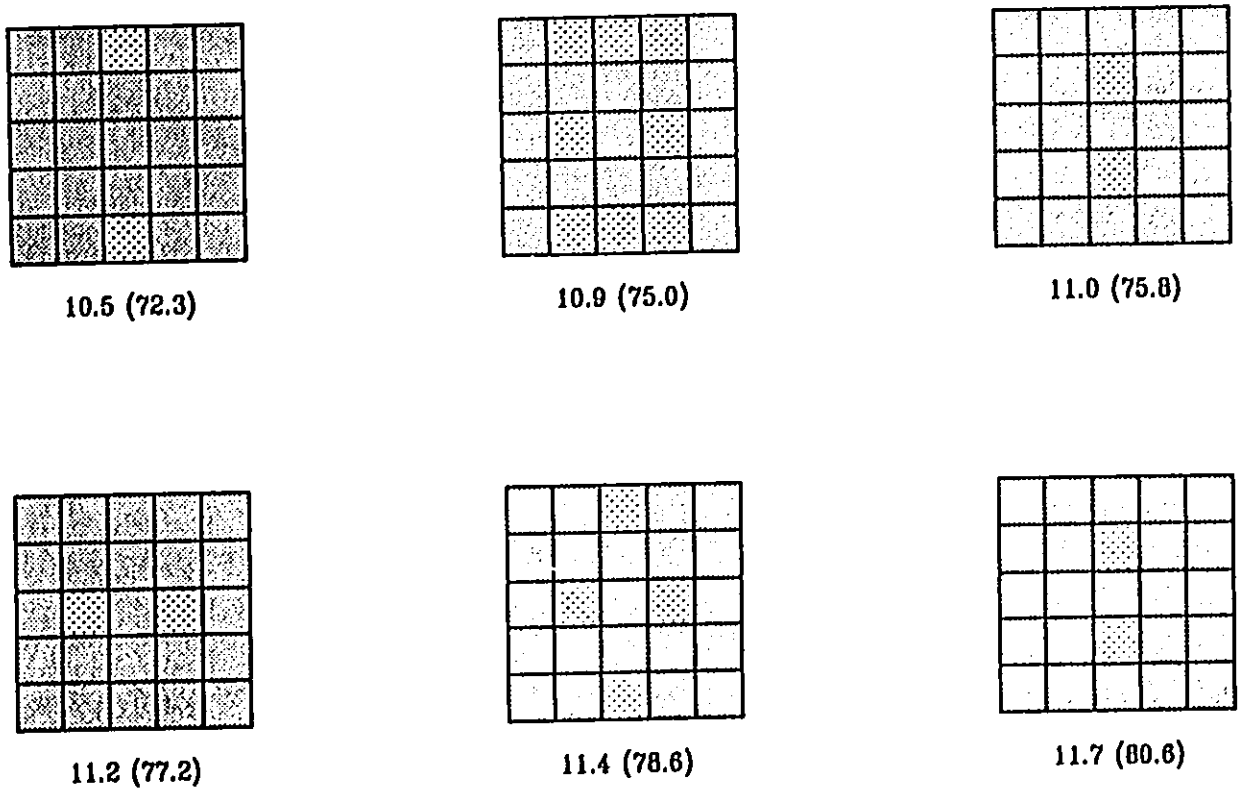

Figure 36 : Element Level Failure Display For $(90_1,0_2,90_1)_s$ Clamped Plate

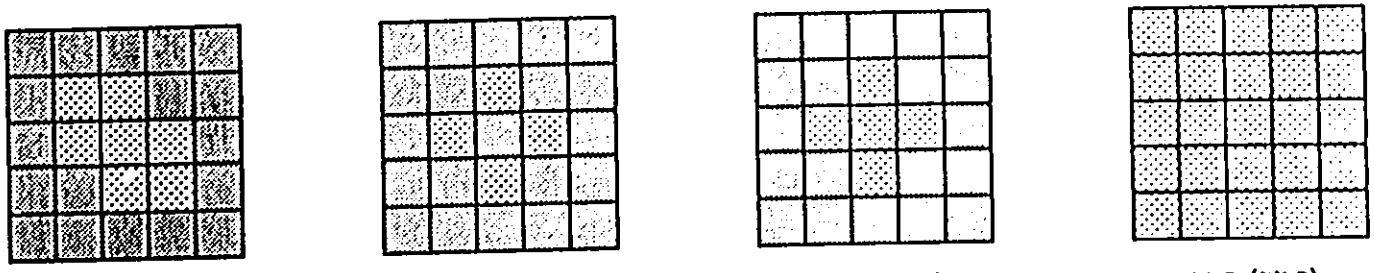

Figure 37 : Element Level Failure Displays For Clamped Plate

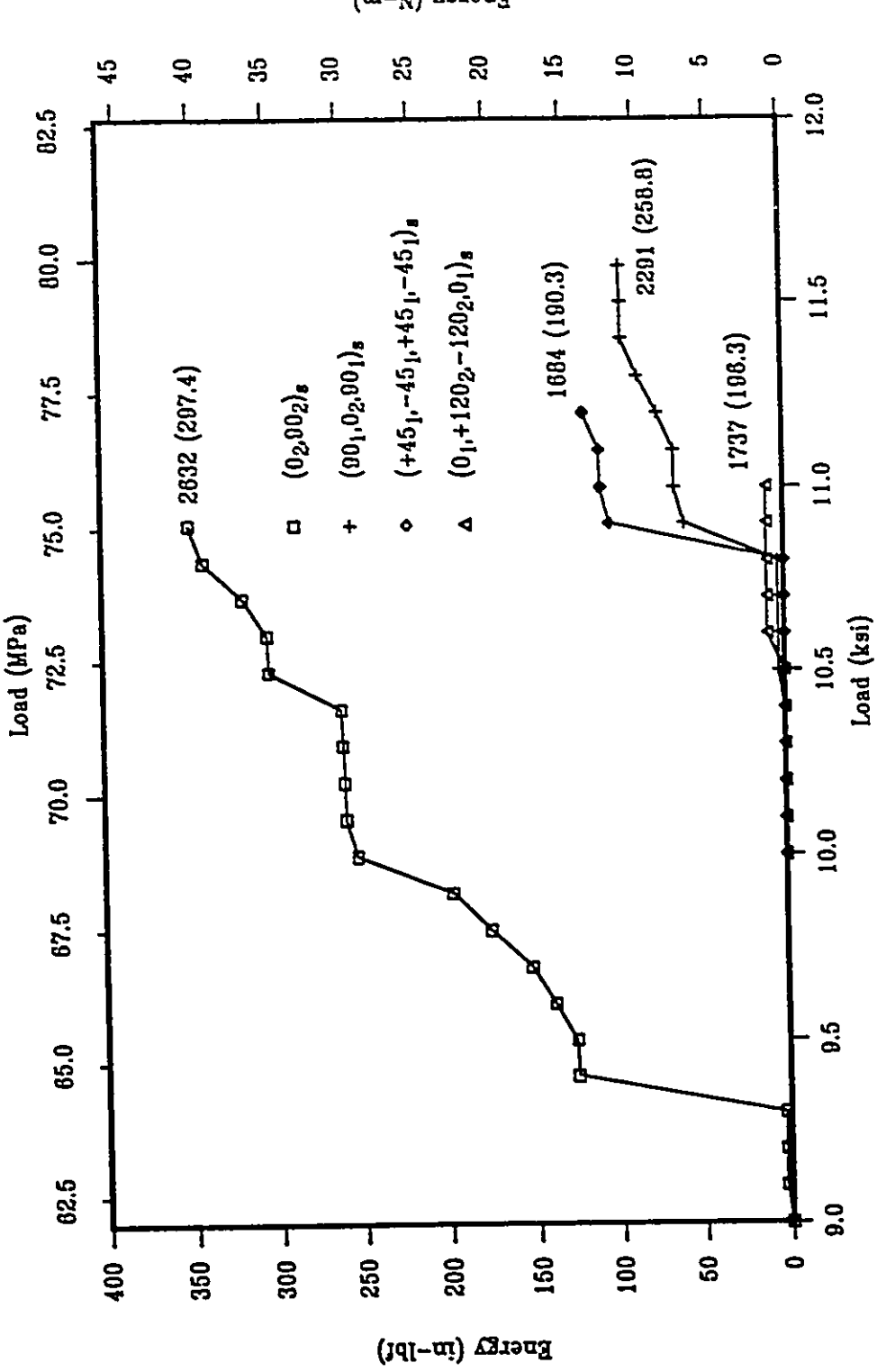

Figure 38 : Comparison Of Energy Absorption For Clamped Laminated Plate

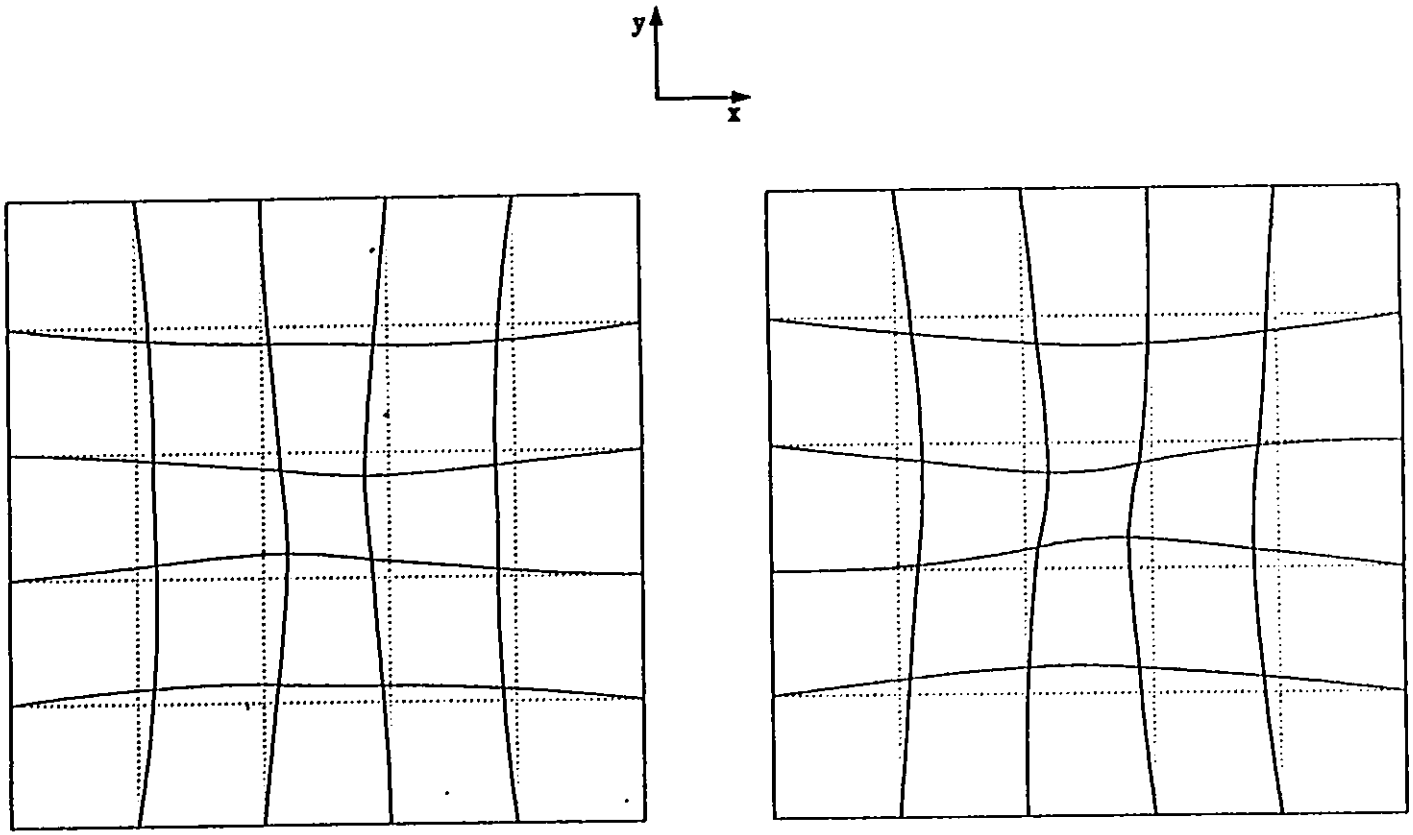

Figure 39 : Surface Skew Deformations For Clamped Laminated Plates

References

1. Timosheko S.P., Goodier J.N.,
Theory of Elasticity, 3'rd edition,
McGraw Hill Book Co., 1970, pp.90-95.

2. Reissner E., Stavsky Y.,
Bending and Stretching of Certain Types of
Heterogeneous Elastic Plates,
J. Appl. Mech., Sep. 1961, pp.402-408.

3. Whitney J.M, Pagano N.J.,
Shear Deformation in Heterogeneous Anisotropic
Plates,
J. Appl. Mec., Dec. 1970, pp.1031-1035.

4. Nelson R.B., Lorch D.R.,
A Refined Theory for Laminated Orthotropic Plates,
J. Appl. Mech., Mar. 1974, pp.177-185.

5. Lo K.H, Christensen R.M., Wu E.M.,
A Higher Order Theory of Plate Deformation,
J. Appl. Mech., Dec. 1977, pp.663-676.

6. Green J.E., Rodgers J.,
Acousto-Ultrasonic Evaluation of Impact-Damaged
Graphite Epoxy Composites,
Proc. 27'th National SAMPE Symposium,
4-6 May 1982, San Diego, California, pp 428-439.

7. Jones R.M.,
Mechanics of Composite Materials,
McGraw Hill Book Co., 1975, p 149.

8. Basset A.B.,
On the Extension and Flexure of Cylindrical and
Spherical Thin Elastic Shells,
Phil. Trans. Royal Soc. (London), Vol 12, 1890,
pp 433-480.

9. Tsai S.W., Hahn H.T.,
Introduction to Composite Materials,
Technomic Publishing Company, 1980, p 68.

10. Reissner E., Stavsky Y.,
Bending and Stretching of Certain Types of
Heterogeneous Aeolotropic Elastic Plates,
J. Appl. Mech., Vol 28, Sep 1961, pp 402-408.

11. Fox N.,
On Asymptotic Expansions in Plate Theory,
Phil. Trans. Royal Soc. (London), 1963, pp 228-233.

12. Reissner E.,
The Effects of Transverse Shear Deformation on the Bending of Elastic Plates,
J. Appl. Mech., Vol 12, Jun 1945, pp A69-A77.

13. Mindlin R.D.,
Influence of Rotary Inertia and Shear on Flexural Motions of Isotropic Elastic Plates,
J. Appl. Mech., Vol 18, Mar 1951, pp 31-38.

14. Whitney J.M., Leissa A.E.,
Analysis of Heterogeneous Anisotropic Plates,
J. Appl. Mech., Vol 36, Jun 1969, pp 261-266.

15. Dong S.B., Tso F.K.W.,
On a Laminated Orthotropic Shell Theory Including Transverse Shear Deformation.
J. Appl. Mech., Vol 39, Dec 1972, pp 1091-1097.

16. Essenberg F.,
On the Significance of the Inclusion of the Transverse Normal Strain in Problems Involving Beams with Surface Constraints.
J. Appl. Mech., Vol 42, Mar 1975, pp 127-132.

17. Whitney J.M, Sun C.T.,
A Refined Theory for Laminated Anisotropic Cylindrical Shells,
J. Appl. Mech., Vol 41, Jun 1974, pp 471-476.

18. Nelson R.B., Lorch D.R.,
A Refined Theory for Laminated Orthotropic Plates,
J. Appl. Mech., Vol 41, Mar 1974, pp 177-185.

19. Hildebrand F.B., Reissner E., Thomas G.B.,
Notes on the Foundations of the Theory of Small Displacements of Orthotropic Shells,
NACA TN#1633, 1949.

20. Naghdi P.M.,
On the Theory of Thin Elastic Shells,
Quat. Appl. Math., Vol 14, Jan 1957, pp 369-380.

21. Reddy J.N.,
A Refined Nonlinear Theory of Plates with Transverse Shear Deformation,
Int. J. Solids Structures, Vol 20, 1984, pp 881-896.

22. Reissner E.,
On Transverse Bending of Plates, Including the Effect of Shear Deformation,
Int. J. Solids Structures, Vol II, 1975, pp 569-573.

23. Lo K.H., Christensen R.M., Wu E.M.,
A Higher Order Theory of Plate Deformation,
J. Appl. Mech., Vol 44, Dec 1977, pp 663-676.

24. Fung Y.C.,
Foundations of Solid Mechanics,
Prentice Hall, 1965, p 457.

25. Pica A., Wood R.D., Hinton E.,
Finite Element Analysis of Geometrically Nonlinear Plate
Behavior Using a Mindlin Formulation.
Computers & Structures, Vol 11, #3, 1980,
pp 203-215.

26. Reddy J.N,
Geometrically Nonlinear Transient Analysis of Laminated Composite Plates,
AIAA J., Vol 21, Apr 1983, pp 621-629.

27. Reddy J.N., Chao W.C.,
Non-Linear Bending of Bimodular Material Plates
Int. J. Solids Structures, Vol 19, #3, 1983,
pp 229-237.

28. Choi I., Horgan C.O.,
Saint-Venant's Principle and End Effects in Anisotropic Elasticity,
J. Appl. Mech., Vol 49, Sep 1977, pp 424-430.

29. Horgan C.O.,
Saint-Venant End Effects in Composites,
J. Composite Materials, Vol 16, Sep 1982, pp 411-422.

30. Pipes R.B., Pagano N.J,
Interlaminar Stresses in Composite Laminates Under Uniform Axial Extension,
J. Composite Materials, Vol 4, Oct 1970, pp 538-548.

31. Whitcomb J.D., Raju I.S., Goree J.G.,
Reliability of the Finite Element Method for Calculating Free Edge Stresses in Composite Laminates,
Computers & Structures, Vol 15, #1, 1982, pp 23-37.

32. Lee J.D.,
Three Dimensional Finite Element Analysis of Damage Accumulation in Composite Laminate,
Computers & Structures, Vol 15, #3, 1982, pp 335-350.

33. Spilker, R.L., Chao S.C.,
Edge Effects in Symmetric Composite Laminates : Importance of Satisfying the Traction Free Edge Condition,
J. Composite Materials, Vol 14, Jan 1980, pp 2-20.

34. Rajagopal S.V., Singh G., Sadasiva Rao Y.V.K.,
Nonlinear Static Analysis of Multilayered Sandwich Plates,
Proc. Int. Conf. Finite Elements in Computational Mechanics,
Bombay, India, 2-6 Dec 1985, pp 221-230.

35. Paul B.,
Prediction of Elastic Constants of Multiphase Materials,
Trans. Metall. Soc. AIME, Vol 218, 1960, pp 36.

36. Hashin Z., Rosen B.W.,
The Elastic Moduli of Fiber Reinforced Materials,
J. Appl. Mech., Vol 31, Jun 1964, pp 223-232.

37. Wu T.T.,
On The Parametrization of the Elastic Moduli of Two Phase Materials,
J. Appl. Mech., Vol 32, Mar 1965, pp 211-214.

38. Cox H.L.,
The Elasticity and Strength of Paper and Other Fibrous Materials,
British J. Appl. Phys., Vol 3, Mar 1952, pp 72-79.

39. Brown R.J., Jr.,
Simplified Stress Analysis of Reinforced Plastic Pressure Vessels,
Soc. Plastics Engrs J., Vol 17, Sep 1961, pp 989-991.

40. Ekvall J.C.,
Elastic Properties of Orthotropic Monofilament Laminates,
ASME Aviation Conference, Los Angeles Ca,
61-AV-56, 1961.

41. Ekvall J.C.,
Structural Behavior of Monofilament Composites,
AIAA,ASME 7'th Structures, Structural Dynamics and Materials Conference, Palm Springs Ca., 1966, pp 250.

42. Shaffer B.W.,
Stress-Strain Relations of Reinforced Plastics Parallel and Normal to the Internal Filaments,
AIAA J., Vol 2, Feb 1964, pp 348-352.

43. Abolin'sh D.S.,
Compliance Tensor for an Elastic Material Reinforced in One Direction,
Polymer Mechanics, Vol 1, #4, 1965, pp 28-32.

44. Greszczuk L.B.,
Theoretical and Experimental Studies on Properties and Behavior of Filamentary Composites,
SPI 21'st Conference, Chicago Ill, 1966.

45. Greszczuk L.B.,
Thermoelastic Properties of Filamentary Composites,
AIAA, ASME 6'th Structures, Structural Dynamics and Materials Conference, Palm Springs Ca., 1965, pp 285.

46 Foster J.M, Smith C.B., Vachon R.I.,
On Predicting Thermal Conductivity of a Binary Mixture of Solids,
J. Spacecraft and Rockets, Vol 3, Feb 1966,
pp 287-288.

47. Springer S.G., Tsai S.W.,
Thermal Conductivities of Unidirectional Materials,
J. Composite Materials, Vol 1, Apr 1967, pp 166-173.

48. Hill R.,
Theory of Mechanical Properties of Fibre-Strengthened Materials,
J. Mech. Phys. Solids, Vol 13, Aug 1965, pp 189-198.

49. Hershey A.V.,
The Elasticity of an Isotropic Agregate of Anisotropic Cubic Crystals,
J. Appl. Mech., Vol 21, Sep 1954, pp 236-240.

50. Frolich H., Sack B.,
Theory of the Reological Properties of Dispersions,
Phil. Trans. Roy. Soc. (London), Vol A185, 1946,
pp 415-430.

51. Whitney J.M, Riley M.B.,
Elastic Properties of Fiber Reinforced Composite Materials,
AIAA J., Vol 4, Sep 1966, pp 1537-1542.

52. Whitney J.M.,
Geometric Effects of Filament Twist on the Modulus and Strength of Graphite Fiber-Reinforced Composites,
Textile Res. J., Vol 36, Sep 1966, pp 765-770.

53. Hermann L.R., Pister K.S.,
Composite Properties of Filament Resin Systems,
ASME Annual General Meeting, PN 63 WA-239, Nov 1963.

54. Leissa A.E., Clausen W.E.,
Application of Point Matching to Problems in Micromechanics,
Fundamental Aspects of Fiber Reinforced Plastic Composites (Ed:R.T.Schwrtz,H.S.Schwrtz),
Wiley Interscience, New York, 1968, pp 29-44.

55. Adams D.F., Dorner D.R.,
Transverse Normal Loading of a Unidirectional Composite,
J. Composite Materials, Jan 1967, pp 152-164.

56. Adams D.F., Dorner D.R.,
Longitudinal Shear Loading of a Unidirectional Composite,
J. Composite Materials, Jan 1967, pp 4-17.

57. Chen C.H., Cheng S.,
Mechanical Properties of Fiber Reinforced Composites,
J. Composite Materials, Vol 1, Jan 1967, pp 30-41.

58. Bloom J.M., Wilson H.B.,
Axial Loading of a Unidirectionsl Composite,
J. Composite Materials, Vol 1, Jul 1967, pp 268-277.

59. Beran M.J.,
Statistical Theory of Heterogeneous Media,
Monographs in Statistical Physics & Thermodynamics (Vol 9) (Ed:I.Prigogine),
J. Wiley & Sons, Ney York, 1968, pp 181-256.

60. Chamis C.C.,
Simplified Composite Micromechanical Equations for Hygral,
Thermal and Mechanical Properties,
SAMPE Quarterly, Apr 1984, pp 14-23.

61. Tsai S.W.,
Strength of Theories of Filamentary Structures,
Fundamental Aspects of Fiber Reinforced Plastic Composites (Ed:R.T.Schwrtz,H.S.Schwrtz),
Wiley Interscience, New York, 1968, pp 3-11.

62. Hill R.,
The Mathematical Theory of Plasticity,
Oxford University Press, London, 1950.

63. Collins J.A.,
Failure of Materials in Mechanical Design,
Van Nostrand, New York, 1972.

64. Griffith J.E., Baldwin W.M.,
Failure Theories of Generally Orthotropic Materials,
Developments in Theoretical and Applied Mechanics,
Vol 1,
Plemun Press, 1963, pp 410-420.

65. Hoffman O.,
The Brittle Strength of Orthotropic Materials,
J. Composite Materials, Vol 1, Apr 1967, pp 200-206.

66. Gol'denblat I.I, Kopnov V.A.,
Strength of Glass-Reinforced Plastics in the Complex Stress State,
Ploymer Mechanics, Vol 1, #2, 1966, pp 54-59.

67. Tsai S.W., Wu E.M.,
A General Theory of Strength for Anisotropic Materials,
J. Composite Materials, Jan 1970, pp 58-80.

68. Pipes B.R, Cole B.W.,
On The Off-Axis Strength Test for Anisotropic Materials,
J. Composite Materials, Apr 1973, pp 246-256.

69. Petit P.H., Waddoups M.E.,
A Method of Predicting the Nonlinear Behavior of Laminated Composites,
J. Composite Materials, Vol 3, Jan 1969, pp 2-19.

70. Whitney J.M., Daniel I.M., Pipes R.B,
Experimental Mechanics of Fiber Reinforced Composites,
SESA Monograph #4, 1982, pp 210-215.

71. Kachanov L.M.,
Time to Failure under Creep Conditions,
Ak Nauk SSR Odt Tekh Nauk #8, 1958 pp 26-31.

72. Sidoroff F.,
Damage Mechanics and Its Application to Composite Materials,
Proceedings of the Colloquium on Mechanical Characterisation of Load Bearing Fibre Composites (Ed:A.H.Cardon,G.Verchery),
Brussels, Aug 1984, pp 21-35.

73. Fitzgerald J.E.,
Some Divagations with Respect to an Operational Definition of Damage,
Workshop on a Continuum Mechanics Approach to Damage and Life Prediction,
Carollton, 1980, pp 153-158.

74. Leckie F.A.,
Tensorial Nature of Damage Measuring Internal Variables,
Physical Nonlinearities in Structural Analysis (Ed:J.Hunt,J.Lemaitre),
Springer 1971, pp 140-155.

75. Krajcinovic D,
Constitutive .Equations for Damaging Materials,
J. Appl. Mech., Vol 50, Jun 1983, pp 355-360.

76. Griffith A.A.,
The Phenomenon of Rupture and Flow of Solids,
Phil. Trans. Roy. Society London,
Ser A, Vol 221, 1921, pp 163-198.

77. DREV Materials Lab,
Experimental Notes on the Evaluation of the Moduli and Failure Strengths of Isolated Graphite Fibers,
Private Communication.

78. Beaumont P.W.R.,
Fracture Mechanics in Fibrous Composites,
Fracture Mechanics : Current Status, Future Prospects,
Pergamon Press, 1979, pp 211-233.

79. Phillips, D.C., Tetelman A.S.,
The Fracture Toughness of Fiber Composites,
Composites, Sep 1972, pp 216-223.

80. Wells A.A.,
Fracture Criteria in Elastic and Elastic/Plastic Solids,
Fracture Mechanics : Current Status, Future Prospects,
Pergamon Press, 1979, pp 235-246.

81. Wardle M.W.,
Impact Damage Tolerance of Composites Reinforced with Kevlar Aramid Fibers,
Proc. ICCM IV (Ed:T.Hayashi,K.Kawata,S.Umekawa),
Tokyo, Sep 1982., pp 837-844.

82. Winkle J.D., Adams D.F.,
Instrumented Drop Weight Testing of Cross-Ply and Fabric Composites,
Composites, Vol 16 #4, 1985, pp 268-278.

83. Harding J., Welsh L.M.,
Impact Testing of Fibre-Reinforced Composite Materials,
Proc. ICCM IV (Ed:T.Hayashi,K.Kawata,S.Umekawa),
Tokyo, Sep 1982., pp 845-852.

84. Hull D.,
Energy Absorption of Composite Materials Under Crack Conditions,
Proc. ICCM IV (Ed:T.Hayashi,K.Kawata,S.Umekawa),
Tokyo, Sep 1982., pp 861-870.

85. Ohlson N.G.,
The Initiation of Fracture in Fiber Composites at Elevated Loading Rates,
Proc. ICCM IV (Ed:T.Hayashi,K.Kawata,S.Umekawa),
Tokyo, Sep 1982., pp 871-878.

86. Gallagher R.H.,
Finite Element Analysis Fundamentals,
Prentice Hall Inc, 1975, pp 139-143.

87. Carey, C.F.,
Basis Functions In Finite Element Theory and Application,
Proc. 1974 Int. Conf. on Finite Element Methods in Engineering,
Univ. of NSW, Australia, Aug 28-30 1974, pp 55-74.

88. Tarnoplo'skii Y.M., Kincis T.,
Static Test Methods for Composites (Tr:G.Lubin),
Van Nostrand Reinhold, 1985, pp 1-281.

89. Lekhnitskii S.G., (Ed:J.J.Brandstatter,Tr:P.Fern),
Theory of Elasticity of an Anisotropic Body,
Holden Day Inc., 1963, pp 14-15.

90. Jones R.M.,
Mechanics of Composite Materials,
McGraw Hill Book Co., 1975, pp 32-33.

91. Bathe K.J.,
Finite Element Procedures In Engineering Analysis,
Prentice Hall Inc., 1982, pp 258-259.

92. Lustman L.R., Rose, M.E.,
A Three Dimensional Calculation of Elastic Equilibrium for Composite Plates,
Int. J. Num. Meth. Engr., Apr 1988, pp 953-971.

93. Gallagher R.H.,
Finite Element Analysis Fundamentals,
Prentice Hall Inc., 1975, pp 139-143.

94. Zienkiewicz O.C.,
The Finite Element Method,
McGraw Hill, New York, 1977, pp 201-204.

95. Conte S.D., deBoor C.,
Elementary Numerical Analysis,
McGraw-Hill Book Co., 1965, pp 150-157.

96. Irons B., Ahmad S.,
Techniques of Finite Elements,
John Wiley & Sons, 1986, pp 185-186.

97. Loxan A.N, Davids N., Levenson A.,
Table of the Zeros of the Legendre Polynomials of Order 1-16 and the Weight Coefficients for Gauss' Mechanical Quadrature Formula.
Bull. Amer. Math. Soc., Vol 48, Oct 1942, pp 739-743.

98. Narayanaswami R., Adelman H.M,
Evaluation of the Tensor Polynomial and Hoffman Strength Theories for Composite Materials,
J. Composite Materials, Vol 11, Oct 1977, pp 366-377.

99. Tsai S.W., Hahn H.T.,
Introduction to Composite Materials,
Technomic Publishing Company, 1980, p 286.

100. Gemert D.Van,
Direct Shear Compliance Measurement for Fibre Reinforced Composites,
Mechanical Characterisation of Load Bearing Fibre Composite Laminates, (Ed:A.H.Cardon,G.Verchery),
Elsivier Applied Science Publishers, 1985,
pp 191-198.

101. Griffith, A.A.,
The Phenomenon of Rupture and Flow of Solids,
Phil. Trans. Roy. Society London,
Ser A, Vol 221, 1921, pp 163-198.

102. Composite Plate Element
ANSYS User's Manual.

103. Warped Semi-Monocoque 4-Node Shell (MOQ4)
ASAS User's Manual (Ver H07), Appendix A.

104. BiLinear 4-Node Shell,
MARC User's Manual (Rev K.3), pp B75 1-1 to 1-6.

105. Barlow J.,
Optimal Stress Locations in Finite Element Models,
Int. J., Num. Meth. Engng., Vol 10, #2, 1976,
pp 243-251.

106. Berkan K.,
INDAP User's Manual,
Technical Report ME/87/FE/R2,
Dept. Mech. Engr.,
McMaster University, May 1987.

107. Grandin H.Jr.,
Fundamentals of the Finite Element Method,
Macmillan Publishing Company, pp 248-255.

108. Norrie D.H., DeVries G.,
An Introduction To Finite Element Analysis,
Acedemic Press Inc., 1978, pp 175-176.

109. Grandin H.Jr.,
Fundamentals of the Finite Element Method,
Macmillan Publishing Company, 1986, pp 271-272.

110. Timoshenko S.P., Goodier J.N.,
Theory of Elasticity, 3'rd Edition,
McGraw Hill Book Company, 1970, pp 254-258.

111. Young W.C.,
Roark's Formula's for Stress and Strain,
McGraw Hill Book Company, 6'th ed., 1989, pp 117-118.

112. Popov E.P,
Introduction to Mechanics of Solids,
Prentice Hall Inc., 1968, pp 412-415.

113. Popov E.P.,
Introduction to Mechanics of Solids,
Precntice Hall Inc., 1968, pp 482-484.

114. Pagano N.J., Halpin J.C.,
Influence of End Constraint in the Testing of
Anisotropic Bodies,
J. Composite Materials, Vol 2, Jan 1968, pp 18-31.

115. Altus E., Rotem A., Shmueli M.,
Free Edge Effect in Angle Ply Laminates - A New Three Dimensional Finite Difference Solution,
J. Composite Materials, Vol 14, Jan 1980, pp 21-30.

116. Ashton J.E., Halpin J.C., Petit P.H.,
Primer On Composite Materials,
Technomic Publishing Co., 1969, p 105.

117. F-15 Composite Wing Flight Test,
AFML Contract #F33615-71-6-1576,
McDonald Douglass Corporation,
AFML-TR-75-78.

118. Dingle L.E., Williams R.G., Parratt N.J.,
The Disproportionate Weakening of Composites by Sub-Millimetre Defects,
Composites-Standards, Testing and Design,
JPC Science and Technology Press, 1974, pp 51-53.

119. Whitney J.M., Browning C.E., Grimes G. C.,
The Relationship Between Significant Damage And The Stress-Strain Response Of Laminated Polymeric Matrix Composites,
Proceedings of the Sixth St.Louis Symposium,
May 11-12 1972, pp 441-447.

120. Batdorf S.B., Ghaffarian R.,
Size Effect and Strength Variability of Unidirectional Composites,
Int. J. Fracture, #26, 1984, pp 113-123.

121. Perry C.C.,
Strain-Gage Reinforcement Effects On Orthotropic Materials,
Experimental Techniques, Feb 1986, pp 20-24.

122. Pipes R.B., Kaminski B.E., Pagano J.E.,
Influence of the Free Edge Upon the Strength of Angle-Ply Laminates,
Analysis of the Test Methods for High Modulus Fibers and Composites,
ASTM STP 512, 1973, pp 218.

123. Rybicki F.E., Schmueser D.W.,
Effect of Stacking Sequence and Lay-Up Angle on Free Edge Stresses Around a Hole in a Laminated Plate Under Tension.
J. Composite Materials, Vol 12, Jul 1978, pp 300-313.

124 Pagano N.J., Pipes R.B.,
The Influence of Stacking Sequence on Laminate Strength,
J. Composite Materials, Vol 5, Jan 1971, pp 50-57.

125. Pipes R.B., Daniel I.M.,
Moire Analysis of the Interlaminar Shear Edge Effect in Laminated Composites,
J. Composite Materials, Vol 5, Apr 1971, pp 255-259.

126. Phan N.D., Reddy J.N.,
Analysis of Laminated Composite Plates Using a Higher-Order Shear Deformation Theory,
Int. J. for Num. Meth. in Engineering, Vol 21, #7, 1985, pp 2201-2219.

127. Whitney J.M., Pagano N.J.,
Shear Deformation in Heterogeneous Anisotropic Plates,
J. Appl. Mech., Vol 37, Dec. 1970, pp 1031-1036.

128. Bergan P.G., Cloug R.W.,
Large Deflection Analysis of Plates and Shallow Shells Using the Finite Element Method,
Int. J. Num. Meth. Engng., Vol 5, Mar 1973, pp 543-556.

129. Murray D.W., Wilson E.L.,
Finite Element Large Deflection Analysis of Plates,
A.S.C.E., Vol 95, Feb 1969, pp 143-165.

130. Srinivasan R.S., Bobby, W.,
Nonlinear Analysis of Skew Plates using the Finite Element Method,
Comput. Structure, Vol 6, Dec 1976, 199-202.

131. Ohlson, N.G.,
The Initiation of Fracture in Fiber Composites at Elevated Loading Rates,
Proc. ICCM IV (Ed:T.Hayashi,K.Kawata,S.Umekawa), Tokyo, Sep 1982., pp 871-878.

132. Stellbrink K.,
Examination of Impact Resistance of FRP - Suggestion for a Standard Test Method,
Mechanical Characterisation of Load Bearing Fibre Composite Laminates (Ed:A.H.Cardon,G.Verchery), Elsivier Applied Science Publishers, 1985, pp 169-178.